ETH
Eidgenössische Technische Hochschule Zürich
Swiss Federal Institute of Technology Zurich

Institute for
Dynamic Systems and Control
IDSC
Institut für Dynamische Systeme
und Regelungstechnik

Johannes Stoerkle

Lateral Dynamics of Multiaxle Vehicles

Master Thesis

Institute for Dynamic Systems and Control
Swiss Federal Institute of Technology (ETH) Zurich

Supervision

M. Alberding (ETH Zurich)
Prof. Dr. L. Guzzella (ETH Zurich)
Prof. Dr. W. Schiehlen (University of Stuttgart)
Prof. Dr. P. Eberhard (University of Stuttgart)

July 2013

IDSC-LG-MA-05

Diploma Thesis DIPL-MSC-196

Lateral Dynamics of Multiaxle Vehicles

of
Johannes Stoerkle

Betreuer: M. Alberding (ETH Zurich)
Prof. Dr. L. Guzzella (ETH Zurich)
Prof. Dr. W. Schiehlen (University of Stuttgart)
Prof. Dr. P. Eberhard (University of Stuttgart)

University of Stuttgart
Institute of Engineering and Computational Mechanics
Prof. Dr.–Ing. Prof. E.h. P. Eberhard

July 2013

Abstract

Since standard European semitrailers usually utilize an unsteered rear tri-axle group they are produced with low financial efforts but have a high tire wear (especially at the rearmost axle) and a reduced maneuverability. This work shows that an actively steered rearmost axle at a semitrailer can improve the performance during low-speed turning maneuvers, high-speed cornering and could intervene during critical situations such as rollover. After some general fundamentals of vehicle dynamics are summarized, the current state of art with respect to steered semitrailers is discussed. Linear and nonlinear tractor-semitrailer single-track models are derived, which take the lateral and yaw motion of the coupled vehicles into account and can be used for the development of different steering strategies for an enhanced maneuverability. In this scope a steady-state and feedback control strategy is developed. In addition, a 2-degree of freedom controller combines both strategies. Furthermore, the models are extended in order to account for the roll motions of the system at high-speed. A simple "active rollover damping control law" is proposed and investigated, which intervenes with the trailer steering and aims to reduce the risk of a rollover. In conclusion, the 2-degree of freedom control law improves the maneuverability of a whole tractor-semitrailer system and the active rollover damping strategy decreases the risk of a rollover significantly during critical maneuvers. The derived models and strategies provide different chances for further optimizations, improvments and implementations on real tractor-semitrailer prototypes.

Contents

Chapter 1

Introduction

1.1 Motivation

Vehicle dynamics control of articulated heavy vehicles, such as tractor-semitrailer (TST) combinations, pose major challenges compared to passenger cars. For instance, a TST results in an increased complexity of the governing dynamics: the available energy is limited, the regarded mass loaded on the vehicle changes, and the requirements towards reliability need to be fulfilled. Articulation and a high center of gravity challenge the tractor and semitrailer combination, especially in terms of road safety i.e. the risk of a rollover (illustrated in figure 1.1) should be decreased. Standard European semitrailers utilize an unsteered tri-axle group. These semitrailers with an unsteered tri-axle group are produced with low financial efforts but later have a high tire wear and reduced maneuverability.

Figure 1.1: Rollover of a real TST in Zhejiang (China) in April 2011. This screen-shots are retouched and extracted from the video of a monitoring camera, published on the website *www.youtube.com*.

The objective of this thesis is to investigate the utilization of a semitrailer steering in order to improve the performance during low-speed turning maneuvers, high-speed cornering and interventions during critical situations such as rollover. Strategies for robust control of the rearmost trailer axle have to be developed and for the implementation of the corresponding control architectures, the numerical simulation environment "MATLAB/Simulink" is available. The controller for the rearmost axle must meet the software and hardware requirements. The performance of the controller can be evaluated with a single track model and a multibody system (MBS) model in the simulation software "SimPack".
Figure 1.2 represents a five-axle articulated tractor with semitrailer which will be the focus of this

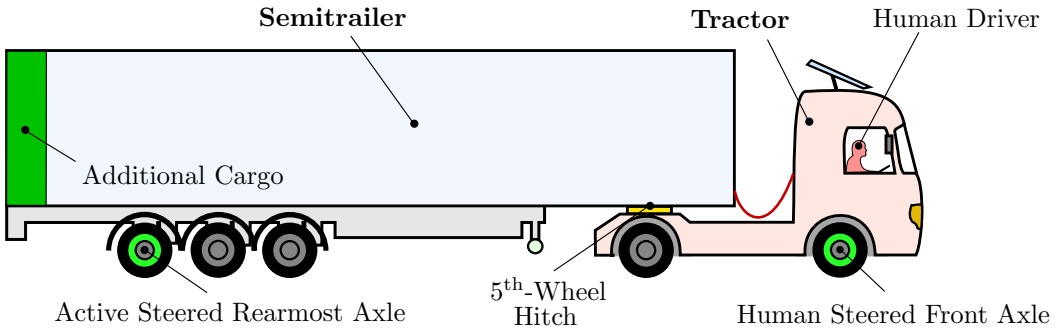

Figure 1.2: Tractor and semitrailer (TST) with an actively steered rearmost axle.

thesis. The tractor unit is considered to be driven by a human, steering the front axle, opening the throttle and pushing the brake. The semitrailer has three axles, whereby the rearmost axle is equipped with an electronically controlled command steering system. The towing unit (tractor) and semitrailer are coupled by a so-called 5^{th}-wheel hitch. It is designed to bear the vertical load imposed by the front of the semitrailer.

Especially during low-speed turning maneuvers the active steering system could not only reduce the tire wear and driving resistance ($\propto CO_2$), but also might allow greater cargo dimensions. Figure 1.3 clarifies the benefits and compares the maneuverability of a steered and unsteered semitrailer.

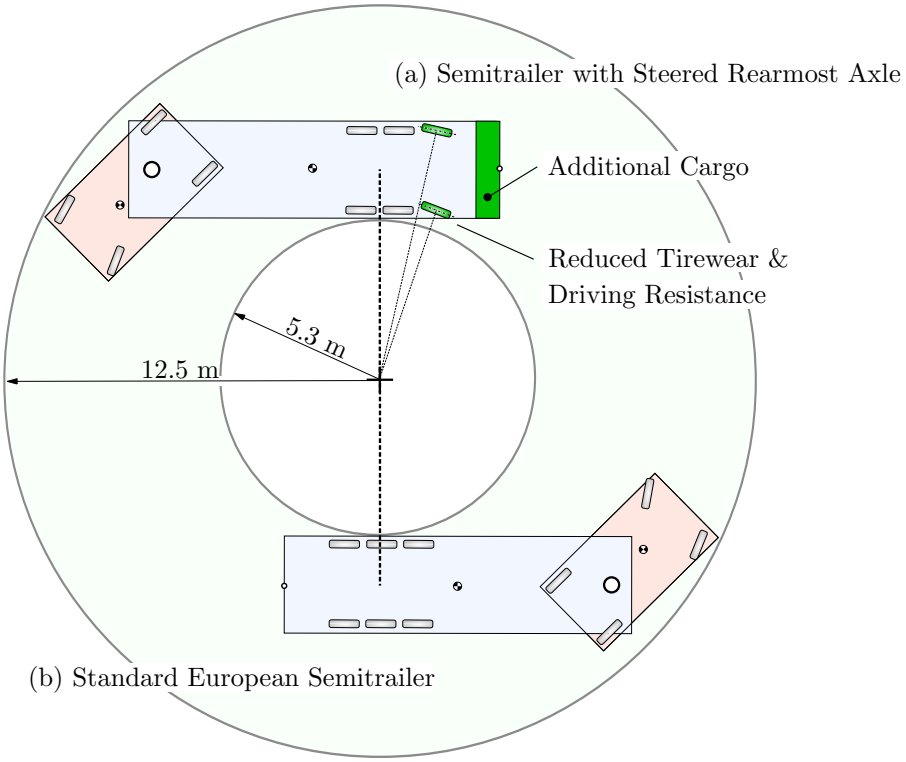

Figure 1.3: Tractor with a steered (a) or unsteered (b) semitrailer during a low-speed turning circle maneuver (german: "*BO-Kraftkreis*"), required by the European road traffic regulations.

Since the steered axle improves the maneuverability, the semitrailer can be increased and additional cargo can be transported. This leads to a higher efficiency, saves costs and resources.

1.2 Structure and Scope

This thesis is structured as follows:

- *Chapter 2* Introduction of fundamentals of vehicle dynamics with respect to the characterization of the tires, basic vehicle modeling and TST specific approaches. Furthermore, insights of previous research are given.
- *Chapter 3* Derivation of a linear and nonlinear horizontal TST model to describe the lateral vehicle dynamics at low-speed. In addition, the derived models will be extended in order to account for the roll motions of the system at high-speed. Finally, an existing SimPack model will be introduced.
- *Chapter 4* Development of control strategies for the tractor front axle steering and the semitrailer rearmost axle steering. A controller will be proposed, which aims to reduce the risk of a trailer rollover.
- *Chapter 5* Implementation of the derived models and controllers in the simulation environments. The influences and improvements of the steering strategies will be investigated, analyzing the simulation results of the horizontal and vertical roll-extended models during certain maneuvers.
- *Chapter 6* Summary of main aspects are given, including conclusion and future research topics.

Chapter 2

Fundamentals and State of the Art

2.1 Basics of Vehicle Dynamics

This chapter is meant to serve as an introduction to ground vehicle dynamics in order to present the characteristics of tires, development of vehicle models and explaining related technical terms. The focus is laid on the description of lateral dynamics during cornering at low and high velocity.

2.1.1 Tire Mechanics

The performance of a ground vehicle is mainly influenced by the tires. The tires interact between the road and the vehicle and their properties are important for the dynamic behavior. This section briefly gives the basic aspects of the force and moment generating properties of a pneumatic tire. Normal and friction forces are transmitted at the point of contact between a tire and the road surface. In figure 2.1 the SAE-standard for axis system [SAE76] is shown. The tire is centered in the wheel plane perpendicular to the axis of rotation. Since it moves with the velocity v in the

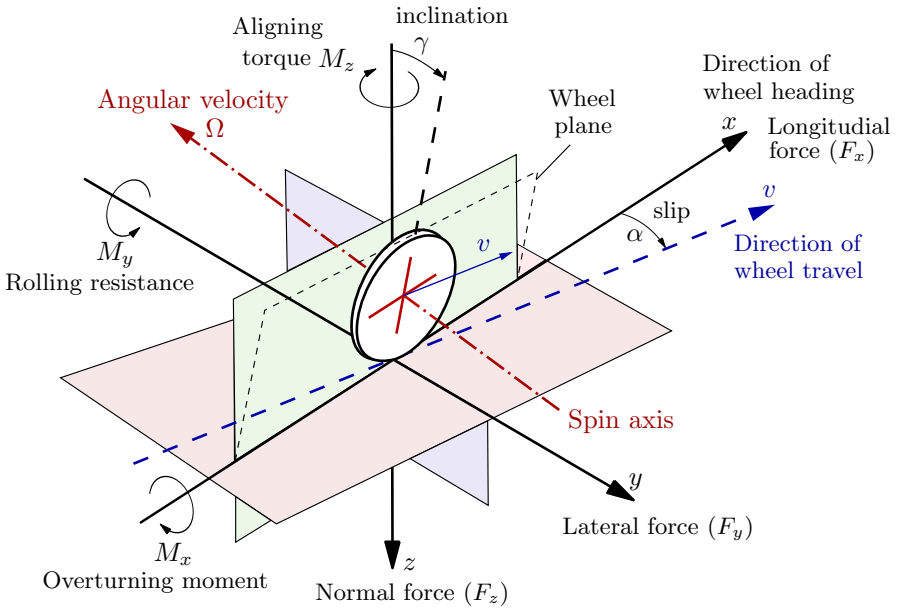

Figure 2.1: Tire axis system and terminology according to SAE-standards [SAE76].

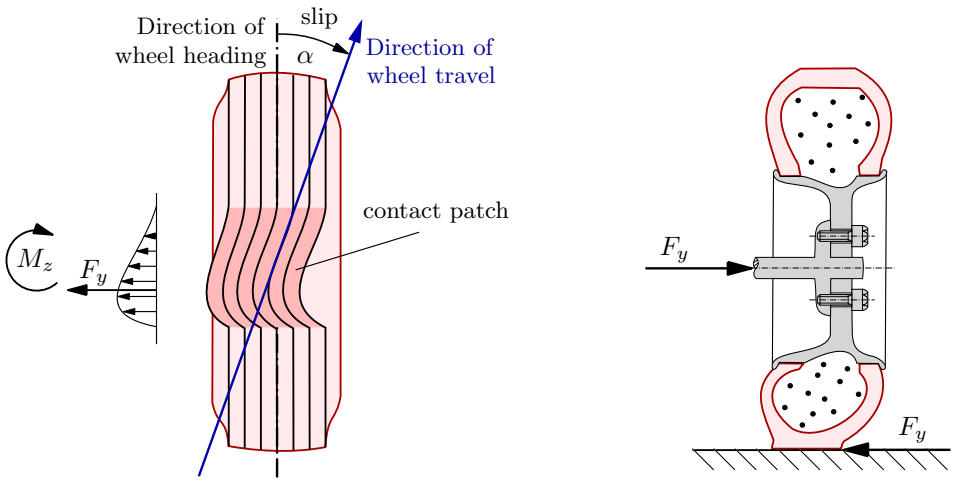

(a) Tire deformation on ground surface (b) Tire deformation in y-direction

Figure 2.2: Origin of lateral forces.

direction of travel, side slip occurs. The lateral component of the slip is described by the tire side slip angle α which effects a lateral force F_y. Because of this slip angle, the material in the contact patch of the elastic tire is drifting to the side, explained in [Gil92] and illustrated in figure 2.2 (a). The deformation of the tire is also indicated in the cross-sectional view of figure 2.2 (b). Since this thesis mainly considers simplified tire behavior of trucks in planar motions, the inclination of the wheels can be neglected. Full details about tire dynamics like e.g. the force and stress distribution at the contact patch are discussed in [Jaz09].
Different tire models are proposed for the calculation of the lateral force during a simulation in the literature of vehicle dynamics. One of the most common tire models is defined by the so-called "magic formula" in [Pac02]. According to this formula, the lateral force F_y can be calculated in dependency of the slip angle α and vertical force F_z,

$$F_y = D \sin\left[\arctan\{B\alpha - E(B\alpha - \arctan(B\alpha))\}\right] \tag{2.1}$$

with the stiffness factor $$B = \frac{C_\alpha}{CD}, \tag{2.2}$$

the peak factor $$D = \mu F_z, \tag{2.3}$$

and cornering stiffness $$C_\alpha = c_1 \sin\left(2 \arctan\left(\frac{F_z}{c_2}\right)\right) \qquad (\text{SAE: } C_\alpha < 0). \tag{2.4}$$

The shape factors C and E as well as the parameters c_1 and c_2 together with the friction coefficient μ are depending on the tire material and design. They can be determined by experiments or empirical values from the literature. The lateral force obtained by the "magic formula" is schematically shown in figure 2.3 with respect to the slip angle. The relation is linear for small slip angles and can be approximated by the function

$$F_{y,\text{lin}}(\alpha) = C_\alpha \, \alpha \qquad (\text{SAE: } C_\alpha < 0). \tag{2.5}$$

As proposed in [Viv12] a saturated tire-force-law can be used in order to characterize the force behavior for larger slip angles,

$$F_{y,\text{sat}}(\alpha) = \begin{cases} C_\alpha \, \alpha & \text{for} \quad |\alpha| < \alpha_{\text{sat}} \\ F_{y,\max} & \text{else} \end{cases} \qquad \text{, where } C_\alpha < 0. \tag{2.6}$$

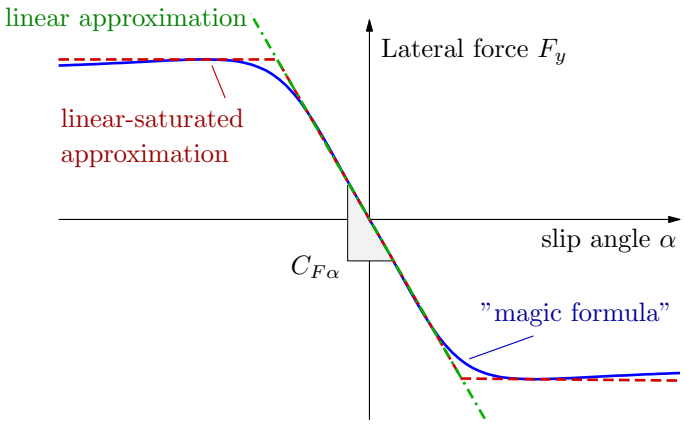

Figure 2.3: Approximation of the lateral force in dependence of the slip angle according to Pacejka's tire model [Pac02] (SAE: $C_\alpha < 0$).

The approximated tire-law also prevents the transgression of the linear range, which may cause excessive lateral forces during a simulation process.

2.1.2 Bicycle Model

This section intends to introduce a simplified model of a four-wheeled vehicle with *Ackermann steering* according to *Riekert and Schunck* (1940). Their linear theories of vehicle modeling has also been published by e.g. [Zom83]. As the two wheels on each axle are modeled by a centered substitute wheel, their models are also known as "bicycle models" or "single-track models". The substitute wheel represents the tire and suspension characteristics of the related axle. Figure 2.4 displays the so-called bicycle model during a steady state cornering of the vehicle at low velocity. The distance between the steered wheels of the front axle is defined by w, and the distance of

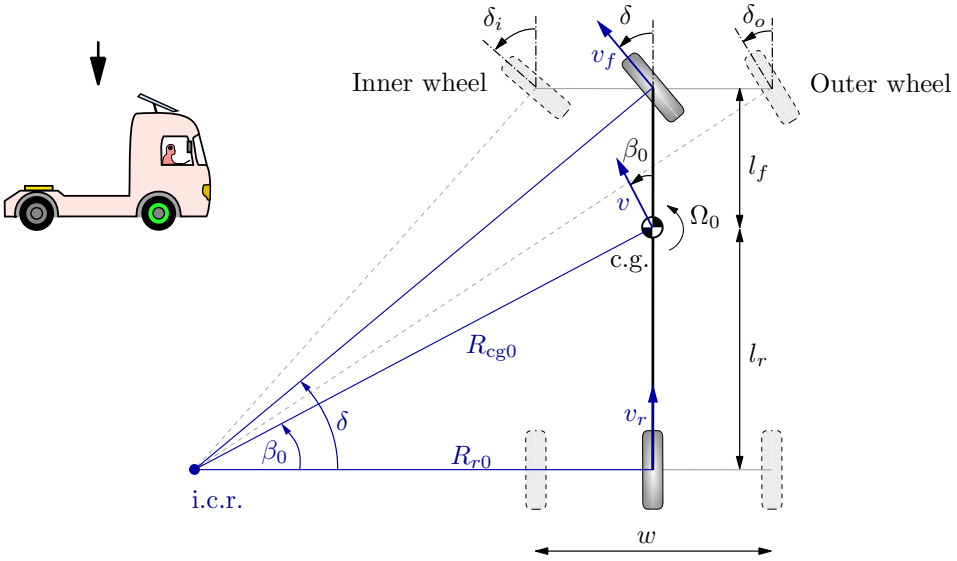

Figure 2.4: Conception of a single-track-model (Bicycle Model) based on an Ackermann steering.

the center of gravity (c.g.) to the front axle respectively to the rear axle is denoted by l_f and l_r. The center of the reared axle moves with the velocity v_r along a circle track with the radius R_{r0}. So the vehicle is turning with a constant angular velocity Ω_0 around the instantaneous center of rotation (i.c.r.). In analogy, the c.g. and the center of the front axle are moving with v and v_f. With the assumption of low velocity, the centrifugal force can be neglected which leads to the following geometric conditions for the inner and outer steer angles

$$\tan\delta_i = \frac{l}{R_{r0} - \frac{w}{2}} \qquad \tan\delta_o = \frac{l}{R_{r0} + \frac{w}{2}} \tag{2.7}$$

$$\Rightarrow \cot\delta_o - \cot\delta_i = \frac{w}{l}. \tag{2.8}$$

This is called the *Ackermann* condition, where $l = l_r + l_f$ describes the wheelbase. The steer angle δ of the single track model relates to the geometric lengths with

$$\tan\delta = \frac{l}{R_{r0}}. \tag{2.9}$$

This equation can be used to eliminate the radius R_{r0} in (2.7),

$$\cot\delta_i = \cot\delta - \frac{w}{2l} \qquad \cot\delta_o = \cot\delta + \frac{w}{2l}. \tag{2.10}$$

The bicycle steer angle is the cot-average of the inner and outer steer angles of the four-wheeled vehicle

$$\cot\delta = \frac{\cot\delta_o + \cot\delta_i}{2}, \tag{2.11}$$

as it is also derived in [Jaz09]. Including the equation (2.9) it can be shown that the mass center of the vehicle turns with the radius

$$R_{\text{cg0}} = \sqrt{l_r^2 + l^2\cot^2\delta} \tag{2.12}$$

on the circle. The introduced relations are only valid for a small steady state cornering velocity v, as already mentioned.
In case of the steady state cornering at high velocity, lateral accelerations must be taken into account. In order to react against the centrifugal forces the tires develop the slip angles causing lateral forces. Figure 2.5 shows the difference between steady state cornering of a bicycle model at low (a) and high (b) velocity. Due to the slip, the position of the i.c.r changes in dependency of the vehicle and the road conditions. According to the equation (2.5), the front and rear tire forces F_{yf} and F_{yr} are linear related to the front and rear slip angles α_f and α_r with

$$F_{yf} = C_{\alpha f}\,\alpha_f \quad \text{and} \quad F_{yr} = C_{\alpha r}\,\alpha_r, \tag{2.13}$$

whereby $C_{\alpha f}$ and $C_{\alpha r}$ are the effective cornering stiffness at the front and rear axle. For the determination of the slip angles, it is necessary to consider the explicit wheel velocities more detailed as shown in figure 2.6. Since the vehicle is turning with the angular velocity (or yaw angular velocity) ω around the c.g. and for a small body slip ($\beta << 1$), the rear and front wheel velocities can be approximately calculated with

$$v_r \approx \sqrt{v^2 + (\omega l_r)^2} \quad \text{and} \quad v_f \approx \sqrt{v^2 + (\omega l_f)^2}, \tag{2.14}$$

where the absolute velocity of the vehicle is denoted by v. Furthermore, the following relationships can be derived for the body slip angle β,

$$\tan(\alpha_r + \beta) \approx \frac{\omega l_r}{v} \quad \text{and} \quad \tan(\delta - \alpha_f - \beta) \approx \frac{\omega l_f}{v}. \tag{2.15}$$

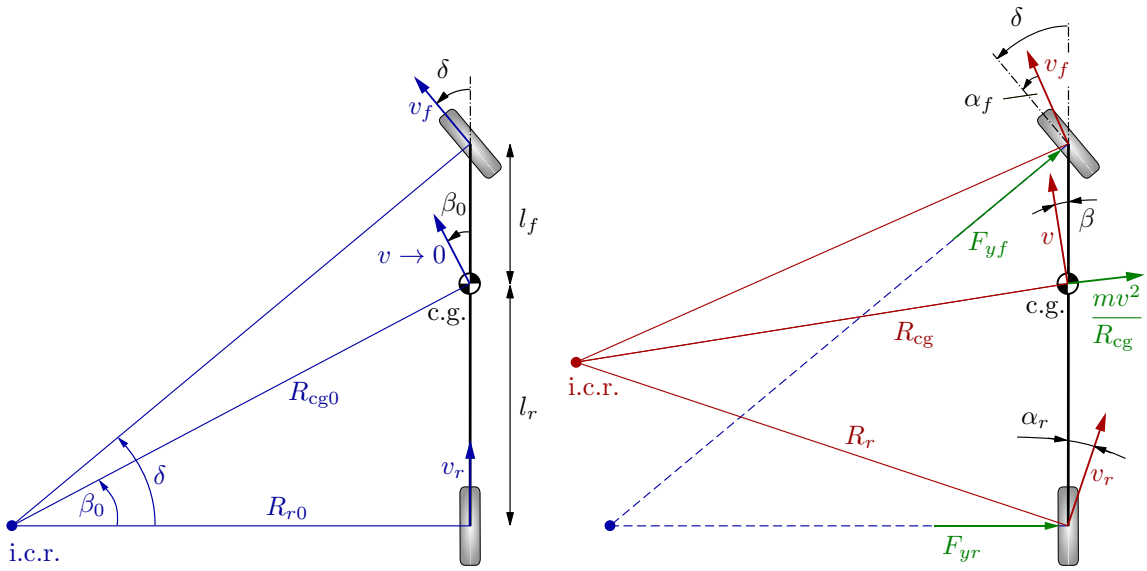

(a) low speed (b) high speed

Figure 2.5: Geometric conditions for a single-track-model of a two-axle vehicle for steady state cornering.

The assumption of small angles ($\tan(\measuredangle) \approx \measuredangle$) leads to simplified calculations of the slip angles,

$$\alpha_r \approx \frac{\omega l_r}{v} - \beta \quad \text{and} \quad \alpha_f \approx \delta - \frac{\omega l_f}{v} - \beta. \tag{2.16}$$

In order to describe the dynamic behavior of the vehicle the equation of motions can be derived as it is proposed in [PS10]. Using the vehicle-fixed frame O^K in correspondence to figure 2.6, the movement of the vehicle in the direction of e_1^K, e_2^K and the rotation around e_3^K can be expressed by

$$\begin{aligned} v_1 &= v \cos\beta \\ v_2 &= v \sin\beta \\ \omega_3 &= \omega, \text{ respectively.} \end{aligned} \tag{2.17}$$

With respect to the inertial coordinate system, the time derivative leads to the acceleration

$$\begin{aligned} a_1 &= \dot{v}\cos\beta - v\dot{\beta}\sin\beta - \omega\, v \sin\beta \\ a_2 &= \dot{v}\sin\beta + v\dot{\beta}\cos\beta + \omega\, v \cos\beta \\ \alpha_3 &= \dot{\omega}. \end{aligned} \tag{2.18}$$

For most applications it is sufficient to assume a small body slip angle $\beta << 1$ and $v = \text{const}$, which leads in a matrix notation to

$$\begin{bmatrix} a_1 \\ a_2 \\ \alpha_3 \end{bmatrix} = \underbrace{\begin{bmatrix} 0 & 0 \\ v & 0 \\ 0 & 1 \end{bmatrix}}_{\bar{\boldsymbol{L}}} \underbrace{\begin{bmatrix} \dot{\beta} \\ \dot{\omega} \end{bmatrix}}_{\dot{\boldsymbol{z}}} + \begin{bmatrix} -v\,\omega\,\beta \\ v\omega \\ 0 \end{bmatrix}. \tag{2.19}$$

The matrix $\bar{\boldsymbol{L}}$ denotes the *Jacobian* matrix and the vector $\dot{\boldsymbol{z}}$ of the generalized velocities. As proposed in [PS10] an air resistance force A_x, lateral aerodynamic force A_y and an external moment M_A react on the vehicle. Furthermore F_{x_r} and F_{x_f} are the longitudinal forces acting on the

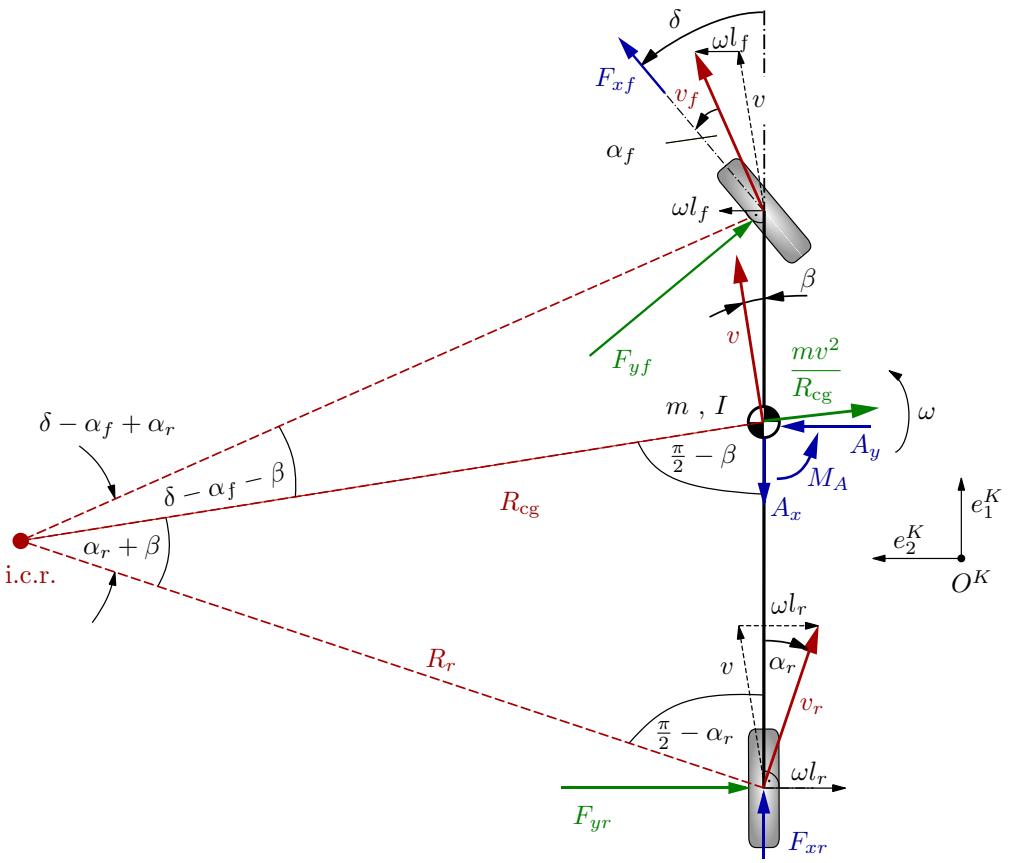

Figure 2.6: Single-track-model of a two-axle vehicle at high velocity.

tires in the direction of the wheel heading. Neglecting small quadratically terms, the *Newton-Euler* equations for the vehicle with the mass m and moment of inertia I results in

$$\begin{bmatrix} 0 & 0 \\ mv & 0 \\ 0 & I \end{bmatrix} \begin{bmatrix} \dot{\beta} \\ \dot{\omega} \end{bmatrix} + \begin{bmatrix} -mv\,\omega\,\beta \\ mv\omega \\ 0 \end{bmatrix} = \begin{bmatrix} F_{xf} + F_{xr} - A_x \\ -F_{yf} - F_{yr} + A_y \\ F_{yr} l_r - F_{yf} l_f + M_A \end{bmatrix}. \tag{2.20}$$

Applying the *Jourdain's principle*, the equations of motion followed by a left multiplication with the transposed *Jacobian* matrix $\bar{\boldsymbol{L}}^T$,

$$\begin{bmatrix} mv^2 & 0 \\ 0 & I \end{bmatrix} \begin{bmatrix} \dot{\beta} \\ \dot{\omega} \end{bmatrix} + \begin{bmatrix} mv^2\omega \\ 0 \end{bmatrix} \begin{bmatrix} v(-F_{yf} - F_{yr} + A_y) \\ F_{yr} l_r - F_{yf} l_f + M_A \end{bmatrix}. \tag{2.21}$$

With the linear tire model from (2.13), it leads to

$$\begin{bmatrix} mv^2 & 0 \\ 0 & I \end{bmatrix} \begin{bmatrix} \dot{\beta} \\ \dot{\omega} \end{bmatrix} + \begin{bmatrix} mv^2\omega \\ 0 \end{bmatrix} = \begin{bmatrix} v(-C_{\alpha f}\,\alpha_f - C_{\alpha r}\,\alpha_r + A_y) \\ C_{\alpha r}\,\alpha_r\,l_r - C_{\alpha f}\,\alpha_f\,l_f + M_A \end{bmatrix}. \tag{2.22}$$

Using (2.16) it yields the *Riekert and Schunck's* equations, also mentioned in [Zom83],

$$mv\dot{\beta} - (C_{\alpha f} + C_{\alpha r})\,\beta + \left(mv - \frac{l_f C_{\alpha f} - l_r C_{\alpha r}}{v} \right) \omega = A_y - C_{\alpha f}\,\delta \tag{2.23}$$

$$I\dot{\omega} - \frac{1}{v}(C_{\alpha r}\,l_r^2 + C_{\alpha f}\,l_f^2)\,\omega - (C_{\alpha f}\,l_f - C_{\alpha r}\,l_r)\beta = M_a - C_{\alpha f}\,\delta\,l_f. \tag{2.24}$$

Condition	Case	Required Driver Intervention
$\lvert C_{\alpha r}\rvert l_r > \lvert C_{\alpha f}\rvert l_f$	understeering	increasing required
$\lvert C_{\alpha r}\rvert l_r = \lvert C_{\alpha f}\rvert l_f$	neutral steering	-
$\lvert C_{\alpha r}\rvert l_r < \lvert C_{\alpha f}\rvert l_f$	oversteering	decreasing required

Table 2.1: Cases of vehicle steer behavior

Remark 2.1. *The sign of the cornering stiffness differs, since the SAE-terminology is used in this work.*

The derived equations can also be used to explain the oversteer and understeer phenomena. In consideration of a steady-state cornering ($\dot{\beta} = 0$) and with the neglection of the aerodynamic force ($A_y = 0$), the equation (2.23) can be rearranged to

$$\delta = \frac{l\omega}{v}\left(1 + \frac{C_{\alpha f}l_f - C_{\alpha r}l_r}{C_{\alpha f}C_{\alpha r}l^2}mv^2\right) \quad \text{, where } \{C_{\alpha f}, C_{\alpha r}\} < 0. \tag{2.25}$$

This means that the driver has to steer in relation to the velocity and the cornering stiffness of the front and rear axle in order to follow a constant cornering path. The steering behavior can be summarized with the cases specified in table 2.1.

2.1.3 Multiple Non-Steered Axles

Non-steered multiple-axle suspensions are typically used to sustain the weighty cargo, especially within the scope of heavy vehicles. The two- and three-axle varieties are the most common types of multiple-axle running gear for trucks or semitrailers. They are generally called tandem and tridem suspensions, respectively. Non-steered multiple-axle suspensions not only increase tire wear particular during cornering maneuvers, but also influence the directional response with the development of large tire slip angles [FW07].
Figure 2.7 (a) illustrates the bicycle model of a three-axle truck with the constant steer angle δ at low-speed steady-state turning. It is assumed that the tires of the non steering rear axles have the same cornering stiffness and that kinematic and compliant steering effects are ignored. The geometric wheelbase l_g is the distance between the tandem center and front axle. In contrast to the two-axle vehicle of figure 2.5 (a), a truck tire can not operate with a zero slip angle, which generates lateral forces in a low-speed turn. The lateral force balance requires that the lateral tire force at the center axle is equal in magnitude to the sum of the front and rear lateral forces, clarified in figure 2.7 (a). Since the cornering stiffness of the two rear axles are identical, the center of the low-speed turn lies on a line perpendicular to the vehicle's longitudinal axis, but differs to the geometric center. As it is proposed in [FW07] an equivalent wheelbase l_eq can be calculated. It characterizes the ideal cornering of an equivalent two-axle vehicle without slip. In particular, figure 2.7 (b) illustrates that both vehicles have the same steer angle δ. If all non-steering axles of the vehicle have the same cornering stiffness, the equivalent wheelbase of the correspond ing two axle vehicle can be calculated with

$$l_\mathrm{eq} = l_\mathrm{g} + \frac{T}{l_\mathrm{g}} + \frac{T}{l_\mathrm{g}}\frac{C_{\alpha r}}{C_{\alpha f}} \quad \text{where} \quad T = \frac{\sum_{i=1}^{N}\Delta_i^2}{N}. \tag{2.26}$$

The sum of the cornering stiffness of all front and rear tires are denoted by $C_{\alpha r}$ and $C_{\alpha f}$. Respectively, N is the number of non-steering axles and Δ_i is the distance of the $i^{\text{ th}}$ non-steered axle to the geometric center of the rear axle group. The detailed derivation of this equation was documented by Winkler in [Win98] and will be explained for a three-axle truck in the following.

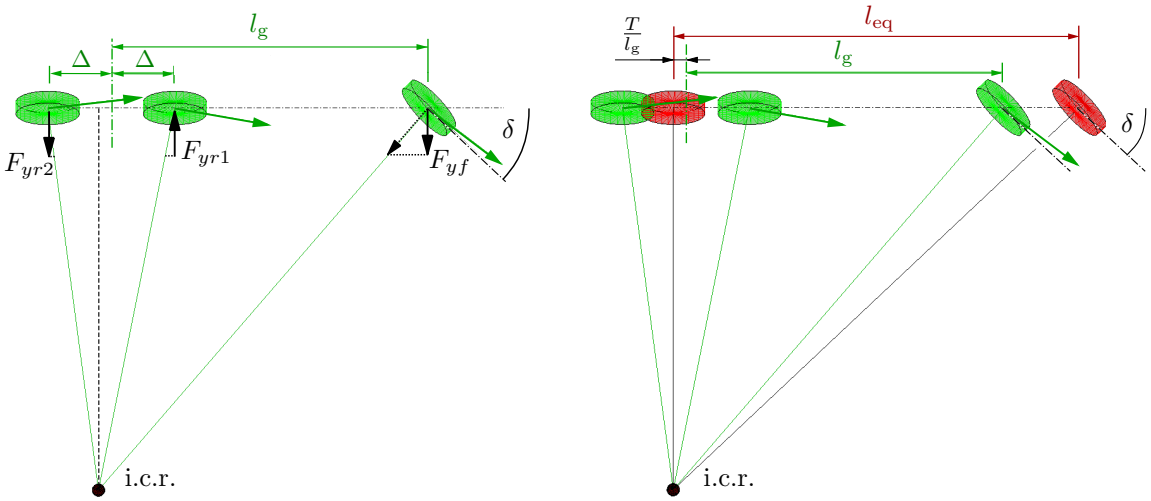

(a) three-axle truck with slip (b) equivalent, two-axle vehicle without slip

Figure 2.7: Single-track-model of a three-axle truck in a steady-state, very low-speed turn.

Consider the three-axle vehicle illustrated in figure 2.8, which is in a steady-state turn at very low velocity such that the centrifugal forces are neglect-able. The requirements of static equilibrium of lateral forces and yaw moment lead to

$$\sum F_y = 0 = -F_{yf} + F_{yr1} - F_{yr2} \quad \text{and} \tag{2.27}$$

$$\sum M_{r1} = 0 = -F_{yf}(l_g - \Delta) + 2F_{yr2}\Delta, \tag{2.28}$$

whereby Δ is the distance from the axles to the geometric center of the group. The tire forces in the direction of y are linear related to the slip angles α_f, α_{r1} and α_{r2}. Assuming small angles, it yields

$$\delta = \tan\left(\frac{l_{eq}}{R}\right) \approx \frac{l_{eq}}{R} \tag{2.29}$$

$$\delta - \alpha_f = \tan\left(\frac{l_{eq} - a}{R}\right) \approx \frac{l_{eq} - a}{R} \Rightarrow \alpha_f \approx \frac{a}{R} \tag{2.30}$$

$$\alpha_{r1} = \tan\left(\frac{\Delta + b}{R}\right) \approx \frac{\Delta + b}{R} \tag{2.31}$$

$$\alpha_{r2} = \tan\left(\frac{\Delta - b}{R}\right) \approx \frac{\Delta - b}{R}. \tag{2.32}$$

The geometric distances a, b and R are defined in figure 2.8. According to [Win98] it can be assumed, that the complete front tire force F_{yf} acts in the direction of y. This leads to the result that (2.27) and (2.28) end up in

$$-C_f\alpha_f + C_{r1}\alpha_{r1} - C_{r2}\alpha_{r2} = 0 \quad \text{and} \tag{2.33}$$

$$-C_f\alpha_f(l_g - \Delta) + 2C_{r2}\alpha_{r2}\Delta = 0, \tag{2.34}$$

where C_f, C_{r1} and C_{r2} are the related cornering stiffnesses. Furthermore, the rear cornering stiffness can be simplified to

$$C_r = C_{r1} + C_{r2} \quad \text{and} \quad C_{r1} = C_{r2}. \tag{2.35}$$

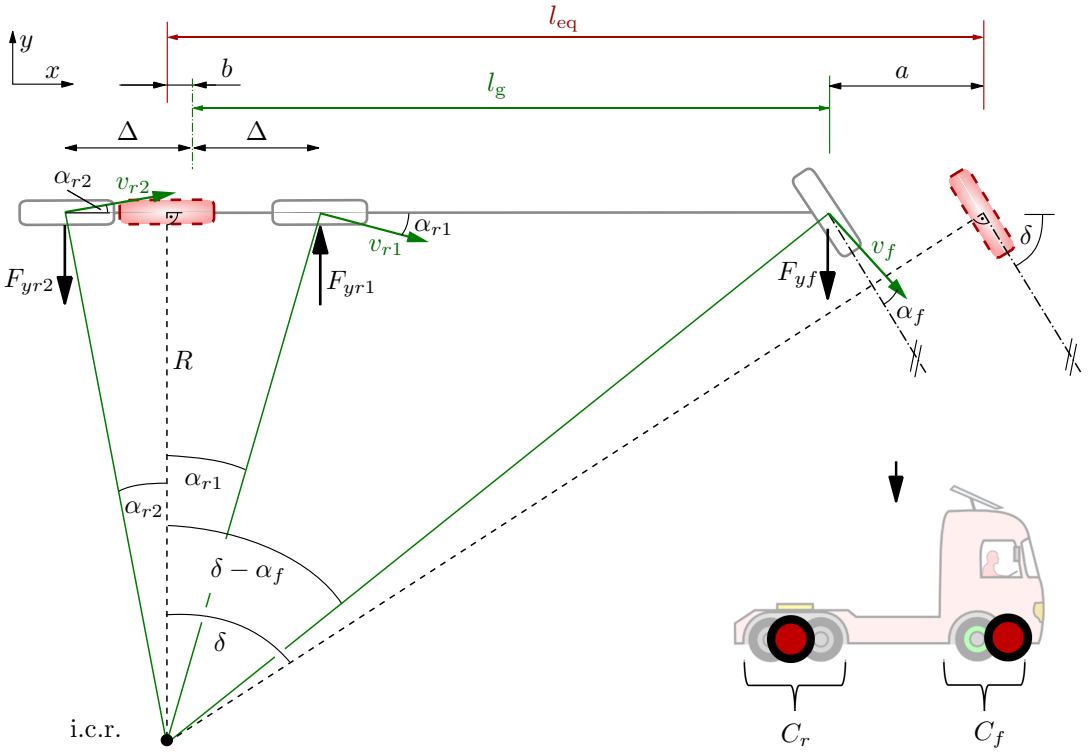

Figure 2.8: Derivation of the equivalent wheelbase l_{eq} of a three-axle truck in a steady-state low-speed turn.

Substituting equations (2.30)-(2.32) into equations (2.33)-(2.34) and the usage of (2.35) yields

$$-C_f \frac{a}{R} + C_r \frac{\Delta + b}{R} - C_r \frac{\Delta - b}{R} = 0 \quad \Rightarrow C_f a = C_r b \quad \text{and} \tag{2.36}$$

$$-C_f \frac{a}{R}(l_g - \Delta) + 2C_r \frac{\Delta - b}{R}\Delta = 0 \quad \Rightarrow C_f a(l_g - \Delta) = C_r(\Delta - b)\Delta. \tag{2.37}$$

The factors a and b can be declared after some calculation with

$$a = \frac{C_r}{C_f}\frac{\Delta^2}{l_g} \quad \text{and} \quad b = \frac{\Delta^2}{l_g}. \tag{2.38}$$

In conclusion, the equivalent wheelbase can be evaluated with

$$l_{\text{eq}} = l_g + b + a = l_g + \frac{\Delta^2}{l_g} + \frac{C_r}{C_f}\frac{\Delta^2}{l_g}. \tag{2.39}$$

This formula displays the same equation as mentioned in (2.26), if one regards the case of two rear axles ($N = 2$). Eventually is should be noted, that the equivalent wheelbase can also be obtained for trailers with multiple non-steering axles on a similar manner.

2.1.4 Trailer Combinations

Nowadays most trucks carry one or more trailers in order to improve cost effectiveness. At low speed tractor-trailer combinations with non-steering rear axles offtrack to the inside during a turn. Similarly, non-steering trailer axles offtrack relative to the path of their forward hitch point, see [FW07].

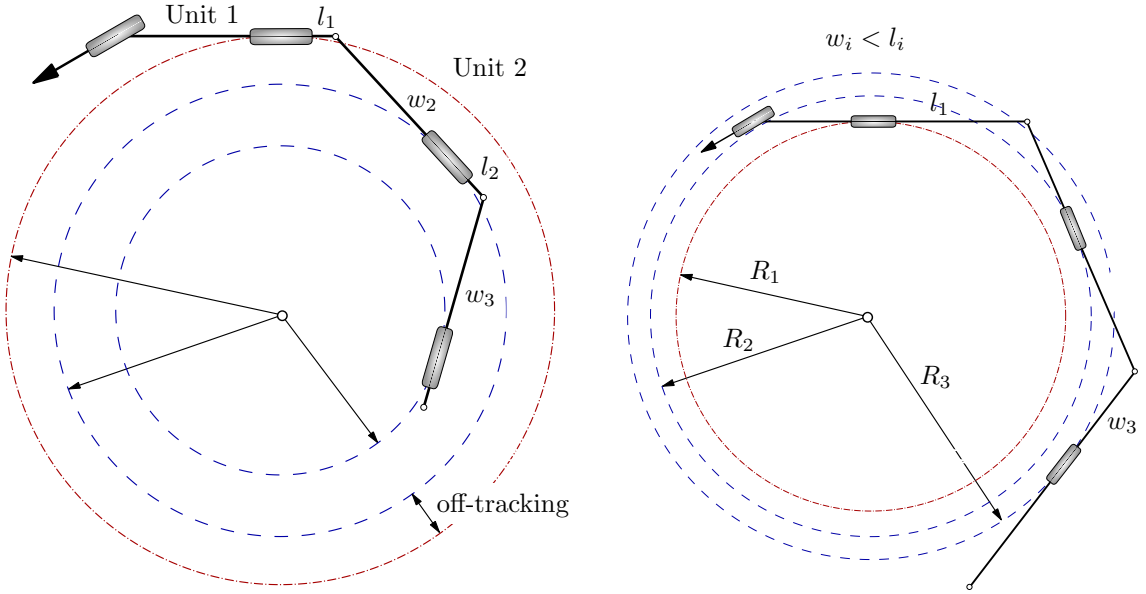

(a) wheelbases are greater than hich distances (b) wheelbases are smaller than hich distances

Figure 2.9: Single-track-model of a three-axle truck in steady-state on a very low-speed turn.

So during a steady-state cornering of a vehicle combination of n-units the path radius of the n^{th} unit depends on the wheelbases $\{w_1, w_2..w_n\}$ and hitch distances $\{l_1, l_l...l_n\}$ of the units ahead. In detail, figure 2.9 shows the geometric relation of a tractor with two trailers. This yields the conditions

$$\begin{aligned} R_1^2 + l_1^2 = w_2^2 + R_2^2 \Rightarrow \quad R_2^2 = R_1^2 + l_1^2 - w_2^2 \quad \text{and} \\ R_2^2 + l_2^2 = w_3^2 + R_3^2 \Rightarrow \quad R_3^2 = R_2^2 + l_2^2 - w_3^2, \end{aligned} \tag{2.40}$$

whereby the radius of the last unit results in

$$R_n^2 = R_1^2 + \sum_{i=2}^{n} l_{i-1}^2 - w_i^2. \tag{2.41}$$

According to the equation above and as shown in figure 2.9 (b), the trailers can even follow on larger radius, if $w_i < l_i$. Furthermore, the coordinates of the units' center of gravity (c.g.) can be calculated in agreement with figure 2.10 with

$$\boldsymbol{r}_n = \boldsymbol{r}_1 - \sum_{i=1}^{n} (b_i + f_i) \begin{bmatrix} \cos\psi_i \\ \sin\psi_i \\ 0 \end{bmatrix} \quad \text{, where } f_1 = 0 \text{ and } b_n = 0. \tag{2.42}$$

The orientation angles are denoted by ψ_i and the distances between the c.g. and the front and the rear hitch points are called f_i and b_i, respectively. Further details about the behavior of multiple-articulated vehicles are described in [dB01].

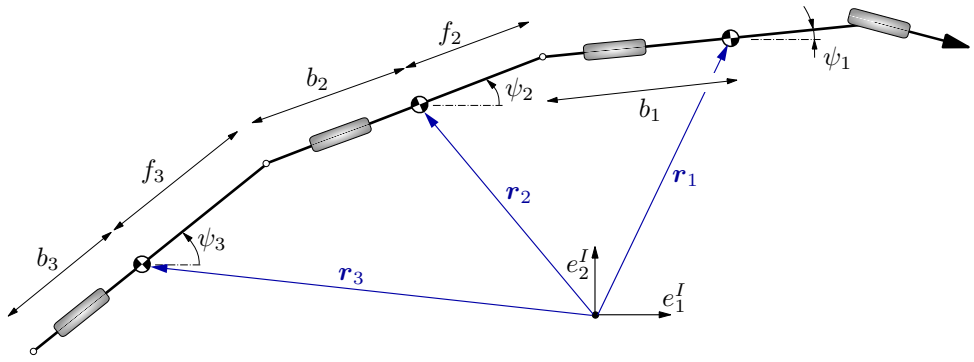

Figure 2.10: Body coordinates of a trailer combination train.

2.2 State of the Art: Steering of Semitrailer's Rearmost Axle

This section introduces steering strategies and control models, developed in the scope of previous research projects ([Boe11], [vdV11], [Viv12]) at the Institute for Dynamic Systems and Control (IDSC). This thesis focuses on the derived control methods, which are designed for an active steering of the semitrailer's rearmost axle, as shown in figure 1.2.

2.2.1 Horizontal Tracking Control Strategies

In literature ([Win98], [FW07], [ORJC10], [dB01], [FMG06]), most of the approaches intend to reduce the off-tracking of trailers with respect to the tractor, as clarified in figure 2.9. Therefore the mid point of the trailer-end should always follow the trajectory of the trailer's front coupling point by articulating the semitrailer actively.

Steady-State Control Strategies

Within the IDSC-research, first proposals for the control of the rearward steer angle called δ_2 were suggested in [Boe11]. For the derivation of the strategy a steady-state cornering maneuver of the TST shown in figure 2.11 was considered. According to this strategy, the steer angle of the trailer results from the superposition of a simplified Ackermann-condition δ_{2r0}, of one part for the velocity compensation δ_{2rV}, and finally the compensation of the yaw moment δ_{2rM}, caused by the non-steered axes. It can be written as

$$\delta_{2r} = \delta_{2r0} + \delta_{2rV} + \delta_{2rM}, \tag{2.43}$$

where the simplified Ackermann condition for the track-tracing of the coupling point, denoted by Ⓒ, can be obtained by

$$\delta_{2r0} = -\frac{1 - \dfrac{b_5}{b_1 + b_4}}{1 + \dfrac{b_5}{b_1 + b_4}}\Gamma. \tag{2.44}$$

The geometrical parameters b_1, b_4, b_5 and the hitch angle Γ, which describes the angle between the tractor and semitrailer, are explained in figure 3.1.

Remark 2.2. *This simplified equation is not explicitly mentioned in [Boe11], but was used in the associated simulation models.*

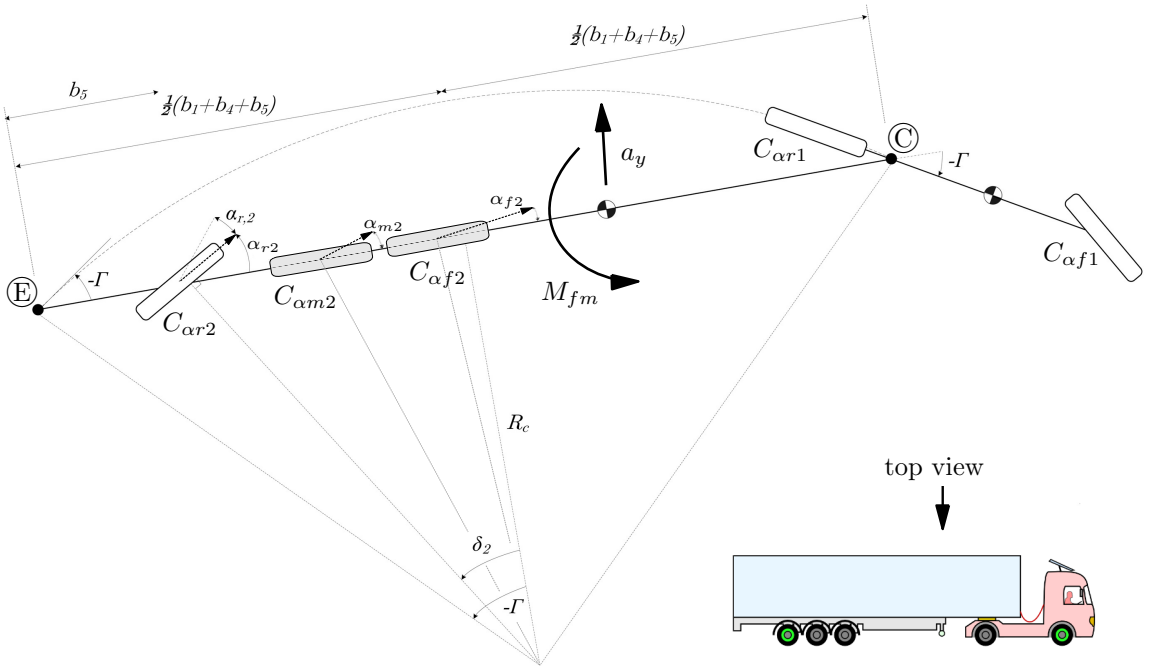

Figure 2.11: Steady-state control strategy according to [vdV11].

The part of the velocity compensation in (2.43) results in

$$\delta_{2rV} = (m_1 + m_2)\frac{b_1(C_{\alpha f1} + C_{\alpha r1}) - b_4 C_{\alpha r2}}{(b_1 + b_4)(C_{\alpha f1} + C_{\alpha r2})C_{\alpha r2}} a_y, \tag{2.45}$$

whereby the centrifugal acceleration is characterized by a_y. The mass of the tractor and trailer are denoted with m_1 and m_2. The quantities $C_{\alpha f1}$, $C_{\alpha r1}$, $C_{\alpha f2}$, $C_{\alpha m2}$ and $C_{\alpha r2}$ characterize the cornering stiffness at the tractor's front, rear and the trailer's front, mid and rear axle. In [Boe11] it is also proposed, that the compensation of the yaw moment can be determined with

$$\delta_{2rM} = \frac{\alpha_{m2} C_{\alpha m2}(b_1 + b_3) + \alpha_{f2} C_{\alpha f2}(b_1 + b_2)}{C_{\alpha r2}(b_1 + b_4)}, \tag{2.46}$$

whereby the slip angles can be approximated with

$$\alpha_{f2} = -\frac{2(b_1 + b_2) - (b_5 + b_1 + b_3 + l_3 - l_2)}{b_5 + b_1 + b_3 - (l_3 - l_2)}\Gamma \quad \text{and} \tag{2.47}$$

$$\alpha_{m2} = -\frac{2(b_1 + b_3) - (b_5 + b_1 + b_3 + l_3 - l_2)}{b_5 + b_1 + b_3 - (l_3 - l_2)}\Gamma. \tag{2.48}$$

In the following this steady-state control strategies will be named as "feed-forward-controller", since they don't compensate any measured error or feedback but just react proportional to the hitch angle Γ.

Path-Following Control Strategies

Moreover, a linear quadratic regulator (LQR)-controller is designed in [vdV11] in order to minimize the transient off-tracking for the three-axle trailer with a feedback control system.
Similarly, in [CC08] a virtual driver steering controller is proposed to control the steering angles of trailer wheels, so as to make the trailer rear end follow the trajectory of 5^{th}-wheel. The "virtual

trailer-driver" is assumed to "sit" at the rear end of the semi-trailer and to use preview information consisting of path-tracking deviations of the trailer body relative to the trajectory of 5^{th}-wheel. The "virtual driver" model for the trailer steering control is introduced to minimise the path-tracking deviation of the trailer's rear end by using a LQR-method. This linear quadratic regulator-approach optimize a cost function which contains weighted input and output states. For the same purpose a PID-Controller with a "reference trailer" is used in [ORJC10]. Thereby the controlled system is investigated for low and high velocity.
At last, in the context of the IDSC-research project an additional thesis [Viv12] exists. It analyzes how the usage of a steerable trailer axle can be beneficial during reversing maneuvers. In conclusion, different feed-forward controllers, feedback controllers, observers and switching strategies particular for the reverse driving problem are developed and tested. In the following this path-following control strategies will be named as "feed-back-controller", since they compensate a measured deviation, which is returned by a feedback.

2.2.2 Rollover Prevention Control

Since a few years, researchers of different institutions are developing a variety of steering strategies for the rollover avoidance of single-unit trucks or tractor-semitrailers. Usually the main challenge is to influence and improve the roll dynamics of these vehicles using the tractor-front or / and a semitrailer rear axle steering.

Roll-Controller for Single-Unit Trucks

In [AO98], [AO99] and [OBA99] control laws for an rollover avoidance of trucks are introduced. Thereby a small auxiliary steering angle is set by an actuator, in addition to the driver's steering angle. The control law is based on proportional feedback of the roll rate and the roll acceleration, so that the vehicle's roll damping is robustly improved for a wide range of speed and height of the center of gravity. Furthermore a rollover coefficient (or so-called load transfer ratio LTR) is defined that basically depends on the lateral acceleration at the center of gravity of the vehicle's sprung mass. For critical values of this variable an emergency steering and braking system is activated.

Roll-Controller for Tractor-Semitrailer

In [KS88] it was found that the stability of tractor-semitrailer systems at high speeds can be significantly improved by the usage of a LQR-controller acting on the tractor-front and trailer-rear axle. Furthermore, some extended LQR-control strategies are designed and investigated, which reduce the rollover occurrence [Sam00].
In order to minimise a combination of the path-tracking deviation of the trailer rear end relative to the path of the hitch point (5^{th}-wheel) and the lateral acceleration of trailer c.g. a LQR-controller is introduced in [CC08]. Thereby the lateral acceleration of trailer c.g. is included as an additional objective of the optimal controller in order to improve roll stability. In [ORJC10] this strategies are extended and investigated for low and high velocities. Finally a similar approach which uses an optimal controller is introduced and tested in [vdV11].

2.3 Basics of Applied Mechanics and System Dynamics

This section gives an overview of the basic model representations which are important in the scope of this work. The theory and formulations are extracted from [PS10] and [Lun08].
Usually, the dynamics of a mechanical system can be described by ordinary differential equations. They can be derived applying the principle laws of the physics and mechanics. In consideration of a holonomic rigid MultiBody System (MBS), the motion behavior is completely described by

f-generalized coordinates $\boldsymbol{q}$, whereby f is the number number of degrees of freedom [PS10]. The nonlinear equations of motion of an ordinary MBS can be read as

$$\boldsymbol{M}(\boldsymbol{q},t)\,\ddot{\boldsymbol{q}} + \boldsymbol{k}(\dot{\boldsymbol{q}},\boldsymbol{q},t) = \boldsymbol{q}^e(\dot{\boldsymbol{q}},\boldsymbol{q},\boldsymbol{u},t), \tag{2.49}$$

where $\boldsymbol{M}$ is the $f \times f$ symmetric inertia matrix, $\boldsymbol{k}$ is a $f \times 1$-vector of generalized gyroscopic forces including the Coriolis and centrifugal forces as well as the gyroscopic torques, and the $f \times 1$-vector $\boldsymbol{q}^e$ represents generalized applied forces. Furthermore, equation (2.49) can be rearranged to

$$\Rightarrow \ddot{\boldsymbol{q}} = \boldsymbol{M}^{-1}(\boldsymbol{q}^e - \boldsymbol{k}) \tag{2.50}$$

and consequently transformed into the nonlinear state-space representation

$$\underbrace{\begin{bmatrix}\dot{\boldsymbol{q}}\\ \ddot{\boldsymbol{q}}\end{bmatrix}}_{\dot{\boldsymbol{x}}_{\mathrm{NonLin}}} = \underbrace{\begin{bmatrix}\dot{\boldsymbol{q}}\\ \boldsymbol{M}^{-1}(\boldsymbol{q}^e - \boldsymbol{k})\end{bmatrix}}_{\boldsymbol{f}(\boldsymbol{x}_{\mathrm{NonLin}},\boldsymbol{u},t)}, \tag{2.51}$$

where $\boldsymbol{x}_{\mathrm{NonLin}}$ is called the state vector and $\boldsymbol{u}$ denominates the input vector of the nonlinear system. In contrast, equation (2.49) can be linearized to

$$\tilde{\boldsymbol{M}}(t)\,\ddot{\boldsymbol{q}}_{\mathrm{lin}} + \tilde{\boldsymbol{P}}(t)\,\dot{\boldsymbol{q}}_{\mathrm{lin}} + \tilde{\boldsymbol{Q}}(t)\,\boldsymbol{q}_{\mathrm{lin}} = \tilde{\boldsymbol{H}}(t)\boldsymbol{u}, \tag{2.52}$$

where $\tilde{\boldsymbol{M}}$ is the symmetric, positive definite inertia matrix. The matrices $\tilde{\boldsymbol{P}}$ and $\tilde{\boldsymbol{Q}}$ characterize the velocity and position dependent forces and the matrix $\tilde{\boldsymbol{H}}$ applied by the input vector $\boldsymbol{u}$ represents the external excitation. The super-scripted "$\sim$" marks the linearity of the matrices. Moreover, this linear representation can also be rearranged and transformed to a linear state-space representation

$$\underbrace{\begin{bmatrix}\dot{\boldsymbol{q}}_{\mathrm{lin}}\\ \ddot{\boldsymbol{q}}_{\mathrm{lin}}\end{bmatrix}}_{\dot{\boldsymbol{x}}} = \underbrace{\left[\begin{array}{c|c}\boldsymbol{0} & \boldsymbol{I}\\ \hline -\tilde{\boldsymbol{M}}^{-1}\tilde{\boldsymbol{Q}} & -\tilde{\boldsymbol{M}}^{-1}\tilde{\boldsymbol{P}}\end{array}\right]}_{\boldsymbol{A}} \underbrace{\begin{bmatrix}\boldsymbol{q}_{\mathrm{lin}}\\ \dot{\boldsymbol{q}}_{\mathrm{lin}}\end{bmatrix}}_{\boldsymbol{x}} + \underbrace{\begin{bmatrix}\boldsymbol{0}\\ \tilde{\boldsymbol{M}}^{-1}\tilde{\boldsymbol{H}}\end{bmatrix}}_{\boldsymbol{B}} \boldsymbol{u}, \tag{2.53}$$

where $\boldsymbol{x}$ is the state vector of the linear model. According to [Lun08] the linear state-space representation of a system with multiple inputs and multiple outputs (MiMo) generally results in

$$\begin{aligned}\dot{\boldsymbol{x}} &= \boldsymbol{A}\boldsymbol{x} + \boldsymbol{B}\boldsymbol{u}\\ y &= \boldsymbol{C}\boldsymbol{x} + \boldsymbol{D}\boldsymbol{u},\end{aligned} \tag{2.54}$$

where $\boldsymbol{A}$ is called the "system matrix", $\boldsymbol{B}$ is named as "input matrix", $\boldsymbol{C}$ is denoted as "output matrix" and $\boldsymbol{D}$ is the"feedthrough matrix" according to the system theories.
In the case of a system with a single input and a single output (SISO) the linear state-space representation can be simplified to

$$\begin{aligned}\dot{\boldsymbol{x}} &= \boldsymbol{A}\boldsymbol{x} + \boldsymbol{b}u\\ y &= \boldsymbol{c}\boldsymbol{x} + du,\end{aligned} \tag{2.55}$$

where $\boldsymbol{b}$ is a column vector and $\boldsymbol{c}$ is a row vector. The scalar feedthrough is named d. In order to consider the system in the frequency domain, the transfer function can be calculated from the SISO-state-space model (2.55) by

$$G(s) = \boldsymbol{c}^T(s\boldsymbol{I} - \boldsymbol{A})^{-1}\boldsymbol{b} + d. \tag{2.56}$$

Chapter 3

Modelling

In order to simulate the behaviour of a tractor-semitrailer vehicle (TST) and develop control strategies for various driving manoeuvres, mathematical models based on physical laws are required. The dynamic motion of these models are characterized by the so-called equations of motions. This chapter derives a nonlinear and linear horizontal planar model to describe the lateral and yaw motion of the vehicle at low-speed. In addition, the derived models will be extended in order to take also the roll motions of the system at high-speed into account. Thereby the TST is always considered as a rigid Multibody System (MBS).

3.1 Nonlinear Single-Track Model

This section deals with the derivation of a nonlinear horizontal planar model according to the theory of MBS [PS10]. In previous student theses [Boe11]&[Viv12] within the same research project at the IDSC, the regarding nonlinear equations were derived on the one hand with the Newton-Euler approach and on the other hand with the Lagrangian approach. This thesis presents the detailed derivation of the nonlinear equations of motions according to the Newton-Euler approach in subsection 3.1.1. In addition to this, the Lagrangian approach is represented in the subsection A.3 with the same result.
The assumptions and simplifications for the nonlinear model are:

- The tires on each axle are combined into one single tire, which is considered to be at the center of the axle (single-track model).
- Only the lateral forces of the tires are taken into account: $F_{\text{tire}} = F_y$ (There are no braking or accelerating forces on the wheels.)
- The lateral tire behavior is considered fully-linear (or linear-saturated) to the related slip angles: $F_y \propto \alpha$ (and $F_y \leq F_{y,\max}$).
- An auxiliary force F_{aux} is used in order to drive the vehicle at constant velocity. It is assumed that this force is known, since it will later be realized with a subordinate control loop and it is necessary for a later comparison of the different models.
- Pitch and bounce motions have small effects on the vehicle and therefore they are neglected.
- Crosswind and road camber effects are neglected.
- The coupling point (5^{th}-wheel) is considered as a rigid connection and both vehicles as rigid bodies.

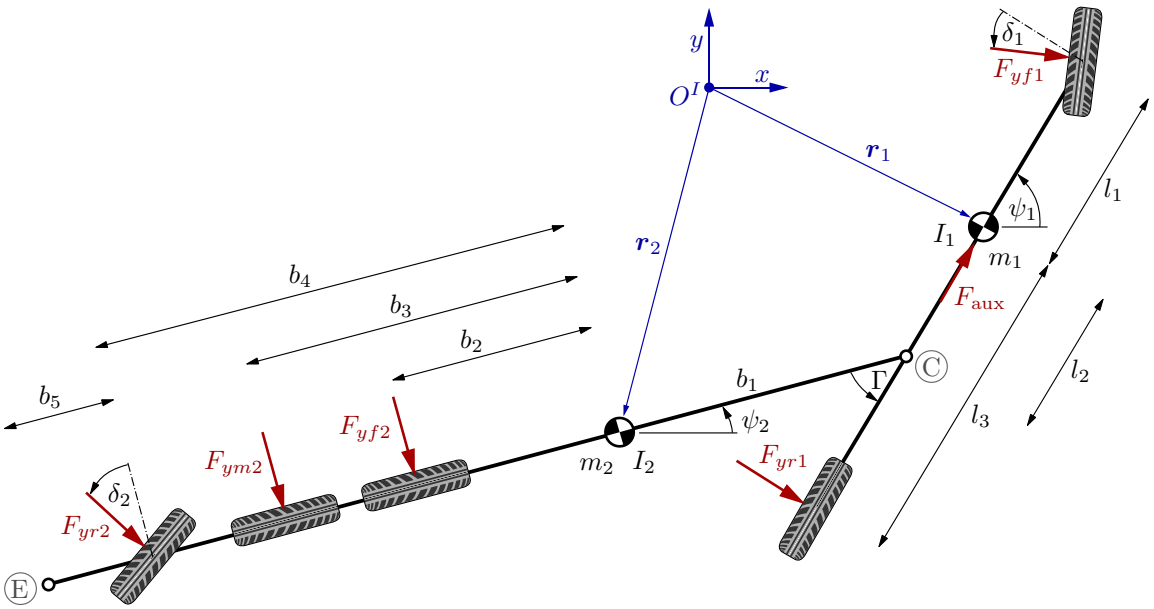

Figure 3.1: Top view of the Single Track Model of a Tractor and Semitrailer(TST) with a steered rearmost axle.

In the first step the planar motion of the TST in the inertial frame O^I will be described. As shown in figure 3.1, the distance from the tractor's front wheel, 5^{th}-wheel Ⓒ and rear wheel to the center of gravity is denoted as l_1, l_2 and l_3. The distance of the 5^{th}-wheel, front wheel, middle wheel and rear wheel of the trailer to it's center of gravity is named as b_1, b_2, b_3 and b_4. The spacing between the rear wheel and the end of the trailer Ⓔ is denoted by b_5. The position of the centers of gravity of the tractor and semitrailer are

$$\boldsymbol{r}_1 = \begin{bmatrix} x_2 + b_1 \cos\psi_2 + l_2 \cos\psi_1 \\ y_2 + b_1 \sin\psi_2 + l_2 \sin\psi_1 \end{bmatrix} \qquad \text{and} \qquad \boldsymbol{r}_2 = \begin{bmatrix} x_2 \\ y_2 \end{bmatrix}, \tag{3.1}$$

where the coordinate tuples x_2 and y_2 define the position of the tractor. The yaw angle of the semitrailer and tractor is called ψ_2 and ψ_1. The tractor has the mass m_1, moment of inertia I_1 and steer angle δ_1 at the front wheel. In analogy, the semitrailer has the mass m_2, moment of inertia I_2 and steer angle δ_2 at the rearward wheel. The tire cornering forces F_{yf1} and F_{yr1} act at the front and rear wheel of the tractor, whereby the forces F_{yf2}, F_{ym2} and F_{yr1} appear at the position of the front, middle and rear axle of the semitrailer.

3.1.1 Equations of motion according to the Newton-Euler Approach

In this section the nonlinear model is derived systematically with the Newton-Euler approach as stated in [SW99]. The proposed method is structured in a certain way and the MBS will now be considered as a three-dimensional system in order to explain the structure generally. Therefore the position vectors to the centers of gravity will be redefined to

$$\boldsymbol{r}_1 = \begin{bmatrix} x_2 + b_1 \cos\psi_2 + l_2 \cos\psi_1 \\ y_2 + b_1 \sin\psi_2 + l_2 \sin\psi_1 \\ 0 \end{bmatrix} \qquad \text{and} \qquad \boldsymbol{r}_2 = \begin{bmatrix} x_2 \\ y_2 \\ 0 \end{bmatrix}. \tag{3.2}$$

With the generalized coordinates $\boldsymbol{q} = \begin{bmatrix} x_2 & y_2 & \psi_2 & \psi_1 \end{bmatrix}^T$, the translational Jacobian matrices $\boldsymbol{J}_{T1}$ and $\boldsymbol{J}_{T2}$ for the tractor and semitrailer can be evaluated with

$$\boldsymbol{J}_{T1} = \frac{\partial \boldsymbol{r}_1}{\partial \boldsymbol{q}} = \begin{bmatrix} 1 & 0 & -b_1 \sin\psi_2 & -l_2 \sin\psi_1 \\ 0 & 1 & b_1 \cos\psi_2 & l_2 \cos\psi_1 \\ 0 & 0 & 0 & 0 \end{bmatrix} \quad \text{and} \quad \boldsymbol{J}_{T2} = \frac{\partial \boldsymbol{r}_2}{\partial \boldsymbol{q}} = \begin{bmatrix} 1 & 0 & 0 & 0 \\ 0 & 1 & 0 & 0 \\ 0 & 0 & 0 & 0 \end{bmatrix}. \tag{3.3}$$

This leads to the conclusion that the velocity and acceleration of the k^{th} body are

$$\boldsymbol{v}_k = \boldsymbol{J}_{Tk}\dot{\boldsymbol{q}} + \underbrace{\frac{\partial \boldsymbol{r}_k}{\partial t}}_{\bar{\boldsymbol{v}}_k} \qquad \text{and} \qquad \boldsymbol{a}_k = \boldsymbol{J}_{Tk}\ddot{\boldsymbol{q}} + \underbrace{\dot{\boldsymbol{J}}_{Tk}\dot{\boldsymbol{q}} + \frac{\partial \bar{\boldsymbol{v}}_k}{\partial t}}_{\bar{\boldsymbol{a}}_k}, \tag{3.4}$$

whereby $\bar{\boldsymbol{v}}_k$ and $\bar{\boldsymbol{a}}_k$ are declared as the local velocity and local acceleration. Due to the fact that any body rotation is not explicit time dependent, the vector of the corresponding angular velocity $\boldsymbol{\omega}_k$ can be described by the rotational Jacobian matrix $\boldsymbol{J}_{Rk}$ and the time derivative of the generalized coordinates,

$$\boldsymbol{\omega}_1 = \begin{bmatrix} 0 \\ 0 \\ \dot{\psi}_1 \end{bmatrix} = \underbrace{\begin{bmatrix} 0 & 0 & 0 & 0 \\ 0 & 0 & 0 & 0 \\ 0 & 0 & 0 & 1 \end{bmatrix}}_{\boldsymbol{J}_{R1}} \dot{\boldsymbol{q}} \quad \text{and} \quad \boldsymbol{\omega}_2 = \begin{bmatrix} 0 \\ 0 \\ \dot{\psi}_2 \end{bmatrix} = \underbrace{\begin{bmatrix} 0 & 0 & 0 & 0 \\ 0 & 0 & 0 & 0 \\ 0 & 0 & 1 & 0 \end{bmatrix}}_{\boldsymbol{J}_{R2}} \dot{\boldsymbol{q}}. \tag{3.5}$$

As reported by [SW99], the equations of motions can be expressed in block matrices,

$$\underbrace{\begin{bmatrix} m_1\boldsymbol{E} & & & \text{sym.} \\ \boldsymbol{0} & m_1\boldsymbol{E} & & \\ \boldsymbol{0} & \boldsymbol{0} & \boldsymbol{I}_1 & \\ \boldsymbol{0} & \boldsymbol{0} & \boldsymbol{0} & \boldsymbol{I}_2 \end{bmatrix}}_{\bar{\boldsymbol{M}}} \underbrace{\begin{bmatrix} \boldsymbol{J}_{T1} \\ \boldsymbol{J}_{T2} \\ \boldsymbol{J}_{R1} \\ \boldsymbol{J}_{R2} \end{bmatrix}}_{\boldsymbol{J}} \ddot{\boldsymbol{q}} + \underbrace{\begin{bmatrix} m_1\bar{\boldsymbol{a}}_1 \\ m_2\bar{\boldsymbol{a}}_2 \\ \boldsymbol{I}_1\bar{\boldsymbol{\alpha}}_1 + \tilde{\boldsymbol{\omega}}_1\boldsymbol{I}_1\boldsymbol{\omega}_1 \\ \boldsymbol{I}_2\bar{\boldsymbol{\alpha}}_2 + \tilde{\boldsymbol{\omega}}_2\boldsymbol{I}_2\boldsymbol{\omega}_2 \end{bmatrix}}_{\bar{\boldsymbol{k}}} = \underbrace{\begin{bmatrix} \boldsymbol{f}_1^e \\ \boldsymbol{f}_2^e \\ \boldsymbol{l}_1^e \\ \boldsymbol{l}_2^e \end{bmatrix}}_{\bar{\boldsymbol{q}}^e} + \underbrace{\begin{bmatrix} \boldsymbol{f}_1^r \\ \boldsymbol{f}_2^r \\ \boldsymbol{l}_1^r \\ \boldsymbol{l}_2^r \end{bmatrix}}_{\bar{\boldsymbol{q}}^r}. \tag{3.6}$$

Each line characterize the force balance in the direction of a Cartesian coordinate of one body. The symmetrical matrix $\bar{\boldsymbol{M}}$ contains the mass and the inertia tensors

$$\boldsymbol{I}_1 = \begin{bmatrix} I_{xx1} & I_{xy1} & I_{xz1} \\ I_{xy1} & I_{yy1} & I_{yz1} \\ I_{xz1} & I_{yz1} & I_1 \end{bmatrix} \quad \text{and} \quad \boldsymbol{I}_2 = \begin{bmatrix} I_{xx2} & I_{xy2} & I_{xz2} \\ I_{xy2} & I_{yy2} & I_{yz2} \\ I_{xz2} & I_{yz2} & I_2 \end{bmatrix}. \tag{3.7}$$

Besides the specified Jacobian matrices are composed to the global Jacobian matrix $\boldsymbol{J}$. Furthermore $\bar{\boldsymbol{k}}$ denotes the vector of Coriolis and gyroscopic forces and torques, where $\bar{\boldsymbol{a}}_k$ and $\bar{\boldsymbol{\alpha}}_k$ denominate the local acceleration and local angular acceleration. The rotation of the bodies is not explicitly time dependent and they spin around their mass centroid axis, so the terms $\boldsymbol{I}_k\bar{\boldsymbol{\alpha}}_k + \tilde{\boldsymbol{\omega}}_k\boldsymbol{I}_k\boldsymbol{\omega}_k$ disappear. The vector $\bar{\boldsymbol{q}}^e$ presents the applied forces and moments which results from the tires. In addition $\bar{\boldsymbol{q}}^r$ contains the reaction forces and moments. The 12 equations stated in (3.6) can be reduced to the minimal number of four ordinary differential equations by a left pre-multiplication with the transposed global Jacobian matrix $\boldsymbol{J}^T$,

$$\underbrace{\boldsymbol{J}^T\bar{\boldsymbol{M}}\boldsymbol{J}}_{\boldsymbol{M}}\ddot{\boldsymbol{q}} + \underbrace{\boldsymbol{J}^T\bar{\boldsymbol{k}}}_{\boldsymbol{k}} = \underbrace{\boldsymbol{J}^T\bar{\boldsymbol{q}}^e}_{\boldsymbol{q}^e} + \cancel{\underbrace{\boldsymbol{J}^T\bar{\boldsymbol{Q}}\boldsymbol{g}}_{\boldsymbol{q}^r}}. \tag{3.8}$$

With that step the reaction forces disappear because of the generalized orthogonality between motion and constraint, i.e. vanishing virtual work of the reaction forces ($\boldsymbol{J}^T\bar{\boldsymbol{Q}} = \boldsymbol{0}$) [PS10]. For the current MBS the only challenge is to evaluate the local accelerations

$$\bar{\boldsymbol{a}}_1 = \begin{bmatrix} -l_2 \mathrm{c}_{\psi 1}\dot{\psi}_1^2 - b_1 \mathrm{c}_{\psi_2}\dot{\psi}_2^2 \\ -l_2 \mathrm{s}_{\psi 1}\dot{\psi}_1^2 - b_1 \mathrm{s}_{\psi_2}\dot{\psi}_2^2 \\ 0 \end{bmatrix} \quad \text{and} \quad \bar{\boldsymbol{a}}_2 = \begin{bmatrix} 0 \\ 0 \\ 0 \end{bmatrix} \tag{3.9}$$

and take the applied forces of the tires acting on the centers of gravity into account. They can be expressed in Cartesian coordinates with

$$\bar{\boldsymbol{q}}^e = \begin{bmatrix} F_{yf1}\mathrm{s}_{\psi_1+\delta_1} + F_{yr1}\mathrm{s}_{\psi_1} + F_{\mathrm{aux}}\mathrm{c}_{\psi_1} \\ -F_{yf1}\mathrm{c}_{\psi_1+\delta_1} - F_{yr1}\mathrm{c}_{\psi_1} + F_{\mathrm{aux}}\mathrm{s}_{\psi_1} \\ 0 \\ F_{yf2}\mathrm{s}_{\psi_2} + F_{ym2}\mathrm{s}_{\psi_2} + F_{yr2}\mathrm{s}_{\psi_2+\delta_2} \\ -F_{yf2}\mathrm{c}_{\psi_2} - F_{ym2}\mathrm{c}_{\psi_2} - F_{yr2}\mathrm{c}_{\psi_2+\delta_2} \\ 0 \\ 0 \\ 0 \\ -F_{yf1}l_1\mathrm{c}_{\delta_1} + F_{yr1}l_3 \\ 0 \\ 0 \\ F_{yf2}b_2 + F_{ym2}b_3 + F_{yr2}b_4\mathrm{c}_{\delta_2} \end{bmatrix}. \tag{3.10}$$

The trigonometric functions are notated according to (A.1). In conclusion, after some calculation the equations of motion in matrix-form and conform to (2.49) results in

$$\begin{aligned} &\begin{bmatrix} m_1+m_2 & 0 & -m_1b_1\mathrm{s}_{\psi_2} & -m_1l_2\mathrm{s}_{\psi_1} \\ 0 & m_1+m_2 & m_1b_1\mathrm{c}_{\psi_2} & m_1l_2\mathrm{c}_{\psi_1} \\ -m_1b_1\mathrm{s}_{\psi_2} & m_1b_1\mathrm{c}_{\psi_2} & m_1b_1^2+I_2 & m_1l_2b_1\mathrm{c}_{\psi_1-\psi_2} \\ -m_1l_2\mathrm{s}_{\psi_1} & m_1l_2\mathrm{c}_{\psi_1} & m_1l_2b_1\mathrm{c}_{\psi_1-\psi_2} & m_1l_2^2+I_1 \end{bmatrix} \ddot{\boldsymbol{q}} + \begin{bmatrix} -m_1l_2\mathrm{c}_{\psi_1}\dot{\psi}_1^2 - m_1b_1\mathrm{c}_{\psi_2}\dot{\psi}_2^2 \\ -m_1l_2\mathrm{s}_{\psi_1}\dot{\psi}_1^2 - m_1b_1\mathrm{s}_{\psi_2}\dot{\psi}_2^2 \\ -m_1\dot{\psi}_1^2l_2b_1\mathrm{s}_{\psi_1-\psi_2} \\ m_1\dot{\psi}_2^2l_2b_1\mathrm{s}_{\psi_1-\psi_2} \end{bmatrix} \ldots \\ &= \begin{bmatrix} F_{yf1}\mathrm{s}_{\delta_1+\psi_1} + F_{yr2}\mathrm{s}_{\delta_2+\psi_2} + F_{yf2}\mathrm{s}_{\psi_2} + F_{ym2}\mathrm{s}_{\psi_2} + F_{yr1}\mathrm{s}_{\psi_1} + F_{\mathrm{aux}}\mathrm{c}_{\psi_1} \\ -F_{yf1}\mathrm{c}_{\delta_1+\psi_1} - F_{yr2}\mathrm{c}_{\delta_2+\psi_2} - F_{yf2}\mathrm{c}_{\psi_2} - F_{ym2}\mathrm{c}_{\psi_2} - F_{yr1}\mathrm{c}_{\psi_1} + F_{\mathrm{aux}}\mathrm{s}_{\psi_1} \\ F_{yf2}b_2 + F_{ym2}b_3 - F_{yr1}b_1\mathrm{c}_{\psi_1-\psi_2} - F_{yf1}b_1\mathrm{c}_{\delta_1+\psi_1-\psi_2} + F_{yr2}b_4\mathrm{c}_{\delta_2} + F_{\mathrm{aux}}b_1\mathrm{s}_{\psi_1-\psi_2} \\ F_{yr1}(l_3-l_2) - F_{yf1}\mathrm{c}_{\delta_1}(l_1+l_2) \end{bmatrix}. \end{aligned} \tag{3.11}$$

In comparison with (A.24), these derived equations of motions are identical.

3.1.2 Transformation to trailer-fixed reference frame

Up to this point, a full non-linear model for the planar motion in the inertial frame is derived. Nevertheless, for the purpose of creating a controller, it is necessary to have all the equations expressed in a frame fixed to one of the two truck units. Since this work mainly focus on the semitrailer, a trailer-fixed reference frame is used. The new vector of generalized coordinates is

$${}_S\boldsymbol{q} = \begin{bmatrix} {}_Sx_2 & {}_Sy_2 & \psi_2 & \psi_1 \end{bmatrix}^T, \tag{3.12}$$

where ${}_Sx_2$ and ${}_Sy_2$ denotes the trailer position with respect to the semitrailer coordinate system O^S, which is fixed to its center of gravity. Figure 3.2 shows the model description at two points of time ($t^{(k)}$ and $t^{(k+1)}$) during a simulation process. Consequently the position of the semitrailer with respect to the initial frame O^I at $t^{(k+1)}$ can be expressed by

$$\boldsymbol{r}_2^{(k+1)} = \begin{bmatrix} x_2 \\ y_2 \end{bmatrix} = \boldsymbol{r}_2^{(k)} + \underbrace{\begin{bmatrix} \cos\psi_2^{(k)} & -\sin\psi_2^{(k)} \\ \sin\psi_2^{(k)} & \cos\psi_2^{(k)} \end{bmatrix}}_{{}_I\boldsymbol{\phi}_S\psi_2^{(k)}} \underbrace{\begin{bmatrix} {}_S\Delta x_2 \\ {}_S\Delta y_2 \end{bmatrix}}_{{}_S\Delta\boldsymbol{r}_2}, \tag{3.13}$$

where $\boldsymbol{r}_2^{(k)}$ is the previous position at $t^{(k)}$ and ${}_I\boldsymbol{\phi}_S$ the rotational matrix of the semitrailer. Moreover ${}_S\Delta\boldsymbol{r}_2$ is the relative displacement after the time-step Δt. With the velocity ${}_S\dot{\boldsymbol{r}}_2 = \begin{bmatrix} {}_S\dot{x}_2 & {}_S\dot{y}_2 \end{bmatrix}^T$ it yields

$${}_S\Delta\boldsymbol{r}_2 = {}_S\dot{\boldsymbol{r}}_2\,\Delta t. \tag{3.14}$$

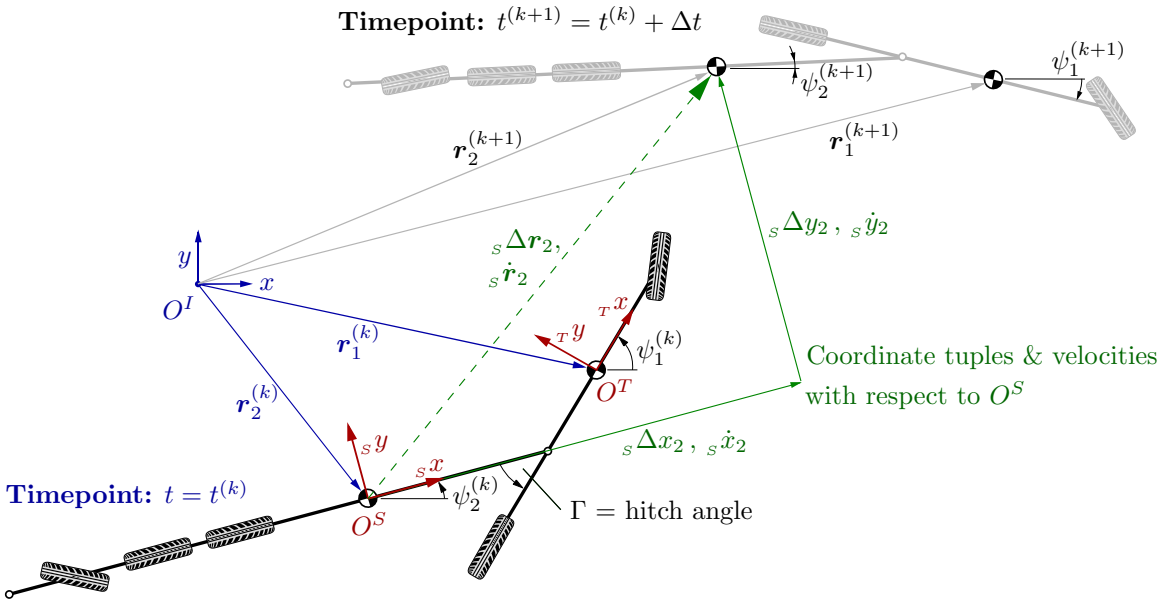

Figure 3.2: Coordinate transformation of the TST-Single Track Model.

Since the ${}_S\Delta\boldsymbol{r}_2$ and ${}_S\dot{\boldsymbol{r}}_2$ have the same direction, the velocity with respect to O^I and O^S are also related to the rotational matrix of the semitrailer ${}_I\boldsymbol{\phi}_S$,

$$\underbrace{\begin{bmatrix}\dot{x}_2\\ \dot{y}_2\end{bmatrix}}_{\boldsymbol{v}_2} = \underbrace{\begin{bmatrix}\cos\psi_2 & -\sin\psi_2\\ \sin\psi_2 & \cos\psi_2\end{bmatrix}}_{{}_I\boldsymbol{\phi}_S(\psi_2)} \underbrace{\begin{bmatrix}{}_S\dot{x}_2\\ {}_S\dot{y}_2\end{bmatrix}}_{{}_S\boldsymbol{v}_2}. \tag{3.15}$$

When considering the angle velocities it is obvious, that they are independent of the reference frame ($\dot{\psi}_1 = {}_S\dot{\psi}_1$ and $\dot{\psi}_2 = {}_S\dot{\psi}_2$). This leads to the transformation matrix ${}_I\boldsymbol{\Phi}_S$, which describes the relation between the previous and current generalized velocities,

$$\underbrace{\begin{bmatrix}\dot{x}_2\\ \dot{y}_2\\ \dot{\psi}_2\\ \dot{\psi}_1\end{bmatrix}}_{\dot{\boldsymbol{q}}} = \underbrace{\begin{bmatrix}\cos\psi_2 & -\sin\psi_2 & 0 & 0\\ \sin\psi_2 & \cos\psi_2 & 0 & 0\\ 0 & 0 & 1 & 0\\ 0 & 0 & 0 & 1\end{bmatrix}}_{{}_I\boldsymbol{\Phi}_S} \underbrace{\begin{bmatrix}{}_S\dot{x}_2\\ {}_S\dot{y}_2\\ \dot{\psi}_2\\ \dot{\psi}_1\end{bmatrix}}_{{}_S\dot{\boldsymbol{q}}}. \tag{3.16}$$

Furthermore it yields ${}_S\boldsymbol{\Phi}_I = {}_I\boldsymbol{\Phi}_S{}^{-1} = {}_I\boldsymbol{\Phi}_S{}^T$, since the linear transformation ${}_I\boldsymbol{\Phi}_S$ is orthogonal. Applying (3.16) to (3.8) it is possible to obtain the equations of motion expressed in the trailer-fixed reference frame in matrix form,

$$\underbrace{{}_S\boldsymbol{\Phi}_I\,\boldsymbol{M}\,{}_I\boldsymbol{\Phi}_S}_{{}_S\boldsymbol{M}}\,{}_S\ddot{\boldsymbol{q}} + \underbrace{{}_S\boldsymbol{\Phi}_I\,\boldsymbol{M}\,{}_I\dot{\boldsymbol{\Phi}}_S\,{}_S\dot{\boldsymbol{q}} + {}_S\boldsymbol{\Phi}_I\,\boldsymbol{k}}_{{}_S\boldsymbol{k}} = \underbrace{{}_S\boldsymbol{\Phi}_I\,\boldsymbol{q}^e}_{{}_S\boldsymbol{q}^e}. \tag{3.17}$$

After some calculations the equations of motions with reference to the trailer-fixed frame results in

$$\begin{bmatrix} m_1+m_2 & 0 & 0 & -m_1 l_2 \mathrm{s}_\Gamma \\ 0 & m_1+m_2 & m_1 b_1 & m_1 l_2 \mathrm{c}_\Gamma \\ 0 & m_1 b_1 & m_1 b_1^2 + I_2 & m_1 l_2 b_1 \mathrm{c}_\Gamma \\ -m_1 l_2 \mathrm{s}_\Gamma & m_1 l_2 \mathrm{c}_\Gamma & m_1 l_2 b_1 \mathrm{c}_\Gamma & m_1 l_2^2 + I_1 \end{bmatrix} {}_S\ddot{\boldsymbol{q}} + \begin{bmatrix} -m_1 \dot{\psi}_2^2 b_1 - m_1 \dot{\psi}_1^2 l_2 \mathrm{c}_\Gamma - (m_1+m_2)\dot{\psi}_2 \, {}_S\dot{y}_2 \\ -m_1 \dot{\psi}_1^2 l_2 \mathrm{s}_\Gamma + \dot{\psi}_2 \, (m_1+m_2) \, {}_S\dot{x}_2 \\ m_1 b_1 (\dot{\psi}_2 \, {}_S\dot{x}_2 - \dot{\psi}_1^2 l_2 \mathrm{s}_\Gamma) \\ m_1 \dot{\psi}_2 l_2 ({}_S\dot{x}_2 \, \mathrm{c}_\Gamma + ({}_S\dot{y}_2 + \dot{\psi}_2 b_1) \mathrm{s}_\Gamma) \end{bmatrix} \ldots$$
$$= \begin{bmatrix} F_{yf1} \mathrm{s}_{\delta_1+\Gamma} + F_{yr2} \mathrm{s}_{\delta_2} + F_{\mathrm{aux}} \mathrm{c}_\Gamma + F_{yr1} \mathrm{s}_\Gamma \\ F_{\mathrm{aux}} \mathrm{s}_\Gamma - F_{yf2} - F_{ym2} - F_{yf1} \mathrm{c}_{\delta_1+\Gamma} - F_{yr2} \mathrm{c}_{\delta_2} - F_{yr1} \mathrm{c}_\Gamma \\ F_{yf2} b_2 + F_{ym2} b_3 - F_{yr1} b_1 \mathrm{c}_\Gamma + F_{\mathrm{aux}} b_1 \mathrm{s}_\Gamma - F_{yf1} b_1 \mathrm{c}_{\delta_1+\Gamma} + F_{yr2} b_4 \mathrm{c}_{\delta_2} \\ F_{yr1}(l_3 - l_2) - F_{yf1} \mathrm{c}_{\delta_1} (l_1 + l_2) \end{bmatrix}, \text{ where} \tag{3.18}$$

$$\Gamma = \psi_1 - \psi_2 \tag{3.19}$$

denotes the hitch angle and the trigonometric functions are notated in agreement with (A.1).

3.2 Model Extensions and Background Analysis

3.2.1 Trajectories with respect to the Initial Reference Frame

The model equations according to (3.18) are formulated with respect to the semitrailer-fixed reference frame O^S. In order to identify the positions of the semitrailer and tractor units, the trajectories in the inertial reference frame O^I must be obtained by the generalized coordinates of the simulation results. Additionally, the following back transformation method is also needed for the determination of the tire forces, at each simulation time-step.
Given are the generalized positions in line with (3.12)and along a simulated time line $\{t^{(1)} \ldots t^{(k)} \ldots t^{(n)}\}$,

$${}_S\boldsymbol{q}_{\mathrm{result}} = \begin{bmatrix} {}_Sx_2^{(1)} & {}_Sx_2^{(2)} & \ldots & {}_Sx_2^{(k)} & {}_Sx_2^{(k+1)} & \ldots & {}_Sx_2^{(n)} \\ {}_Sy_2^{(1)} & {}_Sy_2^{(2)} & \ldots & {}_Sy_2^{(k)} & {}_Sy_2^{(k+1)} & \ldots & {}_Sy_2^{(n)} \\ \psi_2^{(1)} & \psi_2^{(2)} & \ldots & \psi_2^{(k)} & \psi_2^{(k+1)} & \ldots & \psi_2^{(n)} \\ \psi_1^{(1)} & \psi_1^{(2)} & \ldots & \psi_1^{(k)} & \psi_1^{(k+1)} & \ldots & \psi_1^{(n)} \end{bmatrix}. \tag{3.20}$$

The k^{th} displacement vector of the semitrailer unit relative to O^S can be evaluated by

$${}_S\Delta\boldsymbol{r}_2^{(k)} = \begin{bmatrix} {}_Sx_2^{(k+1)} - {}_Sx_2^{(k)} \\ {}_Sy_2^{(k+1)} - {}_Sy_2^{(k)} \end{bmatrix} \quad \text{, for} \quad k = 1(1)n-1. \tag{3.21}$$

In consideration of the initial condition $\boldsymbol{r}_{02}$ and (3.13), the trailer position with respect to the initial reference frame can be calculated,

$$\boldsymbol{r}_2^{(k)} = \begin{cases} \boldsymbol{r}_{02} & \text{for} \quad k = 1 \\ \boldsymbol{r}_2^{(k-1)} + {}_I\boldsymbol{\phi}_S(\psi_2^{(k-1)}) \, {}_S\Delta\boldsymbol{r}_2^{(k-1)} & \text{for} \quad k = 2(1)n, \end{cases} \tag{3.22}$$

where ${}_I\boldsymbol{\phi}_S(\psi_2^{(k-1)})$ denotes the rotation matrix of the semitrailer with the applied angle $\psi_2^{(k-1)}$. Figure 3.2 clarifies the relations again. The trailer position can be alternatively obtained by transforming the relative trailer velocity ${}_S\boldsymbol{v}_2$ to the velocity in the initial reference frame $\boldsymbol{v}_2$ using equation (3.15) and applying an integration in the form of

$$\boldsymbol{r}_2 = \int \boldsymbol{v}_2 \, \mathrm{d}t, \tag{3.23}$$

or for discrete values:

$$\boldsymbol{r}_2^{(k)} = \begin{cases} \boldsymbol{r}_{02} & \text{for} \quad k = 1 \\ \boldsymbol{r}_2^{(k-1)} + \boldsymbol{v}_2^{(k-1)} \Delta t^{(k-1)} & \text{for} \quad k = 2(1)n. \end{cases} \tag{3.24}$$

This thesis also treats a linear model with the generalized coordinates

$$\boldsymbol{q}_{\text{lin}} = \begin{bmatrix} \Gamma & \dot{\psi}_1 & \beta_2 & \dot{\psi}_2 \end{bmatrix}^T. \tag{3.25}$$

Since this model assumes a constant body velocity v, the semitrailer velocity in the initial reference frame results in

$$\boldsymbol{v}_2 = \begin{bmatrix} \dot{x}_2 \\ \dot{y}_2 \end{bmatrix} = \begin{bmatrix} v\cos(\beta_2 + \psi_2) \\ v\sin(\beta_2 + \psi_2) \end{bmatrix}. \tag{3.26}$$

The semitrailer position can be calculated afterwards, using equation (3.23), for discrete values (3.24) respectively.
In conclusion, the trajectory of the tractor's c.g. can be obtained by (3.1), in detail it results

$$\boldsymbol{r}_1^{(k)} = \boldsymbol{r}_2^{(k)} + \begin{bmatrix} b_1\cos\psi_2^{(k)} + l_2\cos\psi_1^{(k)} \\ b_1\sin\psi_2^{(k)} + l_2\sin\psi_1^{(k)} \end{bmatrix} \quad \text{, for} \quad k = 1(1)n. \tag{3.27}$$

3.2.2 Tire Forces and Kinematic Constraints

In order to determine the tire forces during the simulation process, some kinematic relations have to be taken into account. As already discussed in section 2.1.1, the tire forces $F_{\alpha i}$ of the modeled TST linearly depend on the corresponding slip angles α_i,

$$F_{yf1} = C_{\alpha f1}\,\alpha_{f1} \qquad F_{yr1} = C_{\alpha r1}\,\alpha_{r1} \tag{3.28}$$

$$F_{yf2} = C_{\alpha f2}\,\alpha_{f2} \qquad F_{ym2} = C_{\alpha m2}\,\alpha_{m2} \qquad F_{yr2} = C_{\alpha r2}\,\alpha_{r2} \tag{3.29}$$

for the tractor and for the semitrailer, where $C_{\alpha i}$ is the cornering stiffness for the single axles.

Remark 3.1. *The tire forces can be either regarded fully linear as stated in* (2.5) *or saturated according to* (2.6)*. This distinction is especially important for the derivative of the linear model reported by section 3.3. Conveniently, it will treated as fully linear during this section.*

In analogy to (2.16), the resulting slip angles are

$$\alpha_{f1} = \delta_1 - \frac{\dot{\psi}_1 l_1}{|{}_T\boldsymbol{v}_1|} - \beta_1 \qquad \alpha_{r1} = \frac{\dot{\psi}_1 l_3}{|{}_T\boldsymbol{v}_1|} - \beta_1 \tag{3.30}$$

$$\alpha_{f2} = \frac{\dot{\psi}_2 b_2}{|{}_S\boldsymbol{v}_2|} - \beta_2 \qquad \alpha_{m2} = \frac{\dot{\psi}_2 b_3}{|{}_S\boldsymbol{v}_2|} - \beta_2 \qquad \alpha_{r2} = \delta_2 + \frac{\dot{\psi}_2 b_4}{|{}_S\boldsymbol{v}_2|} - \beta_2, \tag{3.31}$$

where the constant distances are depicted in figure 3.1, ${}_T\boldsymbol{v}_1 = [{}_T\dot{x}_1 \quad {}_T\dot{y}_1]^T$ and ${}_S\boldsymbol{v}_2 = [{}_S\dot{x}_2 \quad {}_S\dot{y}_2]^T$ are the body velocities and β_1 ($\measuredangle\,{}_T\dot{x}_1, {}_T\dot{y}_1$) and β_2 ($\measuredangle\,{}_S\dot{x}_2, {}_S\dot{y}_2$) are the body slip angles. Since ${}_S\dot{x}_2$ and ${}_S\dot{y}_2$ are generalized coordinates, the vector norm and body slip angle of the semitrailer are also known as

$$|{}_S\boldsymbol{v}_2| = \sqrt{{}_S\dot{x}_2{}^2 + {}_S\dot{y}_2{}^2} \quad (= v_2) \qquad \text{and} \qquad \beta_2 = \arctan\left(\frac{{}_S\dot{y}_2}{{}_S\dot{x}_2}\right). \tag{3.32}$$

Before the calculation of the tractor's body slip angle it is necessary to obtain the tractor velocity $\boldsymbol{v}_1$ represented in the initial reference frame. This can be done with the derivative of (3.27) with respect to the time,

$$\underbrace{\dot{\boldsymbol{r}}_1}_{\boldsymbol{v}_1} = \underbrace{\dot{\boldsymbol{r}}_2}_{\boldsymbol{v}_2} + \underbrace{\begin{bmatrix} -\dot{\psi}_2 b_1\sin\psi_2 - \dot{\psi}_1 l_2\sin\psi_1 \\ \dot{\psi}_2 b_1\cos\psi_2 + \dot{\psi} l_2\cos\psi_1 \end{bmatrix}}_{\boldsymbol{v}_\psi}, \tag{3.33}$$

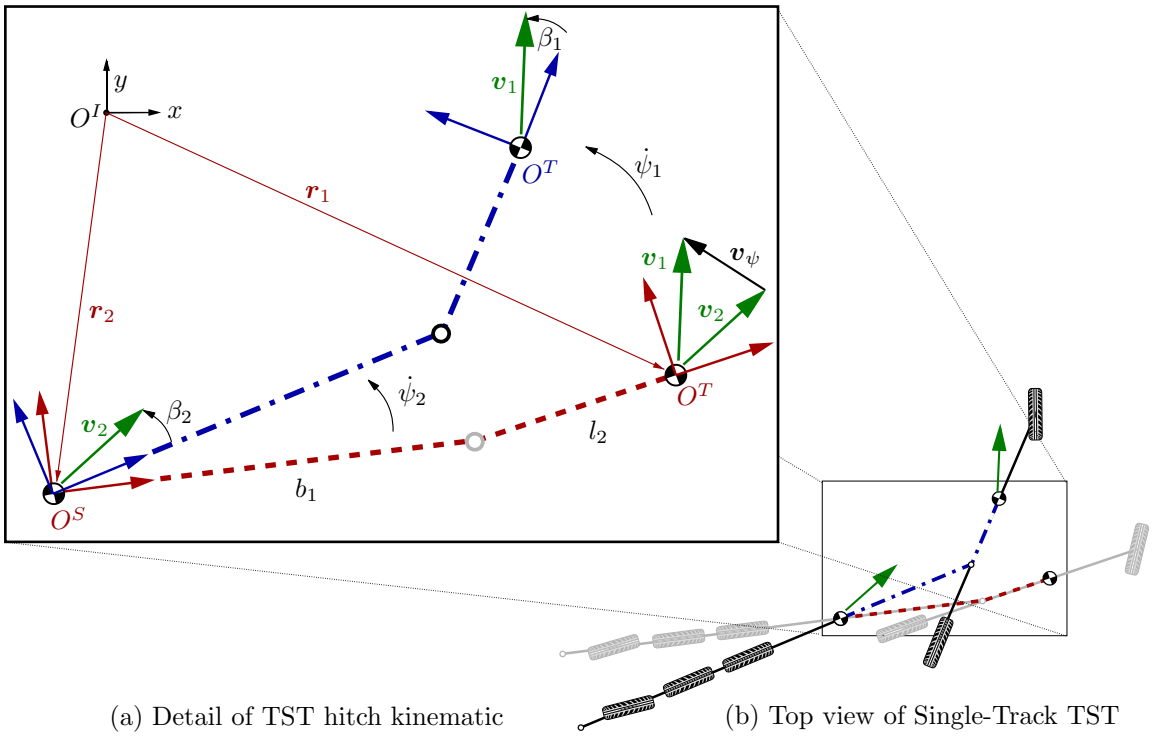

(a) Detail of TST hitch kinematic (b) Top view of Single-Track TST

Figure 3.3: Calculation of the body velocities in order to obtain the body slip angels β_1 and β_2.

where $\boldsymbol{v}_2$ yields from (3.15). The velocity $\boldsymbol{v}_\psi$ results from the angular velocities and is depicted in figure 3.3. On the left site (a) it qualitatively shows the relative movement of the tractor in agreement with the hitch kinematic, where the right site (b) illustrates the rotational motion of the entire tractor semitrailer system with respect to the trailer's center of gravity. Now the velocity with respect to the tractor reference frame (denoted with O^T) can be solved by using the transposed transformation matrix ${}_T\boldsymbol{\phi}_I(\psi_1) = ({}_I\boldsymbol{\phi}_T(\psi_1))^T$,

$$\underbrace{\begin{bmatrix} {}_T\dot{x}_1 \\ {}_T\dot{y}_1 \end{bmatrix}}_{{}_T\boldsymbol{v}_1} = \underbrace{\begin{bmatrix} \cos\psi_1 & \sin\psi_1 \\ -\sin\psi_1 & \cos\psi_1 \end{bmatrix}}_{{}_T\boldsymbol{\phi}_I(\psi_1)} \underbrace{\begin{bmatrix} \dot{x}_1 \\ \dot{y}_1 \end{bmatrix}}_{\boldsymbol{v}_1}. \tag{3.34}$$

The vector norm and body slip angle of the tractor eventually leads to

$$|{}_T\boldsymbol{v}_1| = \sqrt{{}_T\dot{x}_1{}^2 + {}_T\dot{y}_1{}^2} \quad (= v_1) \qquad \text{and} \qquad \beta_1 = \arctan\left(\frac{{}_T\dot{y}_1}{{}_T\dot{x}_1}\right), \tag{3.35}$$

whereby all the tire slip angles and tire forces are determined. The scalar velocities of the bodies are denoted by v_1 and v_2.
Corresponding to figure 3.3, the coupling conditions will be introduced within this section. Since the semitrailer is coupled to the tractor, the orientation ψ_c of the velocity $\boldsymbol{v}_c$ at the coupling point (or so-called "hitch-point" or "5$^{\text{th}}$-wheel") can be described as illustrated in figure 3.4 by both, the tractor's and the trailer's body coordinates,

$$\psi_c \approx \psi_1 + \beta_1 - \tan\frac{\dot{\psi}_1 l_2}{v_1} \qquad \text{and} \qquad \psi_c \approx \psi_2 + \beta_2 + \tan\frac{\dot{\psi}_2 b_1}{v_2}. \tag{3.36}$$

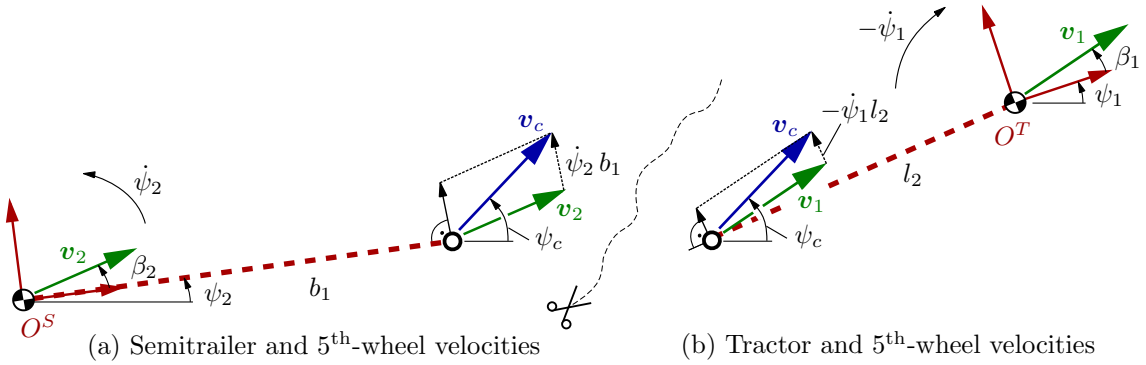

(a) Semitrailer and 5th-wheel velocities (b) Tractor and 5th-wheel velocities

Figure 3.4: Top view of the hitch kinematic for the derivation of the coupling condition.

With the simplification $\tan\measuredangle \approx \measuredangle$ and the elimination of the angle ψ_c, the kinematic constraint equation results equal to [SC98] with

$$\psi_1 + \beta_1 - \frac{\dot{\psi}_1 l_2}{v_1} \approx \psi_2 + \beta_2 + \frac{\dot{\psi}_2 b_1}{v_2} \quad \Leftrightarrow \quad \beta_1 \approx -\Gamma + \beta_2 + \frac{\dot{\psi}_2 b_1}{v_2} + \frac{\dot{\psi}_1 l_2}{v_1}, \tag{3.37}$$

where Γ is defined in (3.19). The derivation with respect to the time and assuming $\dot{v}_1 = 0$ and $\dot{v}_2 = 0$, yields

$$\dot{\psi}_1 + \dot{\beta}_1 - \frac{\ddot{\psi}_1 l_2}{v_1} \approx \dot{\psi}_2 + \dot{\beta}_2 + \frac{\ddot{\psi}_2 b_1}{v_2} \quad \Leftrightarrow \quad \dot{\beta}_1 \approx \dot{\psi}_2 - \dot{\psi}_1 + \dot{\beta}_2 + \frac{\ddot{\psi}_2 b_1}{v_2} + \frac{\ddot{\psi}_1 l_2}{v_1}. \tag{3.38}$$

If the roll motion of the tractor semitrailer should also be taken into account, the model can be extend to a so-called "yaw-roll"-model. The 3D-position of the 5th-wheel can be described with either

$$\boldsymbol{r}_{c1} = \begin{bmatrix} x_1 - l_2\cos\psi_1 + z_1\sin\phi_1\sin\psi_1 \\ y_1 - l_2\sin\psi_1 - z_1\sin\phi_1\cos\psi_1 \\ z_1\cos\phi_1 \end{bmatrix} \quad \text{or} \quad \boldsymbol{r}_{c2} = \begin{bmatrix} x_2 + b_1\cos\psi_2 + z_2\sin\phi_2\sin\psi_2 \\ y_2 + b_1\sin\psi_2 - z_2\sin\phi_2\cos\psi_2 \\ z_2\cos\phi_2 \end{bmatrix}, \tag{3.39}$$

whereby ϕ_1 and ϕ_2 are the roll angle of the tractor and semitrailer. The distances from the roll axis to the 5th-wheel is denoted by z_1 and z_2, respectively. Furthermore, it is assumed that the position of the tractor's c.g. is given with x_1 and y_1. The derivative with respect to the time leads to the velocities

$$\boldsymbol{v}_{c1} = \begin{bmatrix} \dot{x}_1 + \dot{\psi}_1 l_2\sin\psi_1 + \dot{\phi}_1 z_1\cos\phi_1\sin\psi_1 + \psi_1 z_1\sin\phi_1\cos\psi_1 \\ \dot{y}_1 - \dot{\psi}_1 l_2\cos\psi_1 - \dot{\phi}_1 z_1\cos\phi_1\cos\psi_1 + \dot{\psi}_1 z_1\sin\phi_1\sin\psi_1 \\ -\dot{\phi}_1 z_1\sin\phi_1 \end{bmatrix} \quad \text{and} \tag{3.40}$$

$$\boldsymbol{v}_{c2} = \begin{bmatrix} \dot{x}_2 - \dot{\psi}_2 b_1\sin\psi_2 + \dot{\phi}_2 z_2\cos\phi_2\sin\psi_2 + \psi_2 z_2\sin\phi_2\cos\psi_2 \\ \dot{y}_2 + \dot{\psi}_2 b_1\cos\psi_2 - \dot{\phi}_2 z_2\cos\phi_2\cos\psi_2 + \dot{\psi}_2 z_2\sin\phi_2\sin\psi_2 \\ -\dot{\phi}_2 z_2\sin\phi_2 \end{bmatrix}. \tag{3.41}$$

The velocity components of the c.g.'s of the tractor and semitrailer can also be written as

$$\dot{x}_1 = v_1\cos(\psi_1 + \beta_1) \qquad \dot{y}_1 = v_1\sin(\psi_1 + \beta_1)\ , \text{and} \tag{3.42}$$

$$\dot{x}_2 = v_2\cos(\psi_2 + \beta_2) \qquad \dot{y}_2 = v_2\sin(\psi_2 + \beta_2). \tag{3.43}$$

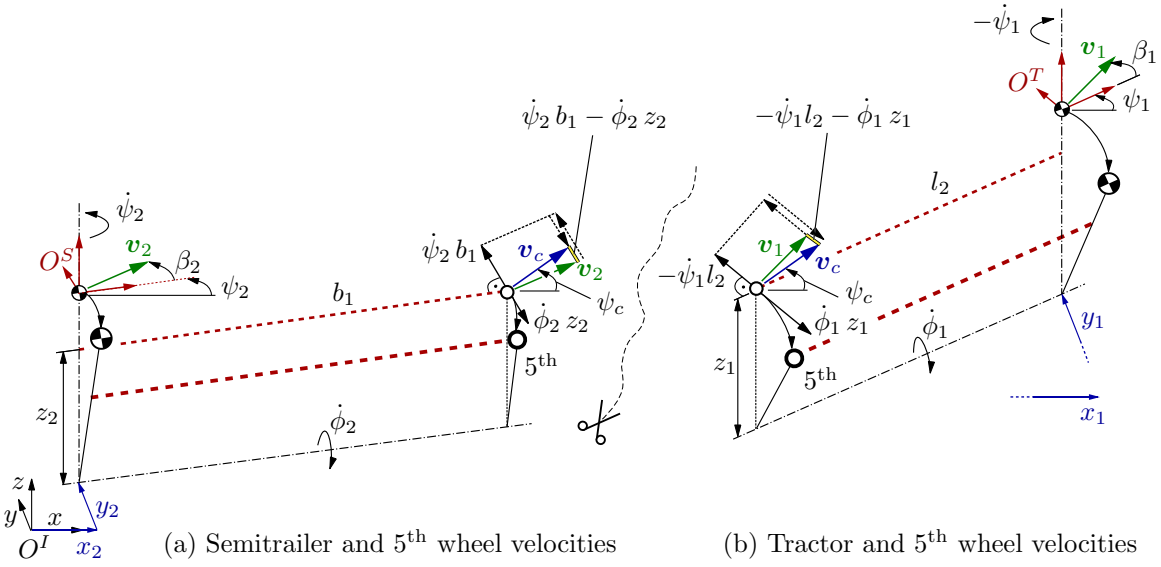

(a) Semitrailer and 5^{th} wheel velocities (b) Tractor and 5^{th} wheel velocities

Figure 3.5: 3D view of the hitch kinematic for the derivation of the coupling condition for a yaw-roll model.

Moreover, the velocities can be represented in the body-fixed reference frames (rotation with ψ_1 or ψ_2 around the z-axis), which leads to

$$ {}_T\boldsymbol{v}_{c1} = {}_T\boldsymbol{\phi}_I \; \boldsymbol{v}_{c1} = \begin{bmatrix} v_1 \cos\beta_1 + \dot{\psi}_1 z_1 \sin\phi_1 \\ v_1 \sin\beta_1 - \dot{\psi}_1 l_2 - \dot{\phi}_1 z_1 \cos\phi_1 \\ -\dot{\phi}_1 z_1 \sin\phi_1 \end{bmatrix} \quad \text{and} \tag{3.44} $$

$$ {}_S\boldsymbol{v}_{c2} = {}_S\boldsymbol{\phi}_I \; \boldsymbol{v}_{c2} = \begin{bmatrix} v_2 \cos\beta_2 + \dot{\psi}_2 z_2 \sin\phi_2 \\ v_2 \sin\beta_2 + \dot{\psi}_2 b_1 - \dot{\phi}_2 z_2 \cos\phi_2 \\ -\dot{\phi}_2 z_2 \sin\phi_2 \end{bmatrix}. \tag{3.45} $$

For the consideration of small angles ($\psi_1, \psi_2, \phi_1, \phi_2 << 1$) the lateral velocities results in

$$ {}_T v_{c1y} = v_1\beta_1 - \dot{\psi}_1 l_2 - \dot{\phi}_1 z_1 \quad \text{and} \quad {}_S v_{c2y} = v_2\beta_2 + \dot{\psi}_2 b_1 - \dot{\phi}_2 z_2, \tag{3.46} $$

This relations are clarified in figure 3.5 for the kinematic of the tractor in fig. 3.5(b) and the semitrailer in fig. 3.5(a). The orientation of the velocities with respect to the body-fixed reference frames and around the z-axis can be approximated with

$$ {}_T\psi_{c1} = \beta_1 - \frac{\dot{\psi}_1 l_2}{v_1} - \frac{\dot{\phi}_1 z_1}{v_1} \quad \text{and} \quad {}_S\psi_{c2} = \beta_2 + \frac{\dot{\psi}_2 b_1}{v_2} - \frac{\dot{\phi}_2 z_2}{v_2}. \tag{3.47} $$

The representation with respect to the initial reference frame can be read as

$$ \psi_{c1} = \psi_1 + \beta_1 - \frac{\dot{\psi}_1 l_2}{v_1} - \frac{\dot{\phi}_1 z_1}{v_1} \quad \text{and} \quad \psi_{c2} = \psi_2 + \beta_2 + \frac{\dot{\psi}_2 b_1}{v_2} - \frac{\dot{\phi}_2 z_2}{v_2}. \tag{3.48} $$

Since the both hitch description have the same velocity orientation ($\psi_{c1} \overset{!}{=} \psi_{c1}$), the kinematic constraint equation (also called algebraic loop) yields

$$ \psi_1 - \psi_2 + \beta_1 - \beta_2 - \frac{l_2}{v_1}\dot{\psi}_1 - \frac{b_1}{v_2}\dot{\psi}_2 - \frac{z_1}{v_1}\dot{\phi}_1 + \frac{z_2}{v_2}\dot{\phi}_2 = 0. \tag{3.49} $$

In conclusion, the derivation with respect to the time and assuming $\dot{v}_1 = 0$ and $\dot{v}_2 = 0$, results in

$$\dot{\psi}_1 - \dot{\psi}_2 + \dot{\beta}_1 - \dot{\beta}_2 - \frac{l_2}{v_1}\ddot{\psi}_1 - \frac{b_1}{v_2}\ddot{\psi}_2 - \frac{z_1}{v_1}\ddot{\phi}_1 + \frac{z_2}{v_2}\ddot{\phi}_2 = 0. \tag{3.50}$$

This constrain equation is also used in e.g. [SC98], [CC08] or [vdV11].

3.3 Linear Single-Track Model

In order to reduce the simulation cost, to develop linear controllers and to use the methods of the linear system theory, a linear model of the TST will be derived by the nonlinear equations within this section. On the one hand subsection 3.3.1 establishes fully linear equations of motion and on the other hand subsection 3.3.2 introduce a linear model with the saturated tire-force-model. An alternative derivation of the fully linear system is described in section A.5.
Assuming the angle between the tractor and semitrailer is very small $\Gamma << 1$, it yields

$$\sin(\Gamma) \approx \Gamma \qquad \text{and} \qquad \cos(\Gamma) \approx 1, \tag{3.51}$$

it can also be simplified for small steering angles,

$$\sin(\delta_1) \approx \delta_1 \qquad \text{and} \qquad \cos(\delta_1) \approx 1, \tag{3.52}$$

$$\sin(\delta_2) \approx \delta_2 \qquad \text{and} \qquad \cos(\delta_2) \approx 1. \tag{3.53}$$

The addition theorems can be used in order to linearize the trigonometric functions,

$$\sin(\delta_1 + \Gamma) \approx \delta_1 + \Gamma \qquad \text{and} \qquad \cos(\delta_1 + \Gamma) \approx 1 - \Gamma\delta_1. \tag{3.54}$$

With these approximations and neglecting the quadratic terms ($\dot{\psi}_2^2 = 0$, $\dot{\psi}_1^2 = 0$), the nonlinear system of equations (3.18) yields

$$\begin{aligned}
&\begin{bmatrix} m_1+m_2 & 0 & 0 & 0 \\ 0 & m_1+m_2 & m_1 b_1 & l_2 m_1 \\ 0 & m_1 b_1 & m_1 b_1^2 + I_2 & l_2 b_1 m_1 \\ 0 & m_1 l_2 & m_1 l_2 b_1 & m_1 l_2^2 + I_1 \end{bmatrix} \begin{bmatrix} {}_S\ddot{x}_2 \\ {}_S\ddot{y}_2 \\ \ddot{\psi}_2 \\ \ddot{\psi}_1 \end{bmatrix} + \begin{bmatrix} -(m_1+m_2)\dot{\psi}_2\, {}_S\dot{y}_2 \\ (m_1+m_2)\dot{\psi}_2\, {}_S\dot{x}_2 \\ m_1 b_1 \dot{\psi}_2\, {}_S\dot{x}_2 \\ m_1 \dot{\psi}_2 l_2 ({}_S\dot{x}_2 + ({}_S\dot{y}_2 + \dot{\psi}_2 b_1)\,\Gamma) \end{bmatrix} \dots \\
&\qquad = \begin{bmatrix} F_{yf1}(\delta_1 + \Gamma) + F_{yr2}\,\delta_2 + F_{\text{aux}} + F_{yr1}\Gamma \\ F_{\text{aux}}\Gamma - F_{yf2} - F_{ym2} - F_{yf1}(1 - \Gamma\delta_1) - F_{yr2} - F_{yr1} \\ F_{yf2} b_2 + F_{ym2} b_3 - F_{yr1} b_1 + F_{\text{aux}} b_1 \Gamma - F_{yf1} b_1 (1 - \Gamma\delta_1) + F_{yr2} b_4 \\ F_{yr1}(l_3 - l_2) - F_{yf1}(l_1 + l_2) \end{bmatrix}.
\end{aligned} \tag{3.55}$$

From (A.35), the movement can approximately be expressed with the resulted body velocity v_2 and the body slip angle of semitrailer β_2,

$${}_S\dot{x}_2 \approx v_2 \qquad \text{and} \qquad {}_S\dot{y}_2 \approx v_2\beta_2, \tag{3.56}$$

$${}_S\ddot{x}_2 \approx \dot{v}_2 \qquad \text{and} \qquad {}_S\ddot{y}_2 \approx \dot{v}_2\beta_2 + v_2\dot{\beta}_2. \tag{3.57}$$

In the following it will be assumed, that the tractor and semitrailer approximately moves with the same constant velocity called v, so it yields $v_1 = v_2 = v$ and $\dot{v} = 0$. As a consequence, the auxiliary force F_{aux} will become a reaction force and it disappears (for more details go to section 3.1). Furthermore, the product of small angles and angle velocities can be neglected ($\Gamma\delta_1 = \beta_2\Gamma = \dot{\psi}_2\Gamma = 0$). So the equation (3.55) simplifies to

$$\begin{bmatrix} -(m_1+m_2)\dot{\psi}_2\, v\beta_2 \\ (m_1+m_2)v(\dot{\beta}_2 + \dot{\psi}_2) + m_1 b_1 \ddot{\psi}_2 + m_1 l_2 \ddot{\psi}_1 \\ b_1 m_1 v(\dot{\beta}_2 + \dot{\psi}_2) + (m_1 b_1^2 + I_2)\ddot{\psi}_2 + m_1 l_2 b_1 \ddot{\psi}_1 \\ m_1 l_2 v(\dot{\beta}_2 + \dot{\psi}_2) + m_1 l_2 b_1 \ddot{\psi}_2 + (m_1 l_2^2 + I_1)\ddot{\psi}_1 \end{bmatrix} = \begin{bmatrix} F_{yf1}(\delta_1 + \Gamma) + F_{yr2}\,\delta_2 + F_{yr1}\Gamma \\ -F_{yf2} - F_{ym2} - F_{yf1} - F_{yr2} - F_{yr1} \\ F_{yf2} b_2 + F_{ym2} b_3 + F_{yr2} b_4 - (F_{yr1} + F_{yf1}) b_1 \\ F_{yr1}(l_3 - l_2) - F_{yf1}(l_1 + l_2) \end{bmatrix}. \tag{3.58}$$

In conclusion, the assumptions and simplifications for the linear model can be summarized by:

- The tires on each axle are combined into one single tire, which is considered to be at the center of the axle (single-track model).
- Only the lateral forces of the tires are taken into account: $F_{\text{tire}} = F_y$. (There are no braking or accelerating forces on the wheels.)
- The angle between the tractor and semitrailer is very small: $\Gamma << 1$.
- The steer angles of the tractor and semitrailer are very small: $\delta_1 << 1$ and $\delta_2 << 1$.
- The velocity of each unit is constant: $v_1 = v_2 = v$ and $\dot{v} = 0$.
- The yaw rates are small: $\dot{\psi}_1 << 1$ and $\dot{\psi}_2 << 1$.
- Pitch and bounce motions have small effects on the vehicle and are therefore neglected.
- Crosswind and road camber effects are neglected.
- The coupling point (5^{th}-wheel) is considered as a rigid connection without compliance.

3.3.1 Fully Linear Equations of Motions

In the following, a fully linear model will be derived by using the additional assumption:

- The lateral tires behavior is considered fully-linear to the related slip angles: $F_y \propto \alpha$.

Since the first equation of (3.58) is of little importance, it can be neglected. The tire forces can be substituted with (3.28) and (3.29), where the slip angles α_i at the tires are explicitly defined in (3.30). Moreover, using the kinematic constraint equation (3.37) for the elimination of β_1, the remaining equations of motion results for the second row in

$$\begin{aligned} m_1 l_2 \ddot{\psi}_1 + (m_1+m_2) v \dot{\beta}_2 + m_1 b_1 \ddot{\psi}_2 + (C_{\alpha f1} + C_{\alpha r1})\Gamma \quad ... \\ + \left(C_{\alpha r1} \frac{l_3 - l_2}{v} - C_{\alpha f1} \frac{l_1 + l_2}{v} \right) \dot{\psi}_1 - (C_{\alpha f2} + C_{\alpha m2} + C_{\alpha r2} + C_{\alpha f1} + C_{\alpha r1})\, \beta_2 ... \\ + \left((m_1+m_2) v + C_{\alpha f2} \frac{b_2}{v} + C_{\alpha m2} \frac{b_3}{v} + C_{\alpha r2} \frac{b_4}{v} - (C_{\alpha f1} + C_{\alpha r1}) \frac{b_1}{v} \right) \dot{\psi}_2 = ... \\ - C_{\alpha f1} \delta_1 - C_{\alpha r2} \delta_2, \end{aligned} \tag{3.59}$$

the third row it leads to

$$\begin{aligned} m_1 l_2 b_1 \ddot{\psi}_1 + m_1 b_1 v \dot{\beta}_2 + (m_1 b_1^2 + I_2) \ddot{\psi}_2 + (C_{\alpha r1} + C_{\alpha f1}) b_1 \Gamma \quad ... \\ + \left(C_{\alpha r1} b_1 \frac{l_3 - l_2}{v} - C_{\alpha f1} b_1 \frac{l_1 + l_2}{v} \right) \dot{\psi}_1 + (C_{\alpha f2} b_2 + C_{\alpha m2} b_3 + C_{\alpha r2} b_4 - C_{\alpha r1} b_1 - C_{\alpha f1} b_1)\, \beta_2 ... \\ + \left(m_1 v b_1 - C_{\alpha f2} \frac{b_2^2}{v} - C_{\alpha m2} \frac{b_3^2}{v} - C_{\alpha r2} \frac{b_4^2}{v} - C_{\alpha r1} \frac{b_1^2}{v} - C_{\alpha f1} \frac{b_1^2}{v} \right) \dot{\psi}_2 = ... \\ - C_{\alpha f1} b_1 \delta_1 + C_{\alpha r2} b_4 \delta_2 \end{aligned} \tag{3.60}$$

and the fourth row can be formulated as

$$\begin{aligned} (m_1 l_2^2 + I_1) \ddot{\psi}_1 + m_1 l_2 v \dot{\beta}_2 + m_1 l_2 b_1 \ddot{\psi}_2 + (C_{\alpha f1}(l_1 + l_2) - C_{\alpha r1}(l_3 - l_2))\Gamma \quad ... \\ + \left(-C_{\alpha r1} \frac{(l_3 - l_2)^2}{v} - C_{\alpha f1} \frac{(l_1 + l_2)^2}{v} \right) \dot{\psi}_1 + (C_{\alpha r1}(l_3 - l_2) - C_{\alpha f1}(l_1 + l_2))\, \beta_2 ... \\ + \left(m_1 l_2 v + C_{\alpha r1} b_1 \frac{l_3 - l_2}{v} - C_{\alpha f1} b_1 \frac{l_1 + l_2}{v} \right) \dot{\psi}_2 = ... \\ - C_{\alpha f1}(l_1 + l_2) \delta_1. \end{aligned} \tag{3.61}$$

Additionally, the derivation of (3.19) with respect to the time leads to

$$\dot{\Gamma} = \dot{\psi}_1 - \dot{\psi}_2. \tag{3.62}$$

In analogy to (2.53) and with the new state vector

$$\boldsymbol{q}_{\text{lin}} = \begin{bmatrix} \Gamma & \dot{\psi}_1 & \beta_2 & \dot{\psi}_2 \end{bmatrix}^T \tag{3.63}$$

and the input vector

$$\boldsymbol{u} = \begin{bmatrix} \delta_1 & \delta_2 \end{bmatrix}^T \tag{3.64}$$

the equations (3.59)-(3.62) can be also written as a linear system

$$\begin{bmatrix} 0 & m_1 l_2 & (m_1+m_2)v & m_1 b_1 \\ 0 & m_1 l_2 b_1 & m_1 b_1 v & m_1 b_1^2 + I_2 \\ 0 & m_1 l_2^2 + I_1 & m_1 l_2 v & m_1 l_2 b_1 \\ 1 & 0 & 0 & 0 \end{bmatrix} \dot{\boldsymbol{q}}_{\text{lin}} + \ldots$$

$$\begin{bmatrix} Y_{\beta_1} & -Y_{\dot{\psi}_1} - Y_{\beta_1}\frac{l_2}{v} & -Y_{\beta_2} - Y_{\beta_1} & (m_1+m_2)v - Y_{\dot{\psi}_2} - Y_{\beta_1}\frac{b_1}{v} \\ Y_{\beta_1} b_1 & -(Y_{\dot{\psi}_1} + Y_{\beta_1}\frac{l_2}{v}) b_1 & -N_{\beta_2} - Y_{\beta_1} b_1 & m_1 v b_1 - N_{\dot{\psi}_2} - Y_{\beta_1}\frac{b_1^2}{v} \\ N_{\beta_1} + Y_{\beta_1} l_2 & -N_{\dot{\psi}_1} - Y_{\dot{\psi}_1} l_2 - Y_{\beta_1}\frac{l_2^2}{v} - N_{\beta_1}\frac{l_2}{v} & -N_{\beta_1} - Y_{\beta_1} l_2 & m_1 l_2 v - (N_{\beta 1} + Y_{\beta_1} l_2)\frac{b_1}{v} \\ 0 & -1 & 0 & 1 \end{bmatrix} \boldsymbol{q}_{\text{lin}} \tag{3.65}$$

$$\ldots = \begin{bmatrix} Y_{\delta_1} & Y_{\delta_2} \\ Y_{\delta_1} b_1 & N_{\delta_2} \\ N_{\delta_1} + Y_{\delta_1} l_2 & 0 \\ 0 & 0 \end{bmatrix} \boldsymbol{u},$$

where the terms

$$Y_{\beta_1} = C_{f1} + C_{r1} \qquad Y_{\dot{\psi}_1} = C_{f1}\frac{l_1}{v} - C_{r1}\frac{l_3}{v} \qquad Y_{\delta_1} = -C_{f1} \tag{3.66}$$

$$N_{\beta_1} = C_{f1} l_1 - C_{r1} l_3 \qquad N_{\dot{\psi}_1} = C_{f1}\frac{l_1^2}{v} + C_{r1}\frac{l_3^2}{v} \qquad N_{\delta_1} = -C_{f1} l_1 \tag{3.67}$$

$$Y_{\beta_2} = C_{f2} + C_{m2} + C_{r2} \qquad Y_{\dot{\psi}_2} = -C_{f2}\frac{b_2}{v} - C_{m2}\frac{b_3}{v} - C_{r2}\frac{b_4}{v} \qquad Y_{\delta_2} = -C_{r2} \tag{3.68}$$

$$N_{\beta_2} = -C_{f2} b_2 - C_{m2} b_3 - C_{r2} b_4 \qquad N_{\dot{\psi}_2} = C_{f2}\frac{b_2^2}{v} + C_{m2}\frac{b_3^2}{v} + C_{r2}\frac{b_4^2}{v} \qquad N_{\delta_2} = \; C_{r2} b_4 \tag{3.69}$$

also describe the partial derivatives of the lateral tire forces and tire yaw moments [Seg57],[Sam00]. The linear system of equations (3.65) can be abbreviated with

$$\tilde{\boldsymbol{P}}\dot{\boldsymbol{q}}_{\text{lin}} + \tilde{\boldsymbol{Q}}\,\boldsymbol{q}_{\text{lin}} = \tilde{\boldsymbol{H}}\boldsymbol{u}, \tag{3.70}$$

where the super-scripted "$\sim$" marks the linearity of the matrices. It can be rearranged in state space representation,

$$\Rightarrow \dot{\boldsymbol{q}}_{\text{lin}} = \underbrace{\tilde{\boldsymbol{P}}^{-1}(-\tilde{\boldsymbol{Q}})}_{\boldsymbol{A}}\,\boldsymbol{q}_{\text{lin}} + \underbrace{\tilde{\boldsymbol{P}}^{-1}\tilde{\boldsymbol{H}}}_{\boldsymbol{B}}\,\boldsymbol{u}, \tag{3.71}$$

where $\boldsymbol{A}$ is called the "system matrix" and $\boldsymbol{B}$ is named as "input matrix" according to the system theories.

3.3.2 Linear Equations of Motion with saturated Tire Forces

In contrast to section 3.3.1, the following assumption yields:

- The lateral tires behavior is considered linear-saturated to the related slip angles: $F_y \propto \alpha$ and $F_y \leq F_{y,\max}$.

This means, that a simplified and linear model is demanded, but the lateral tire forces must be restrictable to certain maximum and minimum values. This can be accomplished regarding the second, third and fourth equation of (3.58) and using (3.62). With the state vector

$$\boldsymbol{q}_{\text{lin},F} = \begin{bmatrix} \Gamma & \dot{\psi}_1 & \beta_2 & \dot{\psi}_2 \end{bmatrix}^T \tag{3.72}$$

and the vector of the saturated input forces stated in (2.6) and (3.28)-(3.31),

$$\boldsymbol{u}_F = \begin{bmatrix} F_{yf1,\text{sat}} & F_{yr1,\text{sat}} & F_{yf2,\text{sat}} & F_{ym2,\text{sat}} & F_{yr2,\text{sat}} \end{bmatrix}^T, \tag{3.73}$$

the model equation results in

$$\begin{aligned} \underbrace{\begin{bmatrix} 0 & m_1 l_2 & (m_1+m_2)v & m_1 b_1 \\ 0 & m_1 l_2 b_1 & m_1 b_1 v & m_1 b_1^2 + I_2 \\ 0 & m_1 l_2^2 + I_1 & m_1 l_2 v & m_1 l_2 b_1 \\ 1 & 0 & 0 & 0 \end{bmatrix}}_{\tilde{\boldsymbol{P}}_F} \dot{\boldsymbol{q}}_{\text{lin},F} + \underbrace{\begin{bmatrix} 0 & 0 & 0 & (m_1+m_2)v_1 \\ 0 & 0 & 0 & m_1 v_1 b_1 \\ 0 & 0 & 0 & m_1 v_1 l_2 \\ 0 & -1 & 0 & 1 \end{bmatrix}}_{\tilde{\boldsymbol{Q}}_F} \boldsymbol{q}_{\text{lin},F} \cdots \\ = \underbrace{\begin{bmatrix} -1 & -1 & -1 & -1 & -1 \\ -b_1 & -b_1 & b_2 & b_3 & b_4 \\ -(l_1+l_2) & (l_3-l_2) & 0 & 0 & 0 \\ 0 & 0 & 0 & 0 & 0 \end{bmatrix}}_{\tilde{\boldsymbol{H}}_F} \boldsymbol{u}_F. \end{aligned} \tag{3.74}$$

This can also be rearranged in state space representation,

$$\Rightarrow \dot{\boldsymbol{q}}_{\text{lin},F} = \underbrace{\tilde{\boldsymbol{P}}_F^{-1}(-\tilde{\boldsymbol{Q}}_F)}_{\boldsymbol{A}_F} \boldsymbol{q}_{\text{lin},F} + \underbrace{\tilde{\boldsymbol{P}}_F^{-1}\tilde{\boldsymbol{H}}_F}_{\boldsymbol{B}_F} \boldsymbol{u}_F. \tag{3.75}$$

Remark 3.2. *This model description requires to pre-calculate the tire forces from the current steer angles and generalized coordinates indeed, but also allows to use other tire models.*

3.4 Roll-extended Single-Track Models

In order to improve the active safety of semitrailers with a steered rearmost axle, the roll stability has to be investigated. Therefore a nonlinear and linear model will be derived within this section.

3.4.1 Nonlinear Lateral-Yaw-Roll Model

The equations of motion for a precise single-track model of the tractor-semitrailer will be derived in the following, using the Newton-Euler approach from section 3.1. This model is intended for the validation of the linear roll-extended model, which will be introduced later in section 3.4.2.
According to figure 3.6 the position of the centers of gravity of the tractor and semitrailer can be

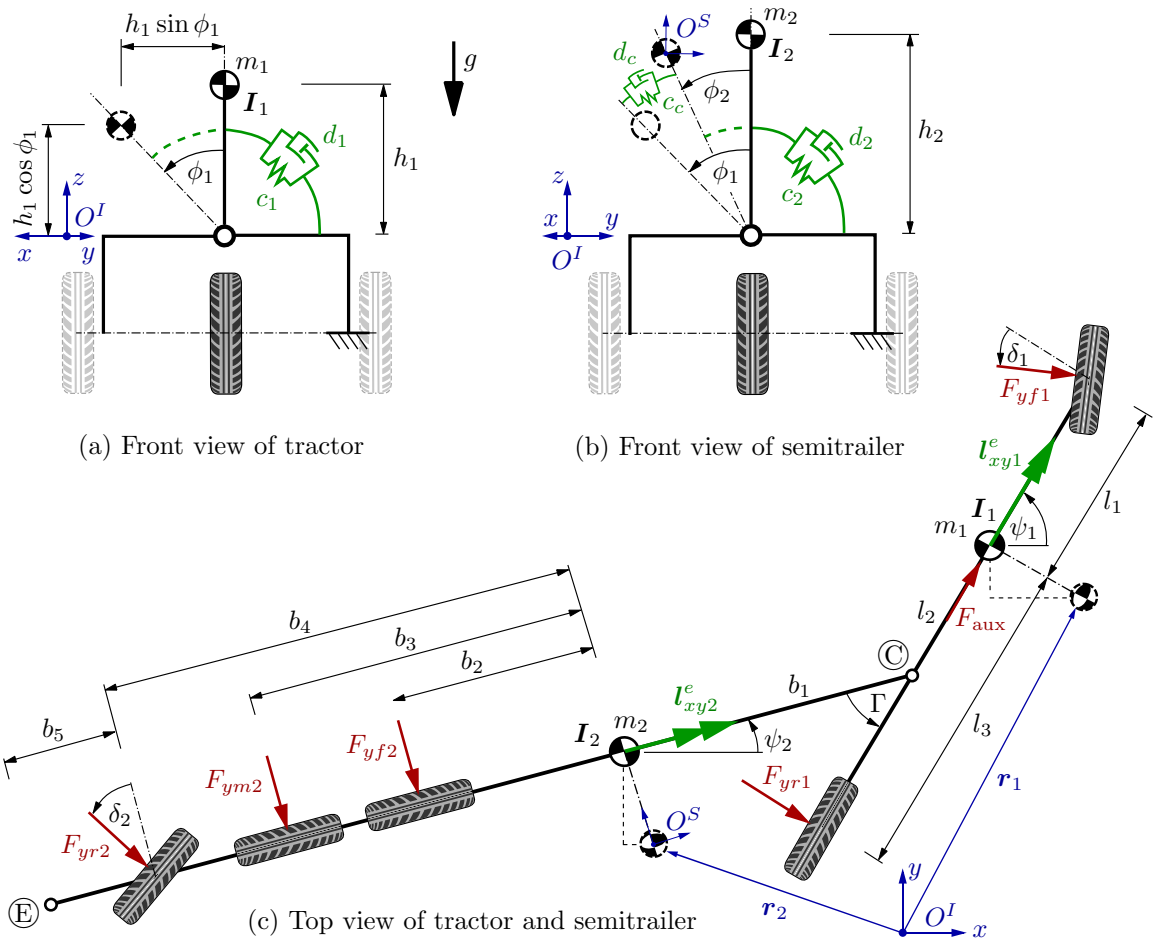

(a) Front view of tractor

(b) Front view of semitrailer

(c) Top view of tractor and semitrailer

Figure 3.6: Roll-extended single track model of the TST with a steered rearmost axle

expressed by

$$\boldsymbol{r}_1 = \begin{bmatrix} x_2 + b_1\cos\psi_2 + l_2\cos\psi_1 + h_1\sin\phi_1\sin\psi_1 \\ y_2 + b_1\sin\psi_2 + l_2\sin\psi_1 - h_1\sin\phi_1\cos\psi_1 \\ h_1\cos\phi_1 \end{bmatrix} \text{ and} \tag{3.76}$$

$$\boldsymbol{r}_2 = \begin{bmatrix} x_2 + h_2\sin\phi_2\sin\psi_2 \\ y_2 - h_2\sin\phi_2\cos\psi_2 \\ h_2\cos\phi_2 \end{bmatrix}. \tag{3.77}$$

With the generalized coordinates $\boldsymbol{q}_r = \begin{bmatrix} x_2 & y_2 & \psi_2 & \psi_1 & \phi_2 & \phi_1 \end{bmatrix}^T$, the translational Jacobian matrices $\boldsymbol{J}_{Tr1}$ and $\boldsymbol{J}_{Tr2}$ for the tractor and semitrailer can be evaluated with

$$\boldsymbol{J}_{Tr1} = \frac{\partial \boldsymbol{r}_1}{\partial \boldsymbol{q}_r} = \begin{bmatrix} 1 & 0 & -b_1\sin\psi_2 & h_1\cos\psi_1\sin\phi_1 - l_2\sin\psi_1 & 0 & h_1\cos\phi_1\sin\psi_1 \\ 0 & 1 & b_1\cos\psi_2 & h_1\sin\phi_1\sin\psi_1 + l_2\cos\psi_1 & 0 & -h_1\cos\phi_1\cos\psi_1 \\ 0 & 0 & 0 & 0 & 0 & -h_1\sin\phi_1 \end{bmatrix}, \tag{3.78}$$

$$\boldsymbol{J}_{Tr2} = \frac{\partial \boldsymbol{r}_2}{\partial \boldsymbol{q}_r} = \begin{bmatrix} 1 & 0 & h_2\cos\psi_2\sin\phi_2 & 0 & h_2\cos\phi_2\sin\psi_2 & 0 \\ 0 & 1 & h_2\sin\phi_2\sin\psi_2 & 0 & -h_2\cos\phi_2\cos\psi_2 & 0 \\ 0 & 0 & 0 & 0 & -h_2\sin\phi_2 & 0 \end{bmatrix}. \tag{3.79}$$

The local accelerations results from (3.4) with

$$\bar{\boldsymbol{a}}_{r1} = \begin{bmatrix} 2\dot{\phi}_1\dot{\psi}_1 h_1 \cos\phi_1 \cos\psi_1 - \dot{\psi}_1^2(l_2\cos\psi_1 + h_1\sin\phi_1\sin\psi_1) - \dot{\psi}_2^2 b_1\cos\psi_2 - \dot{\phi}_1^2 h_1 \sin\phi_1\sin\psi_1 \\ 2\dot{\phi}_1\dot{\psi}_1 h_1 \cos\phi_1 \sin\psi_1 - \dot{\psi}_1^2(l_2\sin\psi_1 - h_1\cos\psi_1\sin\phi_1) - \dot{\psi}_2^2 b_1\sin\psi_2 + \dot{\phi}_1^2 h_1 \cos\psi_1\sin\phi_1 \\ -\dot{\phi}_1^2 h_1\cos\phi_1 \end{bmatrix} \tag{3.80}$$

$$\bar{\boldsymbol{a}}_{r2} = \begin{bmatrix} 0 \\ 0 \\ -\ddot{\phi}_2 h_2 \mathrm{c}_{\phi_2} \end{bmatrix}. \tag{3.81}$$

The angular accelerations can be read as

$$\boldsymbol{\omega}_{rk} = \boldsymbol{J}_{Rrk}\dot{\boldsymbol{q}}_r + \bar{\boldsymbol{\omega}}_{rk} \qquad \text{and} \qquad \boldsymbol{\alpha}_{rk} = \boldsymbol{J}_{Rrk}\ddot{\boldsymbol{q}}_r + \underbrace{\dot{\boldsymbol{J}}_{Rrk}\dot{\boldsymbol{q}}_r + \frac{\partial\bar{\boldsymbol{\omega}}_{rk}}{\partial t}}_{\bar{\boldsymbol{\alpha}}_{rk}}. \tag{3.82}$$

Due to the fact that any body rotation is not explicit time dependent ($\bar{\boldsymbol{\omega}}_{r1} = \bar{\boldsymbol{\omega}}_{r2} = \boldsymbol{0}$), the vector of the corresponding angular velocity $\boldsymbol{\omega}_{r1}$ and $\boldsymbol{\omega}_{r2}$ can be described by the rotational Jacobian matrices

$$\boldsymbol{\omega}_{r1} = \begin{bmatrix} \dot{\phi}_1\cos\psi_1 \\ \dot{\phi}_1\sin\psi_1 \\ \dot{\psi}_1 \end{bmatrix} = \underbrace{\begin{bmatrix} 0 & 0 & 0 & 0 & 0 & \cos\psi_1 \\ 0 & 0 & 0 & 0 & 0 & \sin\psi_1 \\ 0 & 0 & 0 & 1 & 0 & 0 \end{bmatrix}}_{\boldsymbol{J}_{Rr1}} \dot{\boldsymbol{q}}_r \quad \text{and} \tag{3.83}$$

$$\boldsymbol{\omega}_{r2} = \begin{bmatrix} \dot{\phi}_2\cos\psi_2 \\ \dot{\phi}_2\sin\psi_2 \\ \dot{\psi}_2 \end{bmatrix} = \underbrace{\begin{bmatrix} 0 & 0 & 0 & 0 & \cos\psi_2 & 0 \\ 0 & 0 & 0 & 0 & \sin\psi_2 & 0 \\ 0 & 0 & 1 & 0 & 0 & 0 \end{bmatrix}}_{\boldsymbol{J}_{Rr2}} \dot{\boldsymbol{q}}_r. \tag{3.84}$$

The local angular accelerations yield

$$\bar{\boldsymbol{\alpha}}_{\boldsymbol{r1}} = \begin{bmatrix} -\dot{\phi}_1\dot{\psi}_1\sin\psi_1 \\ \dot{\phi}_1\dot{\psi}_1\cos\psi_1 \\ 0 \end{bmatrix} \quad \text{and} \quad \bar{\boldsymbol{a}}_{r2} = \begin{bmatrix} -\dot{\phi}_2\dot{\psi}_2\sin\psi_2 \\ \dot{\phi}_2\dot{\psi}_2 cos\psi_2 \\ 0 \end{bmatrix}. \tag{3.85}$$

Furthermore the applied moments caused by the spring-damping suspensions lead to

$$\boldsymbol{l}^e_{xy1} = \begin{bmatrix} -(d_1\dot{\phi}_1 + c_1\phi_1 + d_c(\dot{\phi}_1 - \dot{\phi}_2) + c_c(\phi_1 - \phi_2))\cos\psi_1 \\ -(d_1\dot{\phi}_1 + c_1\phi_1 + d_c(\dot{\phi}_1 - \dot{\phi}_2) + c_c(\phi_1 - \phi_2))\sin\psi_1 \\ 0 \end{bmatrix} \text{and} \tag{3.86}$$

$$\boldsymbol{l}^e_{xy2} = \begin{bmatrix} -(d_2\dot{\phi}_2 + c_2\phi_2 - d_c(\dot{\phi}_1 - \dot{\phi}_2) - c_c(\phi_1 - \phi_2))\cos\psi_2 \\ -(d_2\dot{\phi}_2 + c_2\phi_2 - d_c(\dot{\phi}_1 - \dot{\phi}_2) - c_c(\phi_1 - \phi_2))\sin\psi_2 \\ 0 \end{bmatrix}, \tag{3.87}$$

whereby the overall applied forces and moments of the tires and of the spring-damping suspensions

can be expressed in Cartesian coordinate with

$$\bar{\boldsymbol{q}}_r^e = \begin{bmatrix} F_{yf1}\mathrm{s}_{\psi_1+\delta_1} + F_{yr1}\mathrm{s}_{\psi_1} + F_{\mathrm{aux}}\mathrm{c}_{\psi_1} \\ -F_{yf1}\mathrm{c}_{\psi_1+\delta_1} - F_{yr1}\mathrm{c}_{\psi_1} + F_{\mathrm{aux}}\mathrm{s}_{\psi_1} \\ -m_1 g \\ F_{yf2}\mathrm{s}_{\psi_2} + F_{ym2}\mathrm{s}_{\psi_2} + F_{yr2}\mathrm{s}_{\psi_2+\delta_2} \\ -F_{yf2}\mathrm{c}_{\psi_2} - F_{ym2}\mathrm{c}_{\psi_2} - F_{yr2}\mathrm{c}_{\psi_2+\delta_2} \\ -m_2 g \\ -(d_1\dot{\phi}_1 + c_1\phi_1 + d_c(\dot{\phi}_1 - \dot{\phi}_2) + c_c(\phi_1 - \phi_2))\mathrm{c}_{\psi_1} \\ -(d_1\dot{\phi}_1 + c_1\phi_1 + d_c(\dot{\phi}_1 - \dot{\phi}_2) + c_c(\phi_1 - \phi_2))\mathrm{s}_{\psi_1} \\ -F_{yf1}l_1\mathrm{c}_{\delta_1} - F_{yf1}\mathrm{s}_{\delta_1}h_1\mathrm{s}_{\phi_1} + F_{yr1}l_3 \\ -(d_2\dot{\phi}_2 + c_2\phi_2 - d_c(\dot{\phi}_1 - \dot{\phi}_2) - c_c(\phi_1 - \phi_2))\mathrm{c}_{\psi_2} \\ -(d_2\dot{\phi}_2 + c_2\phi_2 - d_c(\dot{\phi}_1 - \dot{\phi}_2) - c_c(\phi_1 - \phi_2))\mathrm{s}_{\psi_2} \\ F_{yf2}b_2 + F_{ym2}b_3 + F_{yr2}b_4\mathrm{c}_{\delta_2} - F_{yr2}\mathrm{s}_{\delta_2}h_2\mathrm{s}_{\phi_2} \end{bmatrix}. \tag{3.88}$$

After some calculations the equations of motion can be written in the structure

$$\underbrace{\boldsymbol{J}_r^T\bar{\boldsymbol{M}}_r\boldsymbol{J}_r}_{\boldsymbol{M}_r}\ddot{\boldsymbol{q}} + \underbrace{\boldsymbol{J}_r^T\bar{\boldsymbol{k}}_r}_{\boldsymbol{k}_r} = \underbrace{\boldsymbol{J}_r^T\bar{\boldsymbol{q}}_r^e}_{\boldsymbol{q}_r^e} + \cancel{\underbrace{\boldsymbol{J}_r^T\bar{\boldsymbol{Q}}_r\boldsymbol{g}_r}_{\boldsymbol{q}_r^r}}. \tag{3.89}$$

This representation describes the vehicle dynamics with respect to the initial reference frame. It is not intended to use this equation for further derivations, so it is not necessary to transform it to a body-fixed reference frame. The only purpose is to validate the linear model, which will be described in the following.

3.4.2 Linear Lateral-Yaw-Roll Model

A proposal for a linear model of a single vehicle considering the roll motion, was published by *Segel* (1956). His model takes the lateral, yaw and roll motion of a vehicle at a constant velocity into account [Seg57]. Until today these equations of motion are important and they are revisited of several authors who analyze the rollover behavior of vehicles and trucks e.g. [SC98], [OBA99] or [SMC99]. Furthermore these model approach can be extended for general multi-unit vehicles, as proposed in e.g. [Sam00], [SC03] or [CC08]. In the following a linear lateral-yaw-roll model for a tractor-semitrailer (TST), based on the mentioned references will be explained and derived.
According to [Seg57] the "Dimensional Equations of Motion" describe the equilibrium of the forces in the lateral direction (y), the yaw momentum (around z) and the roll momentum (around x) of a tractor vehicle

$$m_1 v(\dot{\psi}_1 + \dot{\beta}_1) - m_1\ddot{\phi}_1 h_1 = Y_{\beta_1}\beta_1 + Y_{\dot{\psi}_1}\dot{\psi}_1 + Y_{\delta_1}\delta_1 + F_c \tag{3.90}$$

$$I_1\ddot{\psi}_1 - I_{xz1}\ddot{\phi}_1 = N_{\beta_1}\beta_1 + N_{\dot{\psi}_1}\dot{\psi}_1 + N_{\delta_1}\delta_1 - F_c\, l_2 \tag{3.91}$$

$$(I_{xx1} + m_1 h_1^2)\ddot{\phi}_1 - m_1 v(\dot{\psi}_1 + \dot{\beta}_1)h_1 - I_{xz1}\ddot{\psi}_1 = m_1 g h_1\phi_1 - c_1\phi_1 - d_1\dot{\phi}_1 - c_c(\phi_1 - \phi_2) - F_c z_1, \tag{3.92}$$

where F_c represents the internal force at the hitch. The tire forces at the front and rear axle (F_{yf1} and F_{yr1}) can be linearly described by the terms Y_{β_1}, $Y_{\dot{\psi}_1}$ and Y_{δ_1}, the caused torsional moment by N_{β_1}, $N_{\dot{\psi}_1}$ and N_{δ_1}. They are defined in the equations (3.66)-(3.69). As a simplification the sprung and un-sprung masses are not distinguished. Figure 3.7(a) illustrates the nonlinear kinematic relation between the tractor frame, the tractor's center of gravity and the kinematic constraint to the coupled semitrailer in consideration of the roll motion around the angle ϕ_1. Since a linear model has to be derived, the trigonometric terms can be linearized as clarified in figure 3.7(b). The free body diagram is shown in figure 3.8.

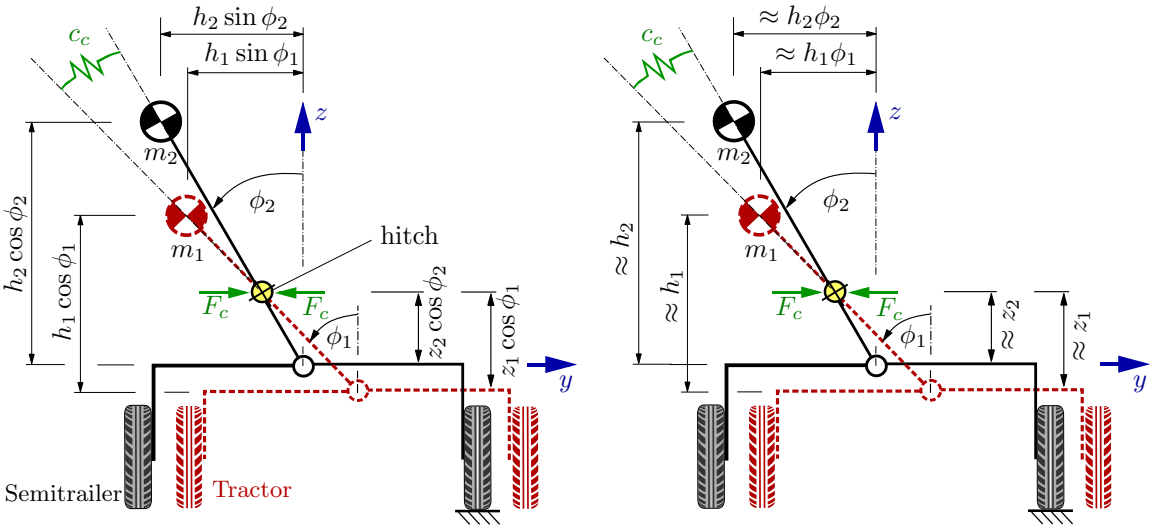

(a) Nonlinear kinematic (b) Linearized kinematic

Figure 3.7: Kinematic of the tractor-semitrailer coupling-hitch in the horizontal and vertical direction.

In analogy, the equations for the semitrailer can be written as

$$m_2 v(\dot{\psi}_2 + \dot{\beta}_2) - m_2 \ddot{\phi}_2 h_2 = Y_{\beta_2}\beta_2 + Y_{\dot{\psi}_2}\dot{\psi}_2 + Y_{\delta_2}\delta_2 - F_c \tag{3.93}$$

$$I_2 \ddot{\psi}_2 - I_{xz2}\ddot{\phi}_2 = N_{\beta_2}\beta_2 + N_{\dot{\psi}_2}\dot{\psi}_2 + N_{\delta_2}\delta_2 - F_c\, b_1 \tag{3.94}$$

$$(I_{xx2} + m_2 h_2^2)\ddot{\phi}_2 - m_2 v(\dot{\psi}_2 + \dot{\beta}_2)h_2 - I_{xz2}\ddot{\psi}_2 = m_2 g h_2 \phi_2 - c_2\phi_2 - d_2\dot{\phi}_2 + c_c(\phi_1 - \phi_2) + F_c z_2. \tag{3.95}$$

Remark 3.3. *For the following derivatives, substitutions and rearrangements a* MATLAB*-Code is provided in A.3.*

The body slip angle of the tractor β_1 and the slip angular velocity $\dot{\beta}_1$ can be substituted using the kinematic coupling constraints (3.49) and (3.50).
Furthermore the internal hitch force F_c can either be eliminated by using ...

... the lateral equations of the tractor and semitrailer (3.90)→(3.93)

$$\begin{aligned} m_1 l_2 \ddot{\psi}_1 + (m_2 + m_1)v\dot{\beta}_2 + m_1 b_1 \ddot{\psi}_2 + m_1(z_1 - h_1)\ddot{\phi}_1 - (m_1 z_2 + m_2 h_2)\ddot{\phi}_2 = \ldots \\ \ldots - Y_{\beta_1}\Gamma + (Y_{\dot{\psi}_1} + Y_{\beta_1}\frac{l_2}{v})\dot{\psi}_1 + (Y_{\beta_2} + Y_{\beta_1})\beta_2 + (Y_{\dot{\psi}_2} + Y_{\beta_1}\frac{b_1}{v} - (m_1 + m_2)v)\dot{\psi}_2 \ldots \\ \ldots + Y_{\beta_1}\frac{z_1}{v}\dot{\phi}_1 - Y_{\beta_1}\frac{z_2}{v}\dot{\phi}_2 + Y_{\delta_1}\delta_1 + Y_{\delta_2}\delta_2, \end{aligned} \tag{3.96}$$

... the lateral equation of the tractor and the yaw equation of the semitrailer (3.90)→(3.94)

$$\begin{aligned} m_1 b_1 l_2 \ddot{\psi}_1 + m_1 b_1 v\dot{\beta}_2 + (m_1 b_1^2 + I_2)\ddot{\psi}_2 + m_1 b_1(z_1 - h_1)\ddot{\phi}_1 - (I_{xz2} + m_1 b_1 z_2)\ddot{\phi}_2 = \\ -Y_{\beta_1} b_1 \Gamma + (Y_{\dot{\psi}_1} + Y_{\beta_1}\frac{l_2}{v})b_1\dot{\psi}_1 + (N_{\beta_2} + Y_{\beta_1} b_1)\beta_2 + (N_{\dot{\psi}_2} + Y_{\beta_1}\frac{b_1^2}{v} - m_1 v b_1)\dot{\psi}_2 \\ + Y_{\beta_1} b_1 \frac{z_1}{v_1}\dot{\phi}_1 - Y_{\beta_1} b_1 \frac{z_2}{v_2}\dot{\phi}_2 + Y_{\delta_1} b_1 \delta_1 + N_{\delta_2}\delta_2, \end{aligned} \tag{3.97}$$

... the lateral and the yaw equation of the tractor (3.90)→(3.91)

$$\begin{aligned}(m_1 l_2^2 + I_1)\ddot{\psi}_1 + m_1 l_2 v\dot{\beta}_2 + m_1 l_2 b_1 \ddot{\psi}_2 + (m_1 l_2(z_1 - h_1) - I_{xz1})\ddot{\phi}_1 - m_1 l_2 z_2 \ddot{\phi}_2 = \\ -(N_{\beta_1} + Y_{\beta_1} l_2)\Gamma + (N_{\dot{\psi}_1} + Y_{\dot{\psi}_1} l_2 + Y_{\beta_1}\frac{l_2^2}{v} + N_{\beta_1}\frac{l_2}{v})\dot{\psi}_1 + (N_{\beta_1} + Y_{\beta_1} l_2)\beta_2 + \\ ((N_{\beta_1} + Y_{\beta_1} l_2)\frac{b_1}{v} - m_1 v l_2)\dot{\psi}_2 + (Y_{\beta_1} l_2 + N_{\beta_1})\frac{z_1}{v}\dot{\phi}_1 - (N_{\beta_1} + Y_{\beta_1} l_2)\frac{z_2}{v}\dot{\phi}_2 \\ +(N_{\delta_1} + Y_{\delta_1} l_2)\delta_1,\end{aligned} \tag{3.98}$$

... the lateral and the roll equation of the tractor (3.90)→(3.92)

$$\begin{aligned}(m_1(z_1 - h_1)l_2 - I_{xz1})\ddot{\psi}_1 + m_1(z_1 - h_1)v\dot{\beta}_2 + m_1(z_1 - h_1)b_1\ddot{\psi}_2 \\ +(I_{xx1} + m_1(h_1^2 + z_1^2) - 2m_1 h_1 z_1)\ddot{\phi}_1 + m_1 z_2(h_1 - z_1)\ddot{\phi}_2 = \\ -Y_{\beta_1} z_1\Gamma + z_1(Y_{\beta_1}\frac{l_2}{v} + Y_{\dot{\psi}_1})\dot{\psi}_1 + Y_{\beta_1} z_1\beta_2 + (m_1 v(h_1 - z_1) + Y_{\beta_1} z_1\frac{b_1}{v})\dot{\psi}_2 \\ +(Y_{\beta_1}\frac{z_1^2}{v} - d_1)\dot{\phi}_1 + (m_1 g h_1 - c_1 - c_c)\phi_1 - Y_{\beta_1} z_1\frac{z_2}{v}\dot{\phi}_2 + c_c\phi_2 + Y_{\delta_1} z_1\delta_1,\end{aligned} \tag{3.99}$$

... or the lateral equation of the tractor and the roll equation of the semitrailer (3.90)→(3.95)

$$\begin{aligned}-m_1 z_2 l_2\ddot{\psi}_1 - (m_2 h_2 + m_1 z_2)v\dot{\beta}_2 - (m_1 z_2 b_1 + I_{xz2})\ddot{\psi}_2 \\ m_1 z_2(h_1 - z_1)\ddot{\phi}_1 + (I_{xx2} + m_2 h_2^2 + m_1 z_2^2)\ddot{\phi}_2 = \\ Y_{\beta_1} z_2\Gamma - z_2(Y_{\beta_1}\frac{l_2}{v} + Y_{\dot{\psi}_1})\dot{\psi}_1 - Y_{\beta_1} z_2\beta_2 + (m_2 h_2 v + m_1 v z_2 - Y_{\beta_1} z_2\frac{b_1}{v})\dot{\psi}_2 \\ -Y_{\beta_1} z_2\frac{z_1}{v}\dot{\phi}_1 + c_c\phi_1 + (Y_{\beta_1}\frac{z_2^2}{v} - d_2)\dot{\phi}_2 + (m_2 g h_2 - c_2 - c_c)\phi_2 - Y_{\delta_1} z_2\delta_1.\end{aligned} \tag{3.100}$$

Moreover, the derivation of (3.19) with respect to the time leads to the additional equation

$$\dot{\Gamma} = \dot{\psi}_1 - \dot{\psi}_2. \tag{3.101}$$

The equations (3.96)-(3.101) can be rearranged in matrix form by using the state vector

$$\boldsymbol{q}_{\mathrm{lin},r} = \begin{bmatrix}\Gamma & \dot{\psi}_1 & \beta_2 & \dot{\psi}_2 & \dot{\phi}_1 & \phi_1 & \dot{\phi}_2 & \phi_2\end{bmatrix}^T \tag{3.102}$$

and the input vector

$$\boldsymbol{u} = \begin{bmatrix}\delta_1 & \delta_2\end{bmatrix}^T. \tag{3.103}$$

This results in equation (3.105) which is reproducible with the MATLAB-Code of A.3. This model equations can be used for the simulation-process, but the roll angles ϕ_1 and ϕ_2 does not directly represent the risk of a tractor and Semitrailer rollover. Therefore a "Load Transfer Ratio" can be introduced.

3.4.3 Load Transfer Ratio (LTR)

A performance index is needed in order to quantify the rollover risk. According to [AO98], [AO99] or [CP01] a rollover coefficient or so-called "Load Transfer Ratio (LTR)" can be used, which is defined as

$$\mathrm{LTR} \quad = \quad \frac{F_{z,R} - F_{z,L}}{F_{z,R} + F_{z,L}}, \tag{3.104}$$

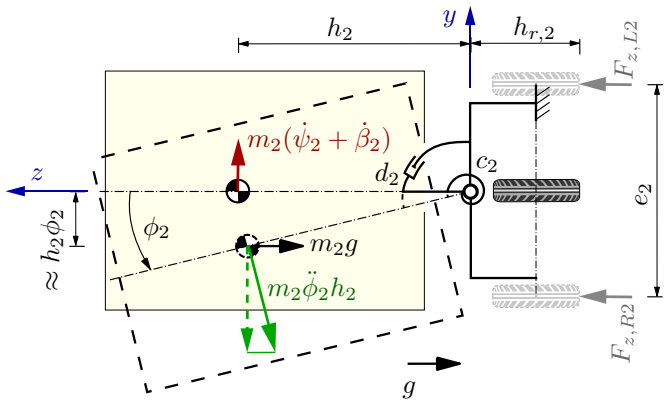

(a) Front view of Semitrailer

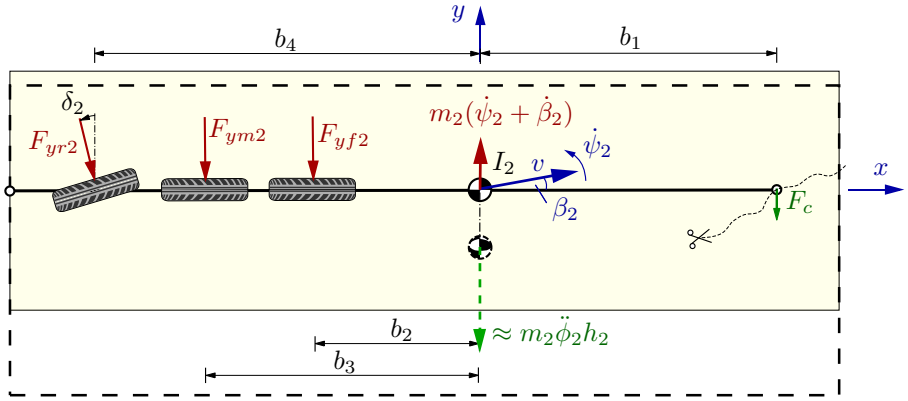

(b) Top view of Semitrailer

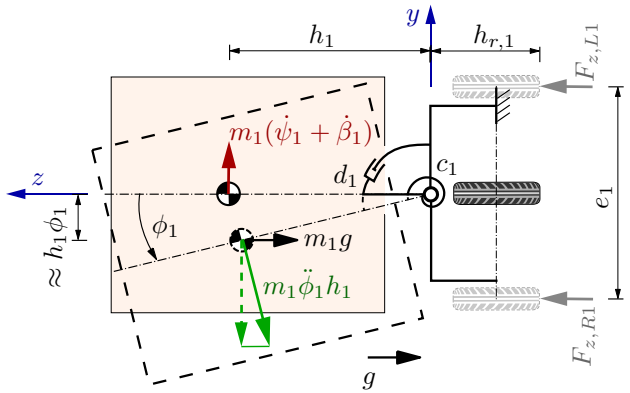

(c) Front view of Tractor

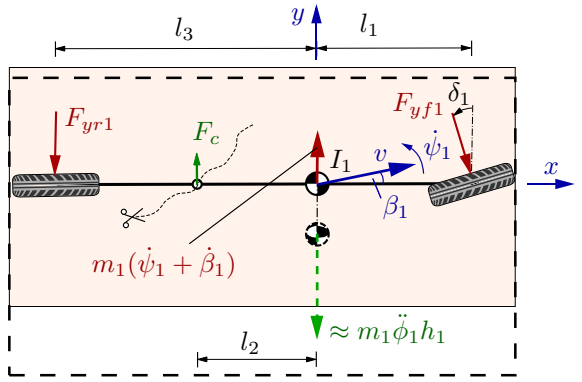

(d) Top view of Tractor

Figure 3.8: Five-DOF tractor-semitrailer model, which includes a rollover consideration.

$$\underbrace{\begin{bmatrix} 0 & m_1 l_2 & (m_1+m_2)v & m_1 b_1 & m_1(z_1-h_1) & 0 & -(m_1 z_2+m_2 h_2) & 0 \\ 0 & m_1 l_2 b_1 & m_1 b_1 v & m_1 b_1^2+I_2 & m_1 b_1(z_1-h_1) & 0 & -(I_{xz2}+m_1 b_1 z_2) & 0 \\ 0 & m_1 l_2^2+I_1 & m_1 l_2 v & m_1 l_2 b_1 & m_1 l_2(z_1-h_1)-I_{xz1} & 0 & -m_1 l_2 z_2 & 0 \\ 1 & 0 & 0 & 0 & 0 & 0 & 0 & 0 \\ 0 & m_1(z_1-h_1)l_2-I_{xz1} & m_1 v(z_1-h_1) & m_1(z_1-h_1)b_1 & I_{xx1}+m_1(h_1^2+z_1^2)-2m_1 h_1 z_1 & 0 & m_1 z_2(h_1-z_1) & 0 \\ 0 & -m_1 z_2 l_2 & -(m_2 h_2+m_1 z_2)v & -(m_1 z_2 b_1+I_{xz2}) & m_1 z_2(h_1-z_1) & 0 & I_{xx2}+m_2 h_2^2+m_1 z_2^2 & 0 \\ 0 & 0 & 0 & 0 & 0 & 1 & 0 & 0 \\ 0 & 0 & 0 & 0 & 0 & 0 & 0 & 1 \end{bmatrix}}_{\tilde{\boldsymbol{P}}_r} \begin{bmatrix} \dot{\Gamma} \\ \ddot{\psi}_1 \\ \dot{\beta}_2 \\ \ddot{\psi}_2 \\ \dot{\phi}_1 \\ \dot{\psi}_1 \\ \ddot{\phi}_2 \\ \dot{\phi}_2 \end{bmatrix} = \ldots$$

$$\underbrace{\begin{bmatrix} -Y_{\beta_1} & Y_{\dot{\psi}_1}+Y_{\beta_1}\frac{l_2}{v} & Y_{\beta_2}+Y_{\beta_1} & Y_{\dot{\psi}_2}+Y_{\beta_1}\frac{b_1}{v}-(m_1+m_2)v & Y_{\beta_1}\frac{z_1}{v} & 0 & -Y_{\beta_1}\frac{z_2}{v} & 0 \\ -Y_{\beta_1} b_1 & (Y_{\dot{\psi}_1}+Y_{\beta_1}\frac{l_2}{v})b_1 & N_{\beta_2}+Y_{\beta_1} b_1 & N_{\psi_2}+Y_{\beta_1}\frac{b_1^2}{v}-m_1 v b_1 & Y_{\beta_1} b_1\frac{z_1}{v} & 0 & -Y_{\beta_1} b_1\frac{z_2}{v} & 0 \\ -(N_{\beta_1}+Y_{\beta_1} l_2) & N_{\psi_1}+Y_{\dot{\psi}_1} l_2+Y_{\beta_1}\frac{l_2^2}{v}+N_{\beta_1}\frac{l_2}{v} & N_{\beta_1}+Y_{\beta_1} l_2 & (N_{\beta_1}+Y_{\beta_1} l_2)\frac{b_1}{v}-m_1 l_2 v & (N_{\beta_1}+Y_{\beta_1} l_2)\frac{z_1}{v} & 0 & -(N_{\beta_1}+Y_{\beta_1} l_2)\frac{z_2}{v} & 0 \\ 0 & 1 & 0 & -1 & 0 & 0 & 0 & 0 \\ -Y_{\beta_1} z_1 & (Y_{\beta_1}\frac{l_2}{v}+Y_{\dot{\psi}_1})z_1 & Y_{\beta_1} z_1 & m_1 v(h_1-z_1)+Y_{\beta_1} z_1\frac{b_1}{v} & Y_{\beta_1}\frac{z_1^2}{v}-d_1 & m_1 g h_1-c_1-c_c & -Y_{\beta_1} z_1\frac{z_2}{v} & c_c \\ Y_{\beta_1} z_2 & -(Y_{\beta_1}\frac{l_2}{v}+Y_{\dot{\psi}_1})z_2 & -Y_{\beta_1} z_2 & m_1 v z_2+m_2 v h_2-Y_{\beta_1} z_2\frac{b_1}{v} & -Y_{\beta_1} z_2\frac{z_1}{v} & c_c & Y_{\beta_1}\frac{z_2^2}{v}-d_2 & m_2 g h_2-c_2-c_c \\ 0 & 0 & 0 & 0 & 1 & 0 & 0 & 0 \\ 0 & 0 & 0 & 0 & 0 & 0 & 1 & 0 \end{bmatrix}}_{-\tilde{\boldsymbol{Q}}_r} \begin{bmatrix} \Gamma \\ \dot{\psi}_1 \\ \beta_2 \\ \dot{\psi}_2 \\ \dot{\phi}_1 \\ \phi_1 \\ \dot{\phi}_2 \\ \phi_2 \end{bmatrix} \quad (3.105)$$

$$\ldots + \underbrace{\begin{bmatrix} Y_{\delta_1} & Y_{\delta_2} \\ Y_{\delta_1} b_1 & N_{\delta_2} \\ N_{\delta_1}+Y_{\delta_1} l_2 & 0 \\ 0 & 0 \\ -Y_{\delta_1} z_1 & 0 \\ -Y_{\delta_1} z_2 & 0 \\ 0 & 0 \\ 0 & 0 \end{bmatrix}}_{\tilde{\boldsymbol{H}}_r} \boldsymbol{u},$$

In analogy to equation (3.71) it can also be formulated in the state-space representation

$$\Rightarrow \dot{\boldsymbol{q}}_{\mathrm{lin},r} = \underbrace{\tilde{\boldsymbol{P}}_r^{-1}(-\tilde{\boldsymbol{Q}}_r)}_{\boldsymbol{A}_r} \boldsymbol{q}_{\mathrm{lin},r} + \underbrace{\tilde{\boldsymbol{P}}_r^{-1}\tilde{\boldsymbol{H}}_r}_{\boldsymbol{B}_r} \boldsymbol{u}. \quad (3.106)$$

whereby $F_{z,R}$ is the sum of the vertical forces on the right tires and $F_{z,L}$ is the sum of the vertical forces on the left tires (with respect to the back view of the concerning vehicle). The LTR ranges from $+1$ to -1. In case of a wheel lift, the vertical tire force on that side will disappear and the LTR will become ± 1. For driving straight, it will result in LTR $= 0$. As recommended in [vdV11], the vertical tire forces for the semitrailer can be estimated by

$$F_{z,R2} = \frac{m_2 b_1}{e_2(b_1+b_3)}\Big(\frac{e_2\, g}{2} + a_{y,2}\big(h_{r,2} + h_2 \cos\phi_2\big)\Big) \tag{3.107}$$

$$F_{z,L2} = \frac{m_2 b_1}{e_2(b_1+b_3)}\Big(\frac{e_2\, g}{2} - a_{y,2}\big(h_{r,2} + h_2 \cos\phi_2\big)\Big), \tag{3.108}$$

with the lateral acceleration of the semitrailer

$$a_{y,2} = v\,(\dot\beta_2 + \dot\psi_2) - h_2\ddot\phi_2, \tag{3.109}$$

the track width e_2 and the height of the roll center $h_{r,2}$ of the semitrailer. These relations results from the force and the moments equilibrium. All the geometric distances are illustrated in figure 3.8(a).

3.5 SimPack Model

Since a real TST system with all the sensors and the actuator for the steerable rearmost axle is not available for this work, the performance of the steering strategies controllers will be verified on a detailed and verified multi-body simulation model. As shown in figure 3.9, it is implemented in the numerical multibody simulation software "SimPack". This model is provided by previous and related research projects. It takes all the relevant sub-systems into account, which form the vehicle structure and characterize several dynamics and forces, e.g. for braking forces, Ackermann steering geometry, additional constraints etc. Moreover, the multibody model relies on a very precise tire model, which is based upon look-up tables identified experimentally. It also provides a "Co-Simulation Interface" (simat_8904_r2010a.dll) to Simulink, which was tested with MATLAB 7.12.0 (R2011a) and can be used to obtain the measurements from the system and to apply the control actions, respectively. At the end of every simulation, all the data is available in the workspace, ready for post-processing and analyzing.

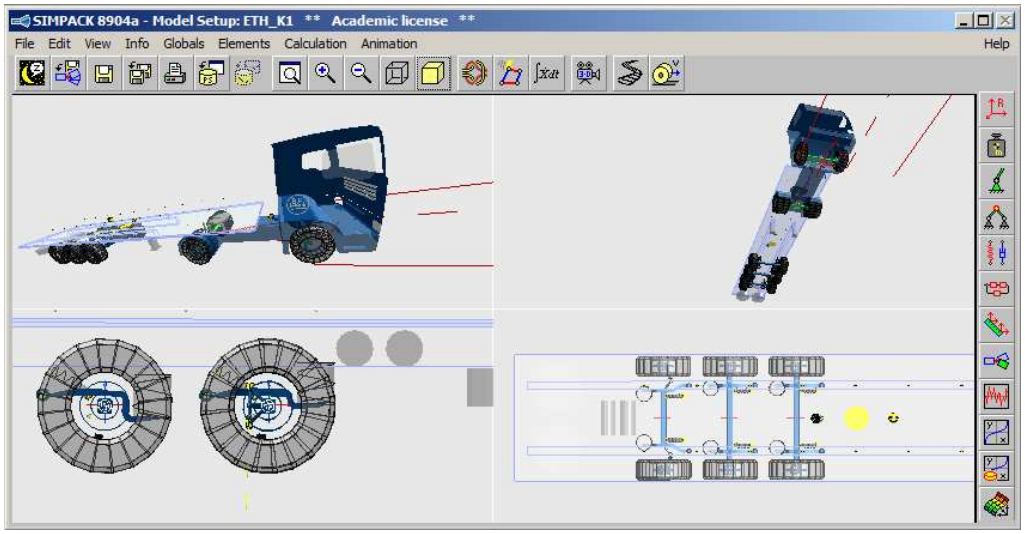

Figure 3.9: Screenshot of the multi-body simulation SimPack model.

Chapter 4

Control Strategies

The developed control strategies are derived and introduced within this chapter. On the one hand controllers for the tractor steering are designed in order to follow a given path constantly and on the other hand trailer-steering strategies for the track-tracing of the semitrailer are proposed. Finally, a controller will be proposed which intervenes with the semitrailer steering and aims to reduce the risk of a trailer rollover.

4.1 Virtual Driver

Since the tractor-semitrailer models should follow a given path with a constant velocity, it is necessary to design a submodel called "virtual driver". During the simulation, it has to emulate the behavior of a human driver, who tries to keep a certain tractor velocity $\boldsymbol{v}_1$ and adapt the front steer angle of the tractor δ_1 to stay on a defined path.

4.1.1 Cruise Control

This section describes the feedback control system, which automatically controls the speed of the semitrailer unit to a specified velocity called v_{target}. Figure 4.1 shows the structure of the closed loop, where $\sum_{\text{NonLin}}$ characterizes the nonlinear tractor-semitrailer system derived by section 3.1 and $PID(s)$ denotes a standard proportional-integral-derivative (PID) control.

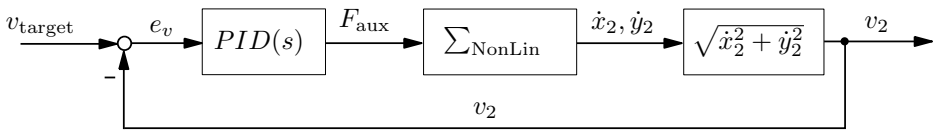

Figure 4.1: Feedback control system for the cruise control.

It will be used to gain the velocity error e_v in order to apply an auxiliary force on the tractor in the longitudinal direction. The scalar velocity v_2 of the semitrailer can be obtained from the system output, independently of the represented reference frame. In this example the target velocity is constant, so that the auxiliary force only compensates the dissipation results from tire slip forces during the cornering.
The velocity of the SimPack-model according to section 3.5 has to be controlled by opening the throttle (0...100%) or pushing the brake (0...100%). In order to control the dynamics of the actors independently, the changed structure of the closed loop results in two $PID(s)$ controls as shown in figure 4.2. Both contain a saturation to the positive range of 0...100%. So if the velocity of the

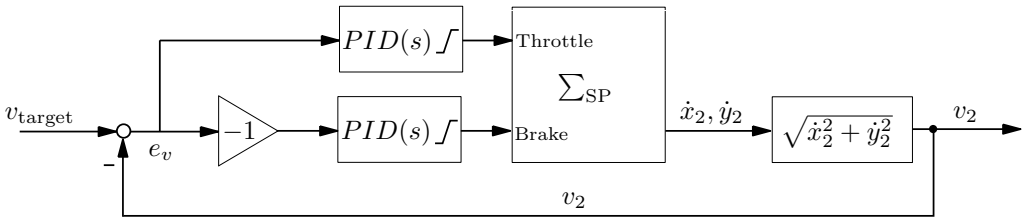

Figure 4.2: Feedback control system for the cruise control.

semitrailer is greater than the target velocity ($e_v < 0$), the break will be pushed and the throttle will be ignored.

Remark 4.1. *Since the linear model derived in section 3.3 is derived with the assumption of a constant body velocity, this control system is not necessary for simulating the linear system.*

4.1.2 Tractors Steering Control

Before the design-process of a steering control for the front angle of the tractor, the definition of the target path has to be discussed. A path can be discretized by a number of path points. Their interconnection shapes a polygon, which describes a certain path. In order to generate various types of paths, during this thesis the following functions are developed:

- *pathAddStraight(...)* $\rightarrow$ generate multiple points on a straight path;
- *pathAddArc(*radius,*...)* $\rightarrow$ generate multiple points on an arg path, specified by a given the radius;
- *pathAddSin(...)* $\rightarrow$ generate multiple points on a sine path.

A hypothetical created polygon of the so-called "target-path" is depicted in figure 4.3.
The target steer angle of the tractor during each simulation time-step depends on the tractor's position, orientation and the given target path-polygon. So the strategy for the steering controller is to detect and follow the path-polygon in the close environment of the tractor's front, similarly as it does a human.

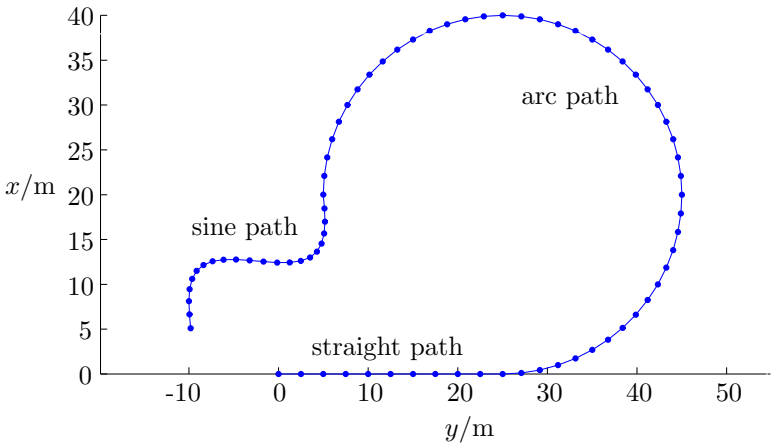

Figure 4.3: A hypothetical target-path polygon, defined by path points and created by developed the functions.

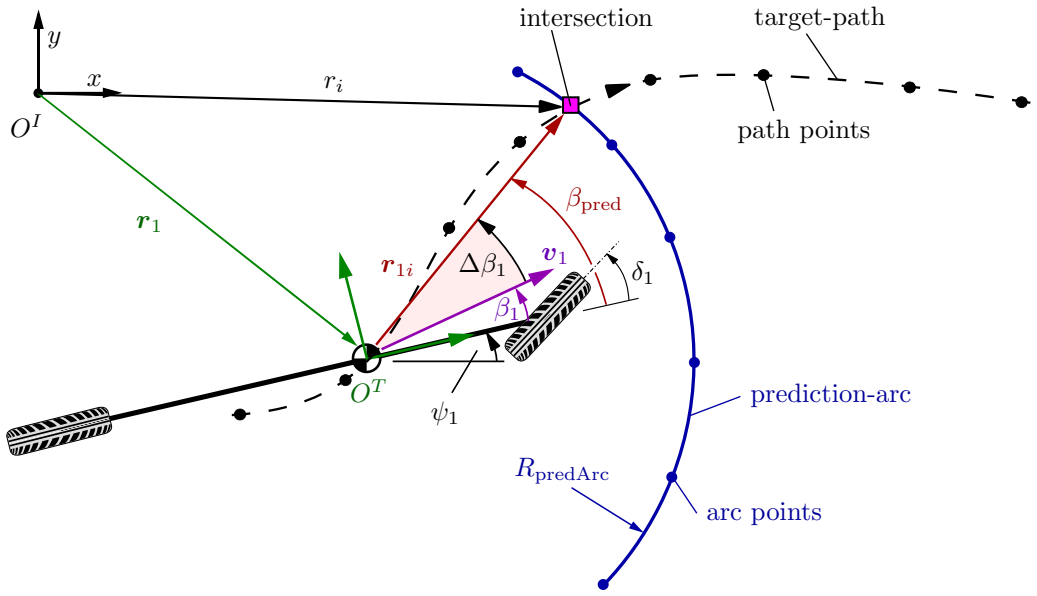

Figure 4.4: Strategy of the virtual drivers controller of the tractor front steer angle δ_1.

Figure 4.4 proposes the usage of a "prediction-arc", which is relatively defined by the tractors center of gravity, the radius R_{predArc} and a wide arc length. In analogy to the target-path, it is defined by arc points which specify a polygon. The intersection r_i of the prediction-arc and the target-path indirectly determines the steer angle δ_1. Since the tractor should move in the direction of r_i, the virtual driver has to calculate the deviation angle $\Delta\beta_1$ and use it for the steering control. In detail, the intersection with respect to the tractors coordinate system O^T can be described with

$$ {}_T\boldsymbol{r}_{1i} = {}_T\boldsymbol{\phi}_I \boldsymbol{r}_{1i} = \phi_I(\boldsymbol{r}_i - \boldsymbol{r}_1), \tag{4.1} $$

where the transformation matrix ${}_T\boldsymbol{\phi}_I$ is defined in (3.15) and $\boldsymbol{r}_1$ is the tractor position vector. The related orientation angle β_{pred} can be computed by the arctangent of the y/x-coordinate tuples. In conclusion, the difference between β_{pred} and the body slip angle β_1 results in

$$ \Delta\beta_1 = \beta_{\text{pred}} - \beta_1. \tag{4.2} $$

This quantity will be used to influence the steer angle δ_1 of the tractor's front wheel to command the orientation of the tractor in the direction of ${}_T\boldsymbol{r}_{1i}$, as it is structured in figure 4.5. The block called $\sum_{\text{TST}}$ can characterize any of the regarded TST models, since this control strategy is independent of the model itself.

The intersection of the two polygons has to be calculated during each simulation time-step. Therefore an algorithm is developed, which calculates the intersection using the theory of the linear algebra. The equations of two lines $(\boldsymbol{g}_a \cap \boldsymbol{g}_b)$, characterized by position vectors $\boldsymbol{r}_a$ and $\boldsymbol{r}_b$ and direction vectors $\boldsymbol{n}_a$ and $\boldsymbol{n}_b$, can be written as

$$ \boldsymbol{g}_a(\alpha_a) = \boldsymbol{r}_a + \alpha_a \boldsymbol{n}_a \quad \text{and} \quad \boldsymbol{g}_b(\alpha_b) = \boldsymbol{r}_b + \alpha_b \boldsymbol{n}_b, \tag{4.3} $$

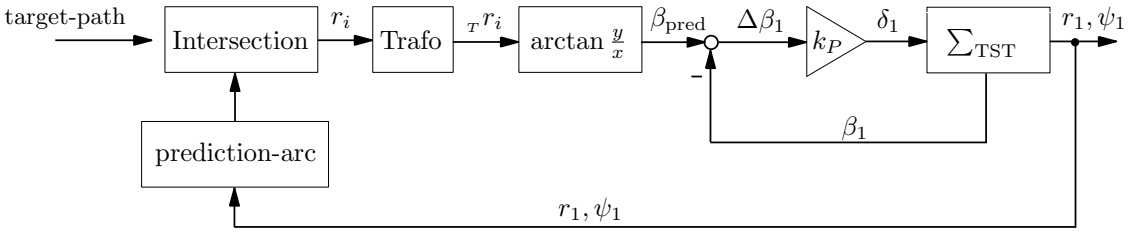

Figure 4.5: Feedback control system for the tractors steering control.

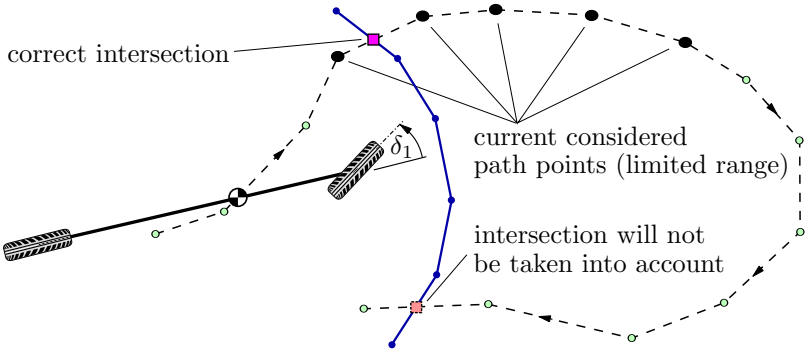

Figure 4.6: Considered path point of the virtual driver are limited to a certain range.

where α_a and α_b are the line parameters. If the two lines intersect ($\boldsymbol{g}_a \stackrel{!}{=} \boldsymbol{g}_b$), there will exist a solution for the inhomogeneous linear system of equations in the form of

$$\begin{bmatrix} \alpha_{ai} \\ \alpha_{bi} \end{bmatrix} = \begin{bmatrix} -\boldsymbol{n}_a & \boldsymbol{n}_b \end{bmatrix}^{-1} (\boldsymbol{r}_a - \boldsymbol{r}_b). \tag{4.4}$$

Ensuring that the lines are only considered in the range between the polygon points, the position vector $\boldsymbol{r}_a^{(k)}$ and direction vector $\boldsymbol{n}_a^{(k)}$ has to be redefined for each intersection calculation at each k^{th}-polygon line part. If the parameters are in the range of

$$0 \leq \alpha_{ai} \leq 1 \quad \text{and} \quad 0 \leq \alpha_{bi} \leq 1, \tag{4.5}$$

the polygon intersection will result from (4.3) with

$$\boldsymbol{r}_i = \boldsymbol{r}_a^{(k)} + \alpha_{ai}\, \boldsymbol{n}_a^{(k)}. \tag{4.6}$$

In some cases there exist additional intersections between the prediction-arc and previous or subsequent target-path parts. This can be prevented with the consideration of path points in a limited range, starting at the recent path point, which took part for the previous calculation of the intersection. Figure 4.6 shows these relations and also clarifies, that the paths are treated as a polygon.

4.2 Steering Strategies for the Track-Tracing of a Semitrailer

The main focus of this thesis is to improve the semitrailer behavior using rear axle steering. In the following, some control strategies for the semitrailer is designed, tracing the trajectory of the coupling point with its rear end. Additionally, an “active rollover damping”-controller will be proposed.

4.2.1 Feedforward Controller for a Steady-State Turn

In section 2.2.1some proposals for a horizontal trailer control strategy according to previous theses are introduced. In contrast the following steady-state approach takes the centrifugal forces and also the tire forces of both, the non-steerable and steerable axles directly into account. A similar steady-state controller was also designed for reversing maneuvers in [Viv12].
The method is based on some assumptions of the equivalent wheelbase derivative as reported in section 2.1.3. Thereby, the influence of non-steered and steered axles of a vehicle will be regarded simultaneously. Additionally, an approximation for the slip angle estimation is proposed, which can also be transferred to a coupled semitrailer. Figure 4.7 illustrates the TST in a steady-state turn. If it is aimed that the trailer end Ⓔ traces the trajectory of the coupling point Ⓒ during a steady turn reliably, the following geometric conditions will result (assuming small angles),

$$\alpha_{f2} = \tan\left(\frac{b_2 - s_R}{R'}\right) \approx \frac{b_2 - s_R}{R'} \tag{4.7}$$

$$\alpha_{m2} = \tan\left(\frac{b_3 - s_R}{R'}\right) \approx \frac{b_3 - s_R}{R'} \tag{4.8}$$

$$-\delta_2 - \alpha_{r2} = \tan\left(\frac{b_4 - s_R}{R'}\right) \approx \frac{b_4 - s_R}{R'}. \tag{4.9}$$

This can be derived, since the orientation of the tire velocity is always perpendicular to the instantaneous center of rotation (i.c.r.). The distance between the center of gravity and the geometrical

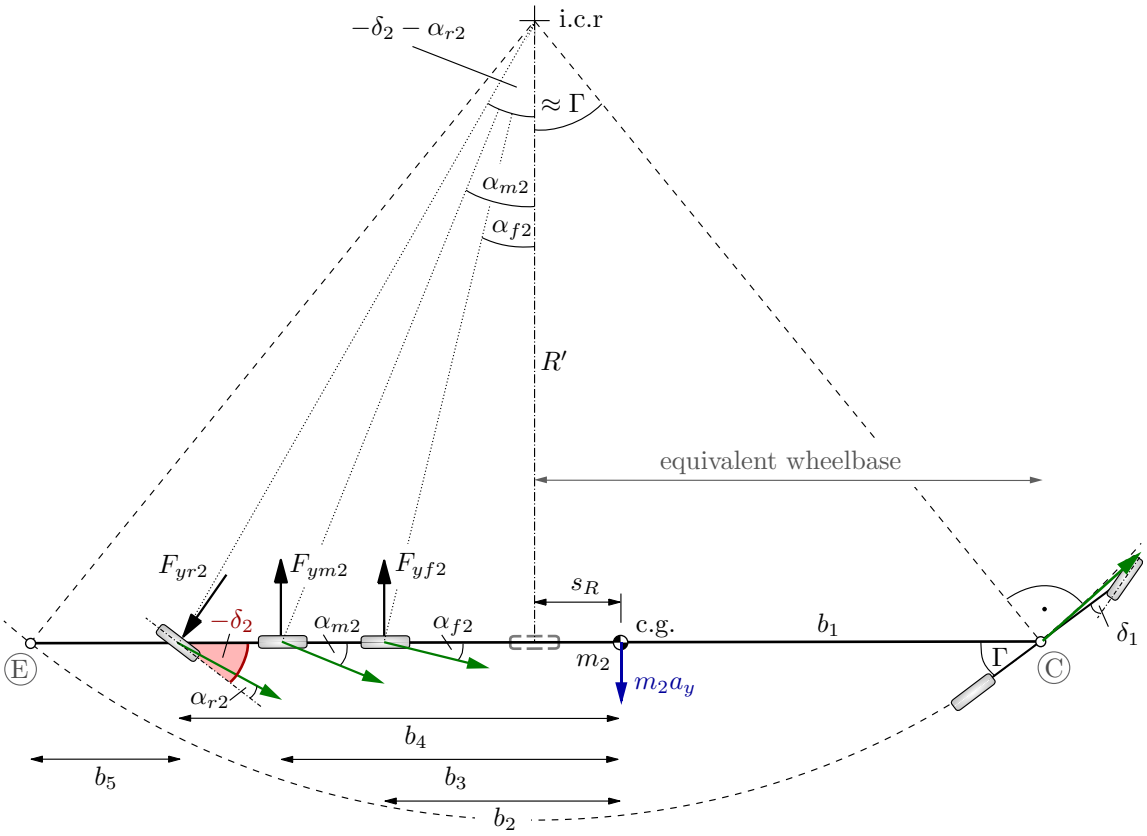

Figure 4.7: Strategy of semitrailer tracking during a steady state turn.

center of Ⓒ and Ⓔ is temporarily denoted with s_R and can be calculated with

$$s_R = \frac{b_4 + b_5 - b_1}{2}. \tag{4.10}$$

Another interpretation is, that the distance of $s_R + b_1$ gives the ideal equivalent wheelbase of the semitrailer, also signified in figure 4.7. The assumption, that the tractor orientation is always tangential to the circle radius, leads to

$$\Gamma \quad = \quad \tan\left(\frac{b_1 + s_R}{R'}\right) \approx \frac{b_1 + s_R}{R'} \quad \Leftrightarrow \quad R' \approx \frac{b_1 + s_R}{\Gamma}. \tag{4.11}$$

Referring to the calculation of the equivalent wheelbase in section 2.1.3, the equilibrium of the yaw moment with respect to the 5^{th}-wheel Ⓒ and taking the inertia force $m_2 a_y$ into account yields

$$\sum M_C = 0 = m_2 a_y b_1 - F_{yf2}(b_1 + b_2) - F_{ym2}(b_1 + b_3) + F_{yr2}\cos(\delta_2)(b_1 + b_4), \tag{4.12}$$

where the front, mid and rear tire forces are named with F_{yf2}, F_{ym2} and F_{yr2}. According to [Win98], it can be supposed that the complete front tire force F_{yf2} acts in the direction of y, which means $\cos\delta_2 \approx 1$. Since the tire forces are linearly related to the slip angles α_{f2}, α_{m2} and α_{r2} with the associated cornering stiffness, equation (4.12) results in

$$0 = m_2 a_y b_1 - C_{\alpha f2}\,\alpha_{f2}(b_1 + b_2) - C_{\alpha m2}\,\alpha_{m2}(b_1 + b_3) + C_{\alpha r2}\,\alpha_{r2}(b_1 + b_4). \tag{4.13}$$

With the substitution of the slip angles from (4.7)-(4.9) it can be written as

$$m_2 a_y b_1 = C_{\alpha f2}\frac{b_2 - s_R}{R'}(b_1 + b_2) + C_{\alpha m2}\frac{b_3 - s_R}{R'}(b_1 + b_3) + C_{\alpha r2}\left(\delta_2 + \frac{b_4 - s_R}{R'}\right)(b_1 + b_4), \tag{4.14}$$

or rearranged to the trailer steer angle and using (4.11),

$$\delta_2 = \underbrace{-\frac{C_{\alpha f2}\,(b_2 - s_R)(b_1 + b_2) + C_{\alpha m2}\,(b_3 - s_R)(b_1 + b_3) + C_{\alpha r2}\,(b_4 - s_R)(b_1 + b_4)}{C_{\alpha r2}(b_1 + b_4)\,(b_1 + s_R)}}_{k_p}\,\Gamma + \underbrace{\frac{m_2 b_1}{C_{\alpha r2}(b_1 + b_4)}}_{k_a}\,a_y. \tag{4.15}$$

This equation finally gives the steady-state control rule for the track-tracing, where k_P is the gain related to the hitch angle Γ and k_a is the gain related to the lateral acceleration. It also considers the centrifugal forces which results from the lateral acceleration a_y. Since the semitrailer moves with the constant velocity v_2 and with the constant angular velocity $\dot{\psi}_2$, it can be estimated by

$$a_y = v_2 \dot{\psi}_2. \tag{4.16}$$

Moreover, in [Viv12] is recommended to extent a steady-state controller for the semitrailer steering in order improve the performance on corner entry and exit. In consideration of a small velocity, the steady-state control method according to equation (4.15) leads to a proportional dependence of the hitch angle Γ and strailer steering angle δ_2. So especially during the entry and exit of a corner, the steering angle changes with the hitch angle simultaneously i.e. too early, which causes a deviation or a so-called "tail-swing". This difference between the trajectory of the coupling point Ⓒ and rear end of the semitrailer Ⓔ is schematically visualized for a TST at the corner entry in figure 4.8(a) and for the corner exit in figure 4.8(b). The suggested extension is the adding of a first-order lag element (PT1) to the steady-state control, which results in a time-delayed reaction and essential improvement. This leads to the steady-state structure

$$\sum\nolimits_{\text{FF}}: \qquad \delta_{2,\text{FF}} = k_p\left(1 + \frac{T_d N}{1 + N\frac{1}{s}}\right)\Gamma + k_a a_y, \tag{4.17}$$

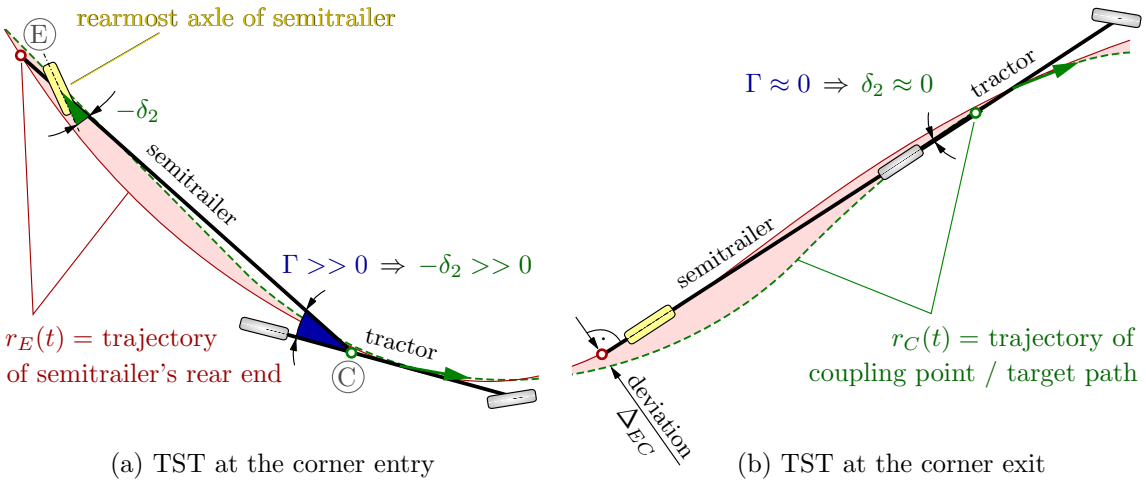

(a) TST at the corner entry (b) TST at the corner exit

Figure 4.8: Off-tracking of a TST with a single steerable rear axle at the corner entry and exit, caused by the steady-state controller.

where T_d and N characterize the time delay and the filter coefficient. The abbreviation "FF" clarifies, that the effect of the method is similar to a feed-forward control. The product $k_p T_d$ is also called the derivative coefficient. As stated in [Viv12], the coefficients can be approximately chosen as

$$T_d = 1 \text{ sec} \quad \text{and} \quad N = 5 \text{ rad/sec}. \tag{4.18}$$

The related simulation results are presented in chapter 5.

Remark 4.2. *Despite of the PT1 extension, the semitrailer rear end does not completely follow the coupling trajectory in all maneuvers, since the steady-state strategy considers no direct feedback of the path.*

Consequentially, a steering closed-loop approach will be introduced in the following.

4.2.2 Feed-Back Controller for a Path-Following

As already mentioned, the trailer rearmost end Ⓔ should always follow the position-trajectory $r_E(t)$ of the coupling point Ⓒ, in order to improve the maneuverability of the TST. So in the ideal case, a trailer steering controller takes as an input the position-trajectory of Ⓒ, denoted by $\boldsymbol{r}_C(t)$, and consistently adjust the trailer's rearmost end position $\boldsymbol{r}_E(t)$ so that it optimally yields

$$\boldsymbol{r}_E(t) \stackrel{!}{=} \boldsymbol{r}_C(t + \Delta t), \tag{4.19}$$

where Δt characterize a delay. This control strategy could be realized using the perpendicular distance of the current Ⓔ position to the coupling point trajectory as a feedback for the trailer steering angle δ_2. The major challenge of this method is to detect the mentioned distance, which can also be called "deviation" Δ_{EC} and is firstly depicted in figure 4.8(b). In detail, it is actually the perpendicular displacement of the semitrailer's rearmost mid point to the trajectory $r_C(t)$, which can be mathematical expressed by

$$\Delta_{EC} = |\boldsymbol{r}_C(t + \Delta t_\perp) - \boldsymbol{r}_E(t)|. \tag{4.20}$$

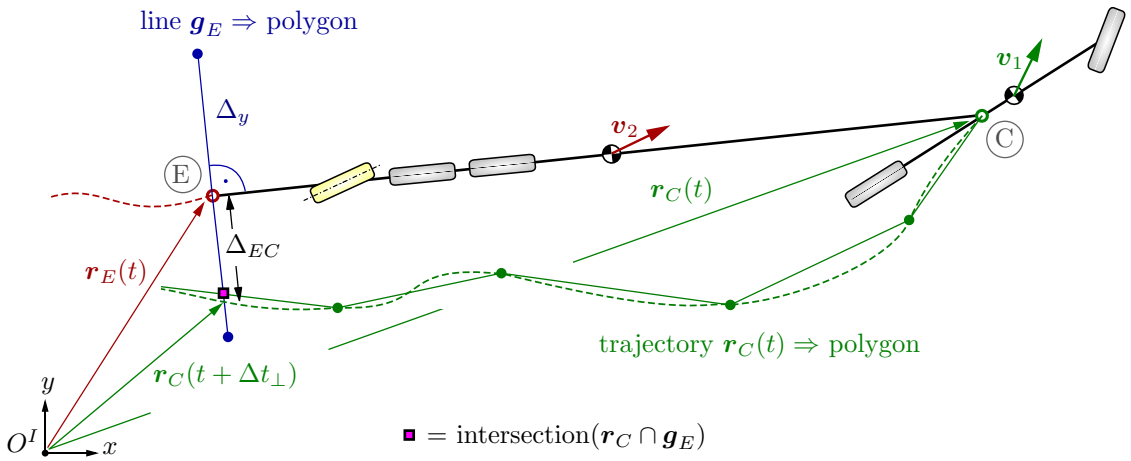

Figure 4.9: Explanation and calculation of the semitrailer deviation Δ_{EC}.

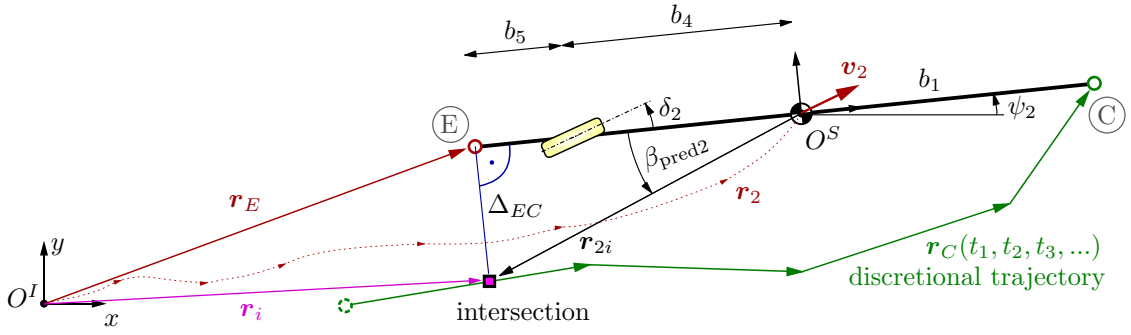

Figure 4.10: Explanation of the horizontal semitrailer control strategy, which uses the trajectory of the coupling point and the trailer position with respect to the initial reference frame O^I.

The consideration of the perpendicular distance to the trajectory of the coupling point at a delayed point in time is indicated by $\Delta t_\perp$, which depends on the former movement of the trailer and thus can not be obtained on a simple way.
Another point of view is to discretize the memorized trajectory $\boldsymbol{r}_C(t_1, t_2, t_3..)$ in order to get an initial polygon. Afterwards, the line normal to the current trailer orientation and crossing (E) will additionally be described by a second polygon called $\boldsymbol{g}_E$. Eventually, the distance from (E) to the intersection of these two polygons ($\boldsymbol{r}_C \cap \boldsymbol{g}_E$) is the deviation Δ_{EC}. Figure 4.9 illustrates the TST at an exemplary maneuver and clarifies the discussed relations. The more precisely the discretisation of the trajectories is, the more accurately the intersection is evaluated.
Since the intersection of polygons can be easily obtained according to section 4.1.2, the only difficulty is to provide the coupling-point trajectory with respect to the initial reference frame O^I for the controller. Figure 4.10 depicts the semitrailer during a maneuver, describes the position relations and explains the control strategy. In the following it is assumed, that the start position of the semitrailer is the origin of the initial reference frame

$$\boldsymbol{r}_E(0) = \begin{bmatrix} 0 & 0 \end{bmatrix}^T, \tag{4.21}$$

and the relative velocity ${}_S\boldsymbol{v}_2$ of the semitrailer with respect to the semitrailer reference frame O^S is measurable. Furthermore it is supposed that the orientation angle of the semitrailer ψ_2 can

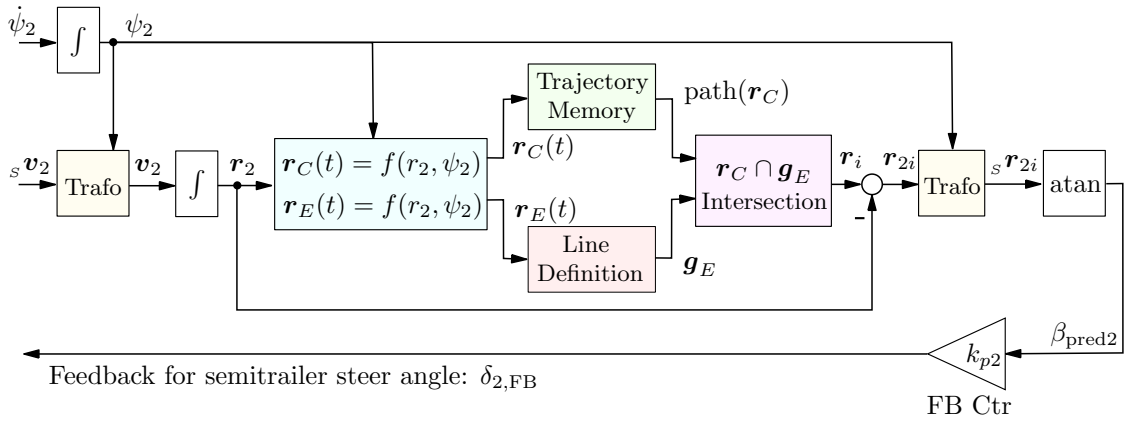

Figure 4.11: Structure of the feedback control strategy $\sum_{\text{FB}}$ for the horizontal semitrailer 5^{th}-wheel tracking.

be calculated, integrating the signal of an angular rate sensor, where the influence of an implied measurement noise will be discussed later. So the absolute trailer position can be obtained by transforming the relative velocity in O^I using (3.15) and apply a time integration using (3.23), which yields

$$\psi_2(t) = \int_0^t \dot{\psi}_2 \, \mathrm{d}t \quad \text{and} \tag{4.22}$$

$$\boldsymbol{r}_2(t) = \int_0^t {}_I\boldsymbol{\phi}_S(\psi_2(t)) \, {}_S\boldsymbol{v}_2 \, \mathrm{d}t. \tag{4.23}$$

Since the distance from the semitrailer c.g. to the coupling point and to the rearmost end is constantly b_1 and $b_4 + b_5$, the trajectory of Ⓒ and Ⓔ results in

$$\boldsymbol{r}_C(t) = \boldsymbol{r}_2(t) + {}_I\boldsymbol{\phi}_S(\psi_2(t)) \begin{bmatrix} b_1 \\ 0 \end{bmatrix} \quad \text{and} \quad \boldsymbol{r}_E(t) = \boldsymbol{r}_2(t) + {}_I\boldsymbol{\phi}_S(\psi_2(t)) \begin{bmatrix} -(b_4 + b_5) \\ 0 \end{bmatrix}. \tag{4.24}$$

As already mentioned, the route of $\boldsymbol{r}_C(t)$ has to be memorized e.g. with the use of small limited memory unit that store the positions every few centimeters and for a range which exceeds the the trailer length. The line (or polygon) perpendicular to the semitrailer and which crosses Ⓔ, can be defined by the two points

$$\boldsymbol{g}_E(t) : \left\{ \boldsymbol{r}_E(t) + {}_I\boldsymbol{\phi}_S(\psi_2(t)) \begin{bmatrix} 0 \\ \Delta_y \end{bmatrix}, \boldsymbol{r}_E(t) + {}_I\boldsymbol{\phi}_S(\psi_2(t)) \begin{bmatrix} 0 \\ -\Delta_y \end{bmatrix} \right\}, \tag{4.25}$$

where Δ_y denotes a certain distance in the y direction relative to the semitrailer, illustrated in figure 4.9. The intersection of both polygons with respect to O^I will be be named by $\boldsymbol{r}_i$. So the distance of the c.g. to the intersection leads to

$$\boldsymbol{r}_{2i} = r_i - r_2, \tag{4.26}$$

or expressed by the semitrailer reference frame O^S,

$${}_S\boldsymbol{r}_{2i} = {}_S\boldsymbol{\phi}_I(\psi_2) \, \boldsymbol{r}_{2i}. \tag{4.27}$$

In conclusion, either the angle between ${}_S\boldsymbol{r}_{2i}$ and the trailer longitudinal axis

$$\beta_{\text{pred2}} = \arctan\left(\frac{{}_S y_{2i}}{{}_S x_{2i}} \right) \tag{4.28}$$

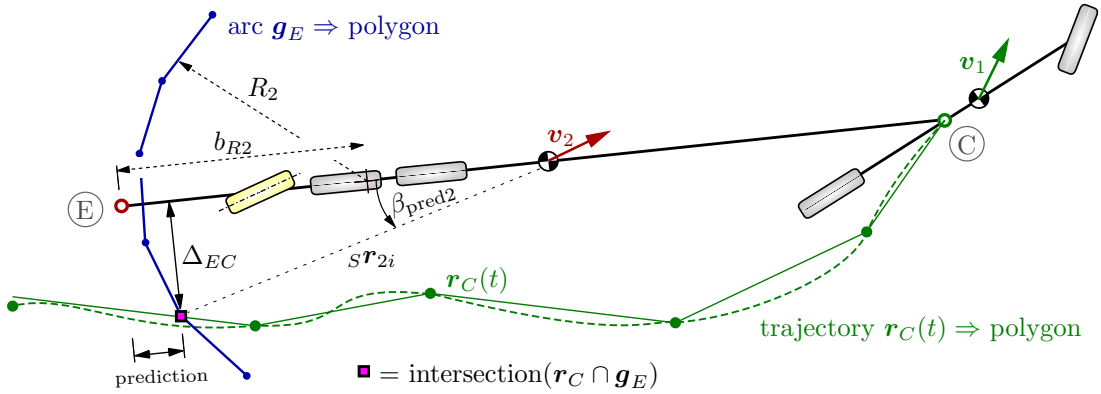

Figure 4.12: Steering strategy for the horizontal semitrailer control, using an "prediction arc".

or the deviation

$$\Delta_{EC} = {}_S y_{2i} \tag{4.29}$$

can be used for the control variable. The gained signal can be used as a feedback to the trailer steering,

$$\sum\nolimits_{\text{FB}}: \qquad \delta_{2,\text{FB}} = k_{p2}\, \beta_{\text{pred2}}. \tag{4.30}$$

According to the angle signs shown in figure 4.10, the gain k_{p2} of the feedback controller (FB Ctr) must be negative so that a positive β_{pred2} leads to steer the trailer in the right direction. Figure 4.11 briefly gives a structured overview of the steering strategy for the horizontal semitrailer control. Instead of a straight line, an arc with the radius R_2 and shifted with b_{R2} can be used for the calculation of the deviation, similar to section 4.1.2. This can lead to an improvement especially during high velocities, since the deviation will be "predicted" in advance for $b_{R2} < R_2$. Figure 4.12 clarifies this case. In analogy to section 4.1.2, the adding of a first-order lag element (PT1) to the feedback control "FB Ctr" results in a time-delayed reaction and can also lead to and further improvement.

Remark 4.3. *The developed strategy assumes that the trailer velocities are precisely measurable, since the* Ⓒ *trajectory will be obtained by a time integration. Unfortunately, measurement noise is always present at the sensors on a real TST system. Therefore the feedback control will be combined with the steady-state control to a two-degree-of-freedom control in the following section 4.2.3, in order to improve the robustness against measurement noise and to ensure a fast reaction of the controller.*

Remark 4.4. *According to the introduced feedback control strategy, the position of the semitrailer will be temporary described with respect to the initial reference frame, which results from the start configuration and leads to very large numbers causing numerical issues. Due to this fact the control strategy has to be extended according to the sections 4.2.4 - 4.2.6, in order to make it applicable in practice.*

4.2.3 Feedforward-Feedback Control (FFFB)

The feedforward steady-state and feedback approach of section 4.2.1 and 4.2.2 will be combined in the following. According to the theory of controls, this is often called "two–degree-of-freedom (2DOF) control schema" [Hor63]. The combination has to be done in order to improve the robustness and

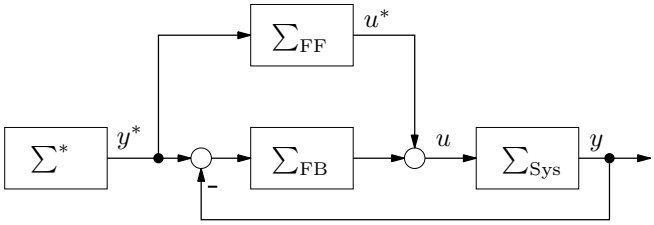

Figure 4.13: Structure of the general feedforward-feedback (FFFB) control schema [Hor63] with a system $\sum_{\mathrm{Sys}}$, a feedback control $\sum_{\mathrm{FB}}$, a steady-state control $\sum_{\mathrm{FF}}$ and a signal generator $\sum^*$.

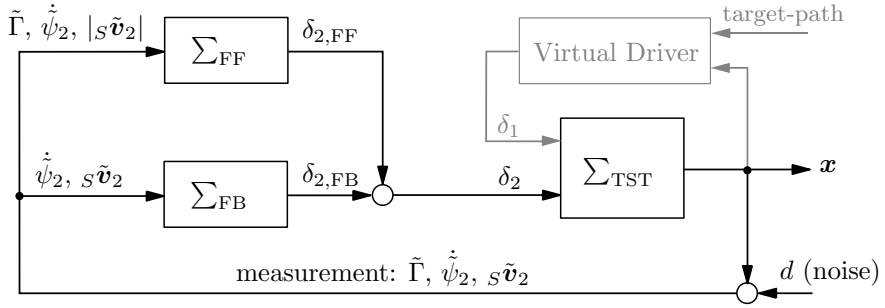

Figure 4.14: Feedforward-feedback (FFFB) control strategy for the horizontal semitrailer 5^{th}-wheel tracking, with the tractor-semitrailer system $\sum_{\mathrm{TST}}$, feedback control $\sum_{\mathrm{FB}}$ and steady-state control $\sum_{\mathrm{FF}}$.

reaction speed of the introduced steering strategies for the horizontal semitrailer 5^{th}-wheel tracking of the trailer's rearmost end.

The FFFB-control schema in figure 4.13 is commonly used to enable the independent design of a steady-state and a feedback control [Hor63]. On the one hand the steady-state control insures that the FFFB structure reacts very fast and on the other hand it uses a compensating feedback which usually leads to a good performance. According to the system control theories the feedforward control $\sum_{\mathrm{FF}}$ is applied to achieve a desired tracking performance of the output y, whereas the feedback control $\sum_{\mathrm{FB}}$ is designed such that the system $\sum_{\mathrm{Sys}}$ is appropriately stabilized and robustified against model uncertainties and disturbances. The signal generator $\sum^*$ normally provides the reference trajectory $y^*(t)$ for both, the feedback and the feedforward control.

In analogy, this control approach can be transferred to the discussed track-tracing task of the semitrailer. Figure 4.14 shows the resulting FFFB-schema which includes the feedforward controller of (4.17), the feedback strategy of (4.30) and the "Virtual Driver" from section 4.1, who steers the tractor along a target-path. The block $\sum_{\mathrm{TST}}$ can characterize any of the regarded TST models of this work, since this control strategy is independent of the model itself. The state vector includes the generalized coordinates and is denoted by $\boldsymbol{x}$. For the application on a real tractor-semitrailer system, it is necessary to measure specific states. As already mentioned, a measurement noise d is always present at unidealised sensors, so it also has to be considered in the control scheme. The noisy signals are super-scripted with $\sim$, whereby the hitch angle $\tilde{\Gamma}$ is used for the feedforward controller. The yaw rate $\dot{\tilde{\psi}}_2$ and the velocity ${}_S\tilde{\boldsymbol{v}}_2$ of the trailer with respect to the semitrailer's reference frame are necessary for both, the feedback and feedforward controller. Finally, the evaluated signals are superposed so that the semitrailer steer angle yields

$$\delta_2 = \delta_{2,\mathrm{FF}} + \delta_{2,\mathrm{FB}}. \tag{4.31}$$

On the one hand the feedforward-part $\delta_{2,\mathrm{FF}}$ depends mainly on the hitch angle $\tilde{\Gamma}$ and leads to a perfect steering during a steady state turn. On the other hand the feedback-part $\delta_{2,\mathrm{FB}}$ is obtained by the estimated deviation of the semitrailer rearmost end to the 5^{th}-wheel trajectory. This part mainly corrects the tracking of the semitrailer during the entry and exit of a corner. The following subsections represents two different realizations of the proposed FFFB control strategy.

4.2.4 FFFB with Reset & Patch-Strategy

According to remark 4.4, the feedback control strategy needs to be extended in order to prevent numerical issues. The issues are caused by large values resulting from the calculation of the absolute trailer position. This section proposes to prevent this by a frequent reset of the integration blocks, which are used for the computation of the position and the angle. Within this action the trajectory-memory (of the measurement) has to be erased, too. That means that the feedback controller loses all data, starts again to record the trajectory of Ⓒ and has to wait for the next founded intersection, since the 5^{th}-wheel hurries a few meters ahead. In order to improve this behavior, a second feedback controller can be used simultaneously, which always resets itself while the first one is running i.e. both controller work alternately. The second feedback controller is called "patch-controller", because it is used to bridge the signal until the first controller detects the intersection after a reset. In the following the described approach of two feedback controllers will be called "Reset & Patch" strategy. In addition, this section takes measurement noise according to remark 4.3 into account. Figure 4.15 illustrates exemplary measurements of a curved driving maneuver of a tractor-semitrailer. The line shows the trajectory of the 5^{th}-wheel position and the points clarify the two noisy measure-

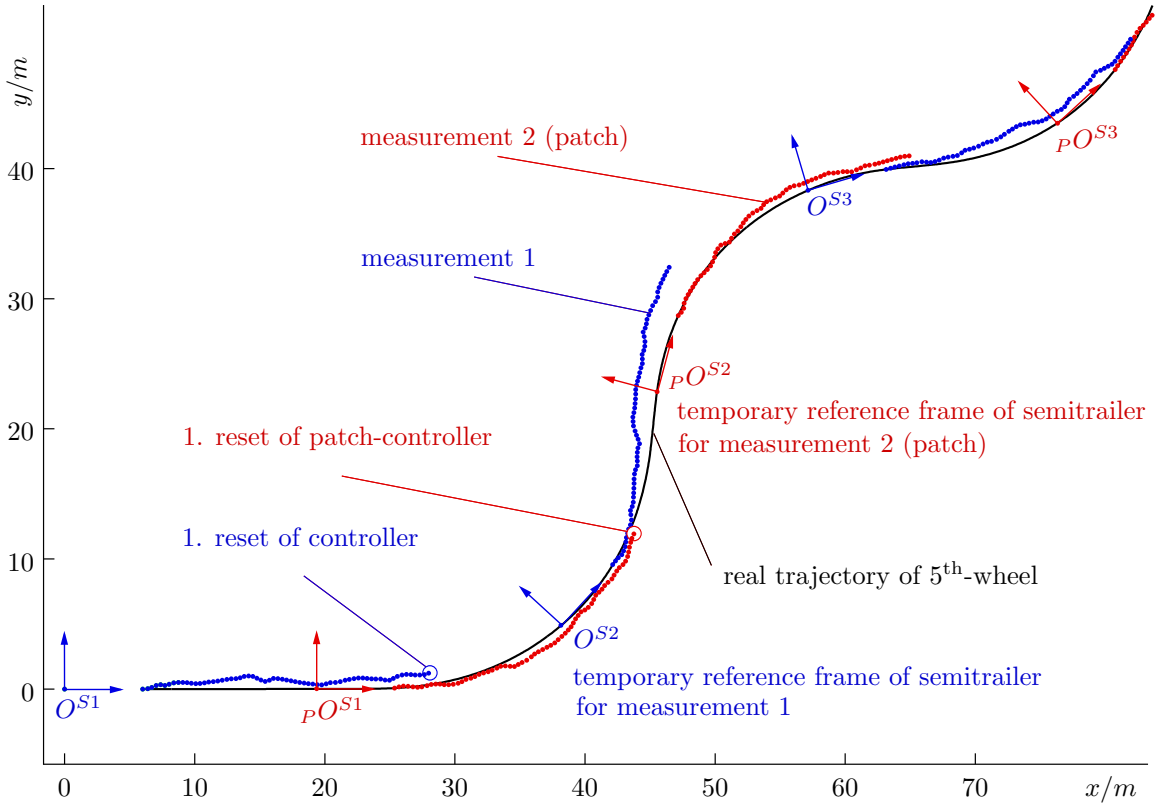

Figure 4.15: Simulated measurement (with noise) of the trajectory of the 5^{th}-wheel, using the introduced "Reset & Patch" strategy.

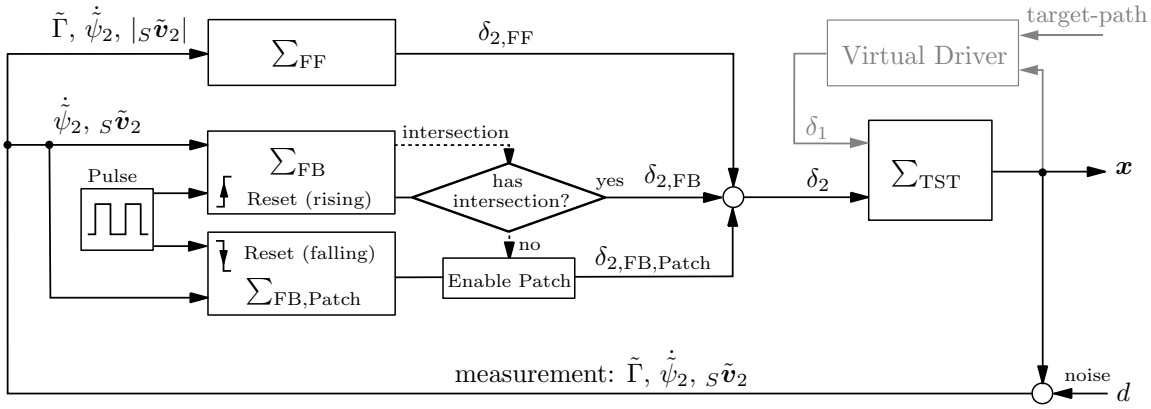

Figure 4.16: Feedforward-feedback (FFFB) control strategy for the horizontal semitrailer 5^{th}-wheel tracking with extensive "Reset & Patch" strategy.

ments of the two feedback controllers. Every few seconds a reset will be applied alternately to make sure that a signal of the feedback controllers is always present. The initial position will be set to zero at a reset of a controller, so the intersections and deviations are always calculated with respect to the related initial reference frames $O^{S1}, O^{S2}, ...$ (or for the patch-controller: ${}_PO^{S1}, {}_PO^{S2}, ...$).

Integration error

The noisy measurements are not only used for the evaluation of the Ⓒ-trajectory, but also for the calculation of the "prediction arc" shown in figure 4.12. So in conclusion, the integrated error between the 5^{th}-wheel and rearmost end of the trailer must only be considered. The relative error is caused by the integration of the noise $d(t)$ until to the time when the rearmost end of the semitrailer reaches the coupling point position. In analogy to equation (4.19) this time can be denominated by Δt, which approximately can be estimated with

$$\Delta t \approx \frac{b_1 + b_4 + b_5}{v_2}, \tag{4.32}$$

whereby the error theoretically results in

$$e(t + \Delta t) = \int_t^{t+\Delta t} d(t)\ \mathrm{d}t. \tag{4.33}$$

This shows that the error only depends on the velocity of the semitrailer and on the measurement noise itself. As faster the TST is, as smaller the error results. Consequently, the control strategy for the horizontal semitrailer 5^{th}-wheel tracking with the extensive "Reset & Patch" strategy can be structured as shown in figure 4.16. The pulse generator regulates the resets of the controllers, whereby the controller $\sum_{\text{FB}}$ resets at a rising edge and the patch-controller $\sum_{\text{FB,Patch}}$ resets at a falling edge. So in dependency of finding an intersection, either the feedback angle $\delta_{2,\text{FB}}$ or $\delta_{2,\text{FB,Patch}}$ is taken into account. This can be formulated mathematically as

$$\delta_2 = \delta_{2,\text{FF}} + \begin{cases} \delta_{2,\text{FB}} & \text{if } (\textstyle\sum_{\text{FB}} \text{ finds intersection}) \\ \delta_{2,\text{FB,Patch}} & \text{else if } (\textstyle\sum_{\text{FB,Patch}} \text{ finds intersection}) \\ 0 & \text{else .} \end{cases} \tag{4.34}$$

The related simulation results are presented in chapter 5.

4.2.5 FFFB with Reset & Shift-Strategy

According to the "Reset & Patch-Strategy" introduced in subsection 4.2.4, two identical feedback controller can be implemented in order to alternate between a reset. This alternating strategy is necessary since the trajectory-memory will also be cleaned up within that reset-action. In this section another approach is suggested for the realization of the FFFB-control strategy.
As stated in figure 4.11 the trajectory $\boldsymbol{r}_C(t)$ of the 5$^{\text{th}}$-wheel is stored in the "Trajectory Memory"-block. The idea of the new approach is to use only one feedback controller shown in figure 4.17 and to keep the trajectory-memory during a reset, but apply a shift of the trajectory coordinates. So in case of a reset, the trajectory $\boldsymbol{r}_C(t)$ has to be transformed from the previous into the new reference frame O^S1 which results from the current position of the semitrailer's center of gravity. Figure 4.18(a) depicts a cornering maneuver of a tractor-semitrailer (TST) with respect to the initial reference frame O^I. It is assumed that the TST starts at the time $t = 0$ at the position $\boldsymbol{r}_2(0)$ and the feedback controller is memorizing the trajectory $\boldsymbol{r}_C(t)$ until to the reset at $t = t_{\text{Reset1}}$ (also with respect to O^I). Since the integrated position and angle are reseted simultaneously with a pulse generator, the coordinate description is shifted to the origin of O^{S1}. So the coordinates of the trajectory has also to be shifted and transformed to current the body fixed reference frame O^{S1} with the previous semitrailer position

$$\hat{\boldsymbol{r}}_2 = \boldsymbol{r}_2(t_{\text{Rest1}} - \mathrm{d}t), \tag{4.35}$$

and the previous semitrailer orientation

$$\hat{\psi}_2 = \psi_2(t_{\text{Rest1}} - \mathrm{d}t), \tag{4.36}$$

whereby "$-\mathrm{d}t$" clarifies that the values at the previous time-step are relevant. In order to calculate the shift inside of the "Trajectory Memory"-block, it has to be extended with the input of ψ_2. Furthermore, the position can be obtained by

$$\hat{\boldsymbol{r}}_2 = \hat{\boldsymbol{r}}_C - {}_I\boldsymbol{\phi}_S(\hat{\psi}_2) \begin{bmatrix} b_1 \\ 0 \end{bmatrix}. \tag{4.37}$$

All of the trajectory coordinates can now be shifted to the trailer's c.g. which yields

$$\boldsymbol{r}_{SC}(t) = \boldsymbol{r}_C(t) - \hat{\boldsymbol{r}}_2. \tag{4.38}$$

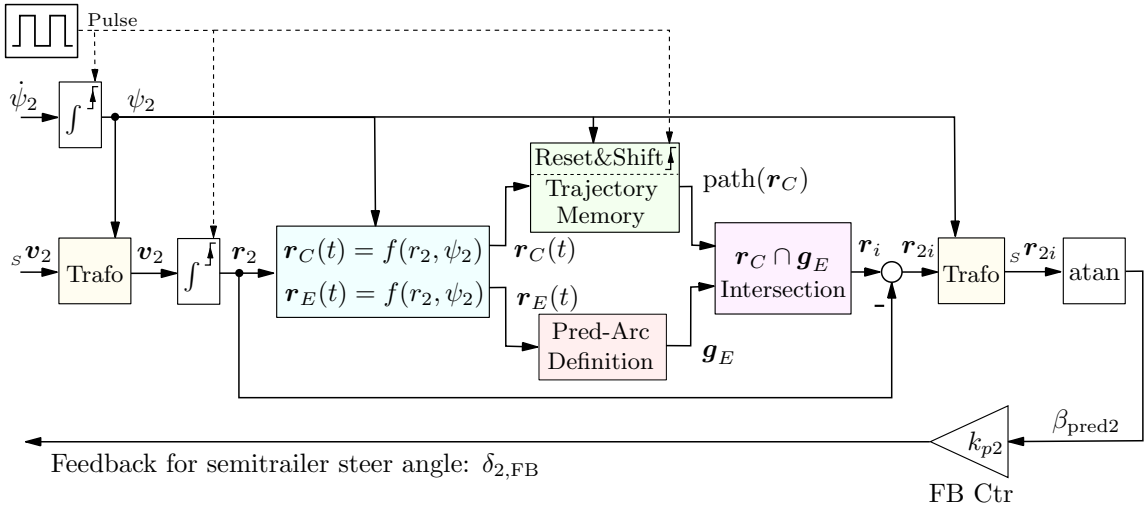

Figure 4.17: Structure of the feedback control strategy $\sum_{\text{FB,Shift}}$ for the horizontal semitrailer 5$^{\text{th}}$-wheel tracking with "Reset & Shift" strategy.

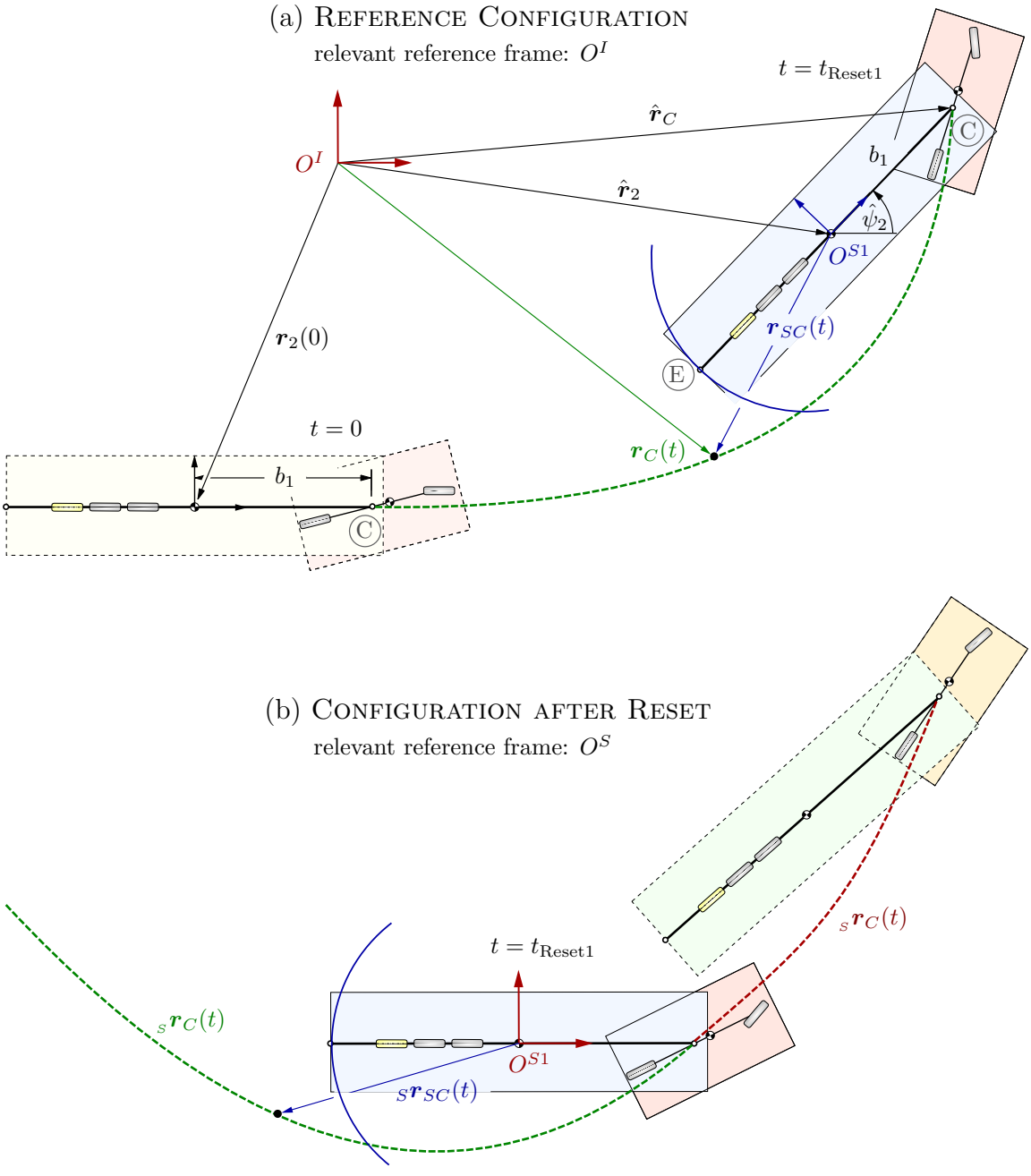

Figure 4.18: Coordinate transformation and shifting for the horizontal semitrailer 5$^{\text{th}}$-wheel tracking with extensive "Reset & Shift" strategy.

Since the reset is also applied to the orientation angle $\hat{\psi}_2$, the coordinates have to be transformed with the rotational matrix ${}_S\boldsymbol{\phi}_I = {}_I\boldsymbol{\phi}_S^T$ of equation (3.15), which yields

$$ {}_S\boldsymbol{r}_{SC}(t) = {}_S\boldsymbol{\phi}_I(\hat{\psi}_2)\, \boldsymbol{r}_{SC}(t). \tag{4.39} $$

Eventually, the new values of the memorized trajectory results in

$$ \boldsymbol{r}_C(t) := {}_S\boldsymbol{r}_{SC}(t). \tag{4.40} $$

The transformed configuration after a reset is depicted in figure 4.18(b).
In conclusion, this new approach uses only one feedback controller, and instead of deleting the trajectory-memory during a reset, it will be shifted and transformed to a temporary reference frame O^{S1}. So this procedure ensures that the intersection can be obtained independently of a reset. The resulting structure of the so-called "Reset & Shift" strategy is illustrated in figure 4.19.

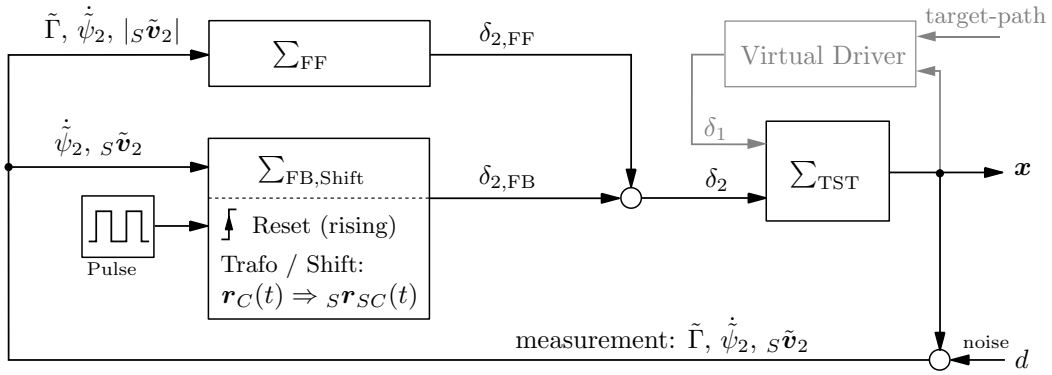

Figure 4.19: Feedforward-feedback (FFFB) control strategy for the horizontal semitrailer 5^{th}-wheel tracking with extensive "Reset & Shift" strategy.

4.2.6 FFFB with Relative Coordinates

This section introduces the third approach for a realization of the FFFB-control strategy. As previously mentioned in remark 4.4, the consideration of the position-trajectory with respect to the initial reference frame may cause numerical issues.
The idea of this approach is to describe the trajectories (of the semitrailer's c.g. and the 5^{th}-wheel) with respect to the semitrailer-fixed reference frame. The relative coordinates of the trajectories are considered in a small area around the semitrailer and are stored in a memory. Afterwards, the relative trajectory of the 5^{th}-wheel can be used to calculate the feedback of the controller.
If a reference frame is rotated against another one around the angle Γ_ψ, the rotational matrix can be formulated with

$$ \boldsymbol{\phi}(\Gamma_\psi) = \begin{bmatrix} \cos\Gamma_\psi & -\sin\Gamma_\psi \\ \sin\Gamma_\psi & \cos\Gamma_\psi \end{bmatrix}. \tag{4.41} $$

According to figure 4.20(a) the motion of a point at the position $\textcircled{P_0}$ to the position $\textcircled{P_k}$ can be discretely characterized by the relative displacement vectors $\{{}_S\Delta\boldsymbol{r}^{(1)}, {}_S\Delta\boldsymbol{r}^{(2)}, ..., {}_S\Delta\boldsymbol{r}^{(k)}\}$ and the incremental angles $\{\Gamma_\psi^{(1)}, \Gamma_\psi^{(2)}, ..., \Gamma_\psi^{(k)}\}$. The first displaced position leads to the trajectory points

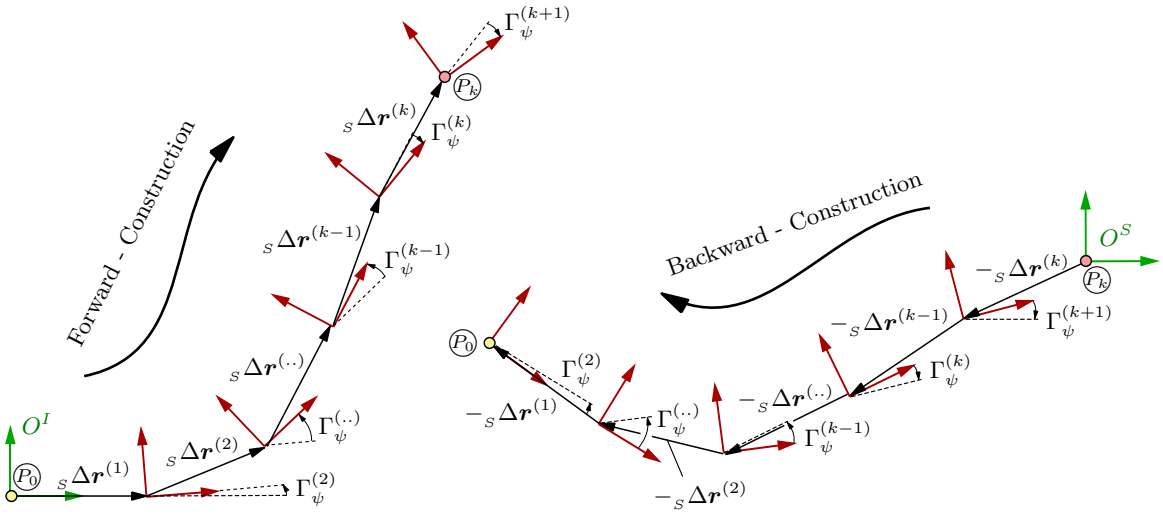

(a) trajectory in the initial reference frame (b) trajectory in the bodx-fixed reference frame

Figure 4.20: Position of the c.g., described by the body-fixed reference frame.

$$\boldsymbol{r}^{(1)} = {}_S\Delta\boldsymbol{r}^{(1)} \tag{4.42}$$

$$\boldsymbol{r}^{(2)} = \boldsymbol{r}^{(1)} + \boldsymbol{\phi}(\Gamma_\psi^{(2)})\,{}_S\Delta\boldsymbol{r}^{(2)} \tag{4.43}$$

$$... \tag{4.44}$$

$$\boldsymbol{r}^{(k-1)} = \boldsymbol{r}^{(k-2)} + \boldsymbol{\phi}(\Gamma_\psi^{(2)} + ... + \Gamma_\psi^{(k-1)})\,{}_S\Delta\boldsymbol{r}^{(k-1)}. \tag{4.45}$$

As a consequence, the k^{th}-position $\textcircled{P_k}$ with respect to the initial reference frame can be generally expressed by

$$\boldsymbol{r}^{(k)} = \sum_{j=1}^{k} \boldsymbol{\phi}\left(\sum_{l=1}^{j} \Gamma_\psi^{(l)}\right)\,{}_S\Delta\boldsymbol{r}^{(j)}. \tag{4.46}$$

Since the rear trajectory points result from the previous ones, the method will be called “Forward Construction”.
In contrast, the trajectory points can also be described with respect to the body-fixed reference frame O^S, as depicted in figure 4.20(b). Since the point $\textcircled{P_k}$ compose the origin of O^S, the previous trajectory points can be constructed in the backward direction by using the negative displacements ’$-{}_S\Delta\boldsymbol{r}$’, and this leads to

$${}_S\boldsymbol{r}^{(k-1)} = -\boldsymbol{\phi}(-\Gamma_\psi^{(k+1)})\,{}_S\Delta\boldsymbol{r}^{(k)} \tag{4.47}$$

$${}_S\boldsymbol{r}^{(k-2)} = -\boldsymbol{\phi}(-\Gamma_\psi^{(k+1)})\,{}_S\Delta\boldsymbol{r}^{(k)} - \boldsymbol{\phi}(-\Gamma_\psi^{(k+1)} - \Gamma_\psi^{(k)})\,{}_S\Delta\boldsymbol{r}^{(k-1)} \tag{4.48}$$

$$... \tag{4.49}$$

$${}_S\boldsymbol{r}^{(0)} = -\boldsymbol{\phi}(-\Gamma_\psi^{(k+1)})\,{}_S\Delta\boldsymbol{r}^{(k)} - ... - \boldsymbol{\phi}(-\Gamma_\psi^{(k+1)} - \Gamma_\psi^{(k)} - ... - \Gamma_\psi^{(2)})\,{}_S\Delta\boldsymbol{r}^{(1)}. \tag{4.50}$$

Eventually, this can also generally expressed for a n^{th}-trajectory point with

$${}_S\boldsymbol{r}^{(n)} = -\sum_{j=n+1}^{k} \boldsymbol{\phi}\left(-\sum_{l=j+1}^{k+1} \Gamma_\psi^{(l)}\right)\,{}_S\Delta\boldsymbol{r}^{(j)}. \tag{4.51}$$

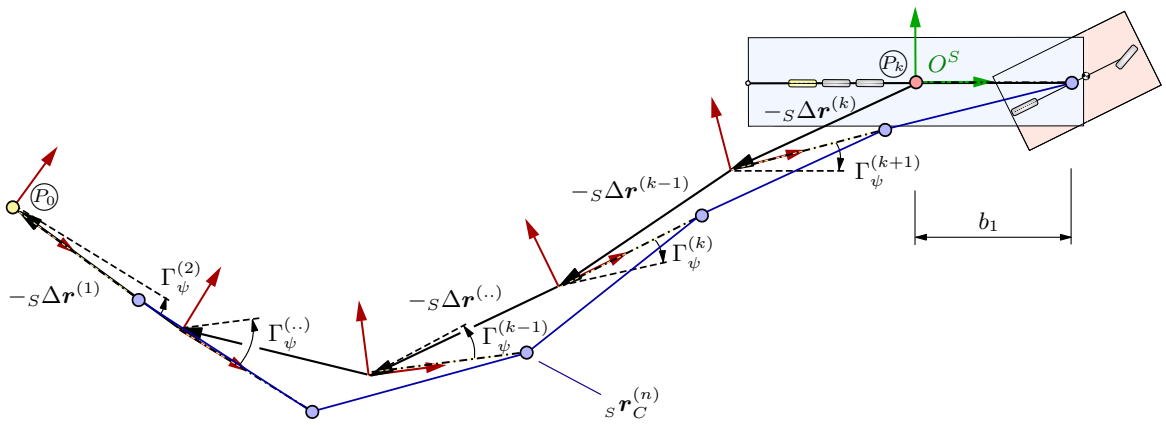

Figure 4.21: Position of the 5th-wheel, described by the body-fixed reference frame.

This equation can be used to describe the trajectory of the semitrailer's c.g. relatively to the current body-fixed reference frame O^S.
The distance of the c.g. and the 5th-wheel is defined by b_1. So the calculation of the 5th-wheel trajectory ${}_S\boldsymbol{r}_c^{(n)}$ with respect to the semitrailer-fixed reference frame can be derived according to figure 4.21, which results in

$$ {}_S\boldsymbol{r}_C^{(n)} = {}_S\,\boldsymbol{r}^{(n)} + \boldsymbol{\phi}\left(-\sum_{l=n+2}^{k+1}\Gamma_\psi^{(l)}\right)\begin{bmatrix} b_1 \\ 0 \end{bmatrix}. \tag{4.52} $$

The equations are derived assuming that the displacement vectors ${}_S\Delta\boldsymbol{r}^{(n)}$ are given. Unfortunately the relative trailer velocity ${}_S\boldsymbol{v}_2$ and angular velocity $\dot{\psi}_2$ are the only signals which are available. So it is proposed to obtain the small displacements and incremental angles Γ_ϕ by an integration of the transformed velocity and angular velocity along the current step n,

$$ {}_S\Delta\boldsymbol{r}^{(n)} = \int_n {}_I\boldsymbol{\phi}_S\;{}_S\boldsymbol{v}_2\,\mathrm{d}t \qquad \text{and} \qquad \Gamma_\phi^{(n)} = \int_n \dot{\psi}_2\,\mathrm{d}t. \tag{4.53} $$

During a simulation this can be realized by resetting the integral-block after the norm of the integrated vector achieves a certain value $|\Delta\boldsymbol{r}_{\text{target}}|$.
The resulting structure of the feedback control strategy is illustrated in figure 4.22. With respect to the previous strategies, the relative trailer velocity is transformed to the initial reference frame and the integration block calculates the current displacement vector. If a target size is reached, the current displacement and angle increment ($\Delta\boldsymbol{r}_2^{(n)}\&\Gamma_\psi^{(n)}$) will be stored in the memory block. This information is necessary since it is needed during the calculation of the trajectories. Eventually the trajectory points will be memorized relative to the trailer-fixed reference frame and the intersection with the predictive arc can be obtained, which is essential for the feedback.
The structure of the FFFB-controller is similar to figure 4.14.

Remark 4.5. *All of the different FFFB-strategies (section 4.2.4 - 4.2.6) lead to the same results, since only the description of the coordinates differs. For the implementation on a real truck system the description with the relative coordinates is recommended, since its control design is very simple and the calculation is faster then using the other methods. In consideration of a measurement noise the resulting integration error of all strategies is equal, see section 4.2.4.*

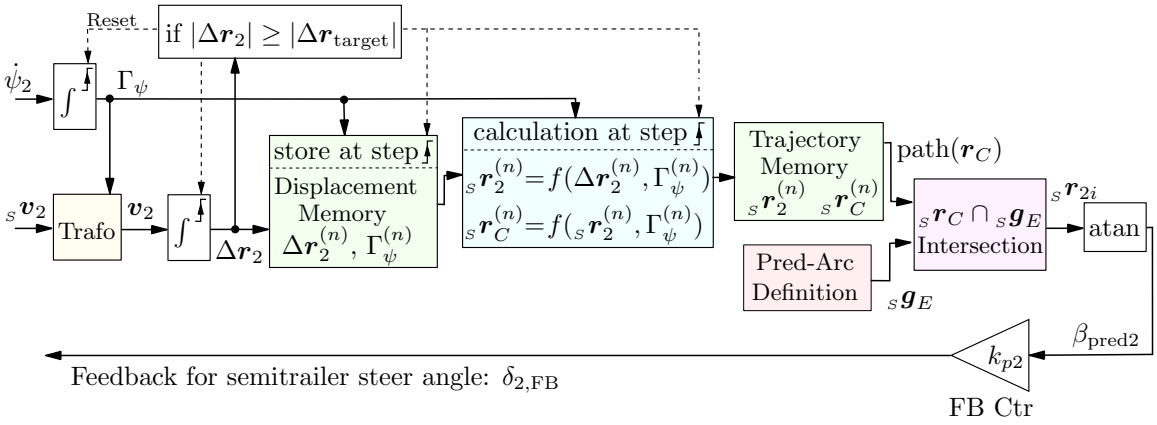

Figure 4.22: Structure of the feedback control strategy $\sum_{\text{FB,relCoord}}$ for the horizontal semitrailer 5^{th}-wheel tracking with the "Relative Coordinate" consideration.

4.3 Steering Strategies for Active Rollover Avoidance

This section represents some trailer steering strategies for the improvement of the roll dynamics during high speed maneuvers. According to subsection 2.2.2 a variety of trailer-steering controllers were investigated for single-unit trucks and tractor-semitrailer within the scope of different research institutions. On the one hand some active damping approaches for single-units were proposed e.g. in [OBA99], and on the other hand different LQR-controllers were designed for tractor-semitrailer combinations [ORJC10]. This work focus on the application of an active roll damping controller. In contrast to previous research, this control-strategy is not applied to a single-unit truck but to a tractor-semitrailer combination.

4.3.1 Rollover of a Single-Unit Vehicle

The intuitive behavior of an experienced driver is clarified by an exemplary driving maneuver of a single-unit vehicle with high velocity in figure 4.23. The left side 4.23(a) indicates the roll motion at the entering of a curve. Since the driver increases the front steer angle δ_1 (to decrease the path radius), the vehicle rolls with the angular velocity $\dot{\phi}_1$ in the positive direction around the roll axis. The right side of figure 4.23(b) shows the countersteering (decreasing of δ_1) of the driver, who wants to prevent a rollover. As a consequence, the increased path radius and the switched tire force F results in a negative roll angular velocity $\dot{\phi}_1$ and the vehicle moves back to a steady position. It can be concluded, that the countersteering in the negative direction of the roll velocity can be beneficial for rollover prevention of single-unit vehicles.

4.3.2 Active Roll Damping of a Tractor-Semitrailer

As proposed in [AO98], an active roll damping (ARD) controller can be designed, which counter-steers with an actuator against the applied driver steer angle δ_{driver} at the front axle of a single-unit truck. The control law should improve the roll dynamics by "damping" the roll motion (with the tire forces) and increasing the path radius in order to avoid a rollover. It can be formulated as

$$\delta_1 = \delta_{\text{driver}} \underbrace{- k_{P1,\text{roll}}\, \dot{\phi}_1}_{\hat{\delta}_{1,\text{ARD}}}, \tag{4.54}$$

whereby the fixed gain is denoted by $k_{P1,\text{roll}}$. It is obvious that the vehicle gets distracted of the desired path, since the controller influences the steer angle. But in most of the cases this off-tracking

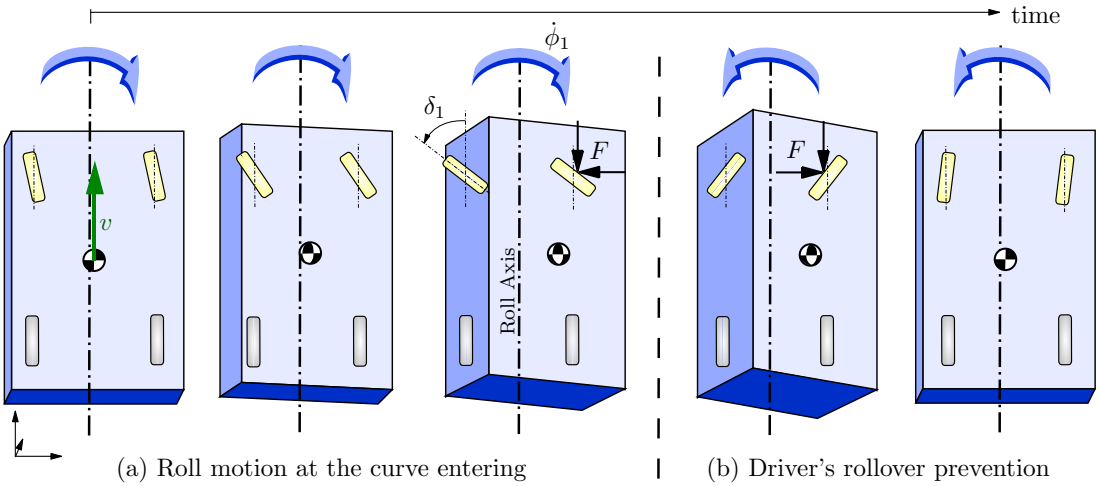

(a) Roll motion at the curve entering (b) Driver's rollover prevention

Figure 4.23: Intuitive driver behavior in order to prevent a rollover of a single-unit vehicle.

can be accepted rather than the occurrence of a rollover. Furthermore it is recommended in [AO98] to add a derivative-part, so that the control law results in

$$\delta_{1,\mathrm{ARD}} = -\,k_{P1,\mathrm{roll}}\;\dot{\phi}_1 - k_{D1,\mathrm{roll}}\;\ddot{\phi}_1. \tag{4.55}$$

It is shown in the concerning publication, that this intervention can decrease the risk of a single-unit truck rollover.

ARD for the Semitrailer

Within the scope of this work it is proposed to test a similar strategy at the semitrailer with the steered rearmost axle. So the basic control law for the steer angle is based on proportional feedback of the trailer roll rate $\dot{\phi}_2$, which can be formulated as

$$\hat{\delta}_{2,\mathrm{ARD}} = -k_{P2,\mathrm{roll}}\;\dot{\phi}_2. \tag{4.56}$$

The fixed gain of the semitrailer controller for the roll damping is denoted by $k_{P2,\mathrm{roll}}$. This means, that in the case of a fast curve-change (e.g. a fishhook maneuver) the controller countersteers the semitrailer during it rolls from one side to another – in dependence of the related roll rate. After the first investigations of the control law effect it was perceived, that indeed it initially improves the load transfer ratio (LTR) during the roll movement. However, after the semitrailer is constantly inclined in the curve, the roll rate – and as a consequence the applied steerangle – are vanishingly low and the countersteering fails to have the desired effect. In some cases this can even increase the LTR and therefore the risk of a rollover, as it will be later shown in the subsection 5.2.4 of the following chapter.
In order to improve the roll dynamic of the semitrailer effectively yet again, it is suggested to add a control part which is proportional to the semitrailer roll angle ϕ_2. Another issue is the intervention of the controller at small transient oscillations with small angels and angular rates. Despite of the uncritical LTR the controller applies a steer angle which can lead to escalations and instabilities because of the reaction delay of the system. This can be prevented by determining a *deathzone* in a certain area with a boundary of $\mathrm{LTR}_{\mathrm{critical}}$. So the final control law results in

$$\delta_{2\mathrm{ARD}} = \begin{cases} 0 & \text{for} \quad |\mathrm{LTR}| \leq \mathrm{LTR}_{\mathrm{critical}} \\ -k_{P2,\mathrm{roll}}\;\dot{\phi}_2 - k_{I2,\mathrm{roll}}\;\phi_2 & \text{else,} \end{cases} \tag{4.57}$$

whereby the gain of the semitrailer roll angle is denoted by $k_{I2,\mathrm{roll}}$. After the proposed control strategies are introduced, the following chapter presents and discusses the influences and benefits on the basis of the simulation results.

Chapter 5

Simulation

The derived tractor-semitrailer (TST) models and steering strategies are implemented in different simulation software in order to analyze the system behavior for different drive maneuvers. This chapter describes the simulation structures and results of the designed models and steering strategies.

5.1 Simulation Structure

Within the scope of this work various models and strategies are developed. This section gives a brief overview of the process chain and introduces the structures of the different simulation models.

5.1.1 Global Process Chain

Figure 5.1 shows the generalized process chain for the tractor-semitrailer simulation. The constant model parameters, simulation settings, controller parameters and initial conditions are defined during the "Pre-Processing". Furthermore the model inputs i.e. the tractor steer angle δ_1 or target path are determined. The next step includes the calculation of the simulation results. On one hand, the derived nonlinear and linear TST-model equations are completely implemented in SIMULINK and on the other hand the complex validation model runs in a "Co-Simulation dll-Interface" with SIMPACK. Afterwards the simulation results can be red and the trajectories can be calculated with respect to the initial reference frame O^I. The summary of the results is plotted in several figures and a 3D-animation of the moving tractor-semitrailer can be generated. This animation is created by the MATLAB-Toolbox "MATCARANIM", which was developed in the scope of this thesis and is documented in the appendix B.

5.1.2 Structure of the Simulation Models

The following TST-models introduced in chapter 3 are considered and investigated in the scope of this thesis:

- Nonlinear Lateral-Yaw Model $\sum_{\text{TST}}$
- Linear Lateral-Yaw Model $\sum_{\text{TST,lin}}$
- SIMPACK-Model $\sum_{\text{TST,SP}}$
- Nonlinear Lateral-Yaw-**Roll** Model $\sum_{\text{TST,Roll}}$
- Linear Lateral-Yaw-**Roll** Model $\sum_{\text{TST,lin,Roll}}$

At first the steering strategies for the track-tracing of the semitrailer will be analyzed using the "Lateral-Yaw Models" and the system structure according to figure 5.2. The equations of motion are implemented in the subsystem "Tractor-Semitrailer-Model" which is involved in the integration loop. The state vector $\boldsymbol{x}$ includes the generalized coordinates $\boldsymbol{q}$ in state-space representation

conforming to equations (2.51) and (3.63), respectively. The model parameters are provided in a structure variable. Normally a human driver steers the tractor, opens the throttle and pushes the brake. So during the simulation these tasks are managed by the "Virtual Driver" which needs the current tractor position with respect to the initial reference frame and the system states. The cruise control ensures that the TST drives with a target velocity. On one hand, it is possible to give a target path which should be followed by the tractor and on the other hand the steer angle of the tractor can be directly defined. The track-tracing strategy of the semitrailer is implemented in the block "Semitrailer Ctr (FFFB)" which contains the steady-state law (4.15) and one of the path-following controllers of the sections 4.2.2-4.2.6.
For the investigations of the roll dynamics the model structures are adjusted as illustrated in figure 5.3. The input steer angle of the tractor is predefined in order to prevent additional excitations of the controller during path-following. Furthermore the roll angular velocity of the tractor $\dot{\phi}_1$, semitrailer $\dot{\phi}_2$ and the related angle ϕ_2 must be measured and provided to the "Active Roll Damping"-Block. According to equation (4.54) the damping part for the tractor $\hat{\delta}_{1,\mathrm{ARD}}$ is superposed to the tractor's front steer angle. In contrast, the damping part of the semitrailer $\delta_{2,\mathrm{ARD}}$ can either be single-applied or can be added to the calculated track-tracing angle $\delta_{2,\mathrm{track}}$. The state vector $\boldsymbol{x}_r$ includes the generalized coordinates $\boldsymbol{q}_r$ in state-space representation again. The different constellation are analysed in the following section.

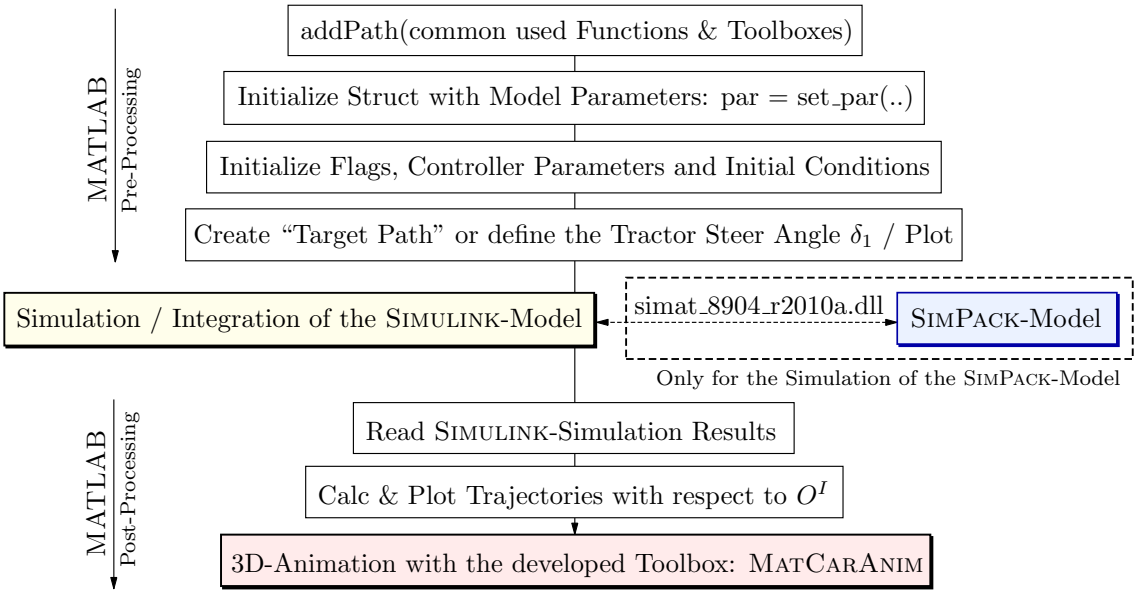

Figure 5.1: Structure of the global process chain for the tractor-semitrailer simulation.

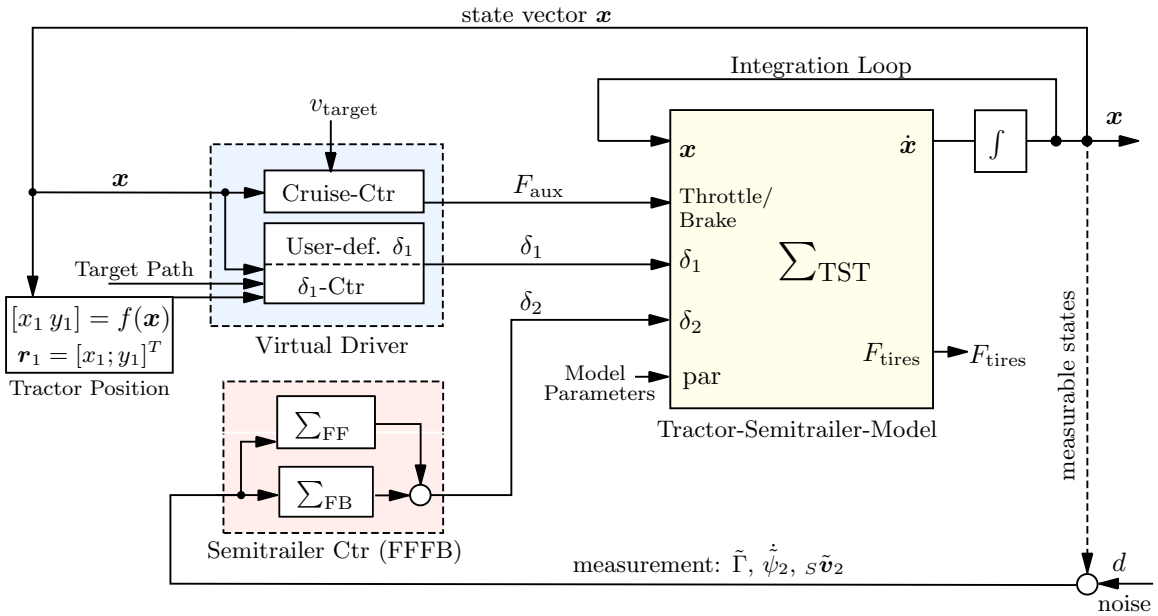

Figure 5.2: Simulation structure of the lateral-yaw models for the investigation of the track-tracing.

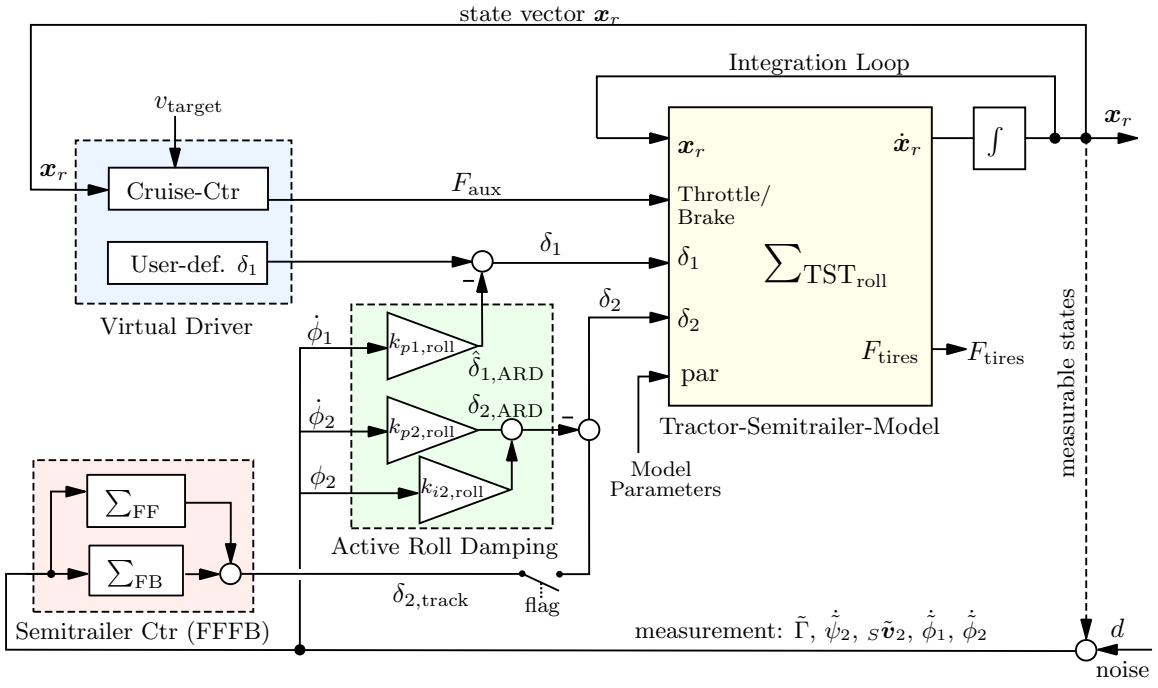

Figure 5.3: Simulation structure of the lateral-yaw-**roll** models for the investigation of the roll dynamics.

5.2 Results and Analysis

This chapter presents and analysis the simulation results of the concerning simulation models and strategies. Beside the validation of the various TST-models, the impacts of steering strategies and the behaviors of the dynamic systems are analyzed. The explicit values of the model parameters and control gains are given in the appendix A.1.

5.2.1 Response Characteristics of the linear Models

The system-dynamics of the linear "Lateral-Yaw Model" ($\sum_{\text{TST,lin}}$) and "Lateral-Yaw-Roll Model" ($\sum_{\text{TST,lin,Roll}}$) can be characterized by multiple transfer functions. They can be formulated from each input to each output and are defined by a single regarded *Laplace* transferred input $U(s)$ and output $Y(s)$. In general it results in

$$G_{yu}(s) := \frac{Y(s)}{U(s)} \ . \tag{5.1}$$

For a system in state-space representation it can be calculated according to (2.56). Initially the model $\sum_{\text{TST,lin}}$ has to be taken into account. One consideration is the influence of the semitrailer steer angle δ_2 on the yaw dynamics (i.e. $\dot{\psi}_2$) of the trailer. According to (3.71) the previous transfer function results in

$$G_{\dot{\psi}_2\delta_2}(s) = \boldsymbol{c}_{\dot{\psi}_2}^T (s\boldsymbol{I} - \boldsymbol{A})^{-1} \boldsymbol{b}_{\delta_2} \ . \tag{5.2}$$

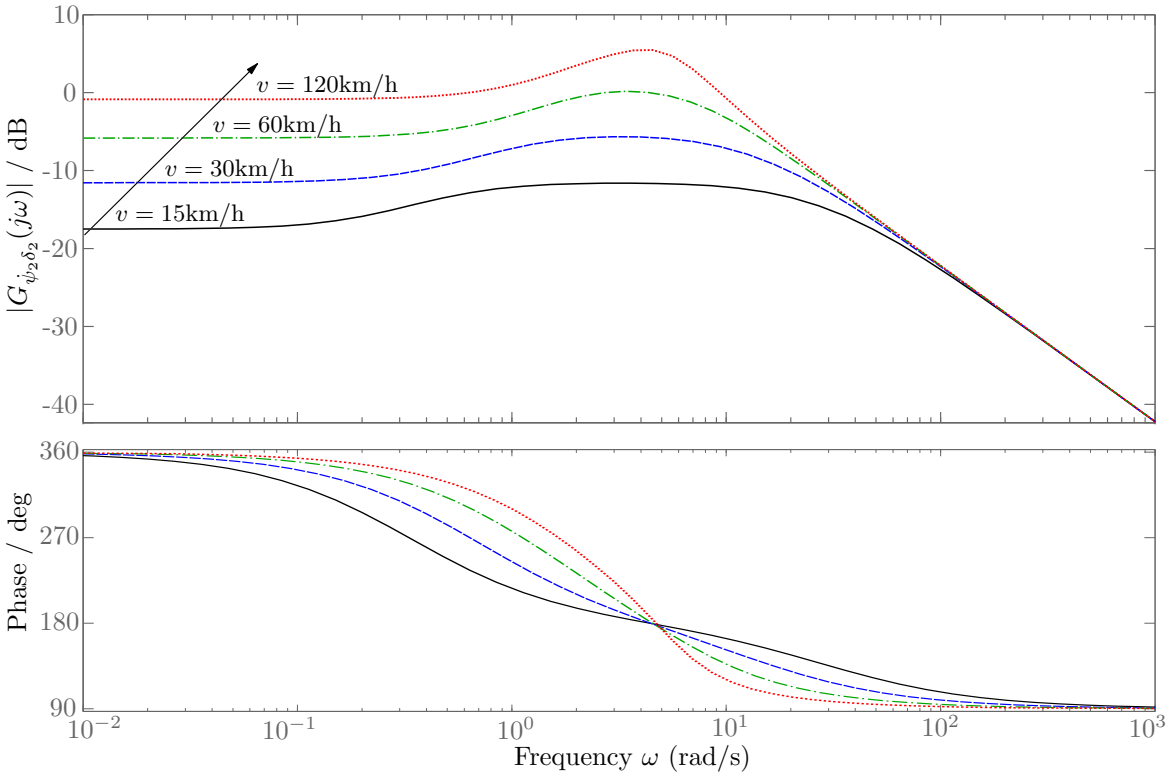

Figure 5.4: Bode diagram of the amplitude frequency response $G_{\dot{\psi}_2\delta_2}(j\omega)$ of the yaw transfer function at different TST velocities.

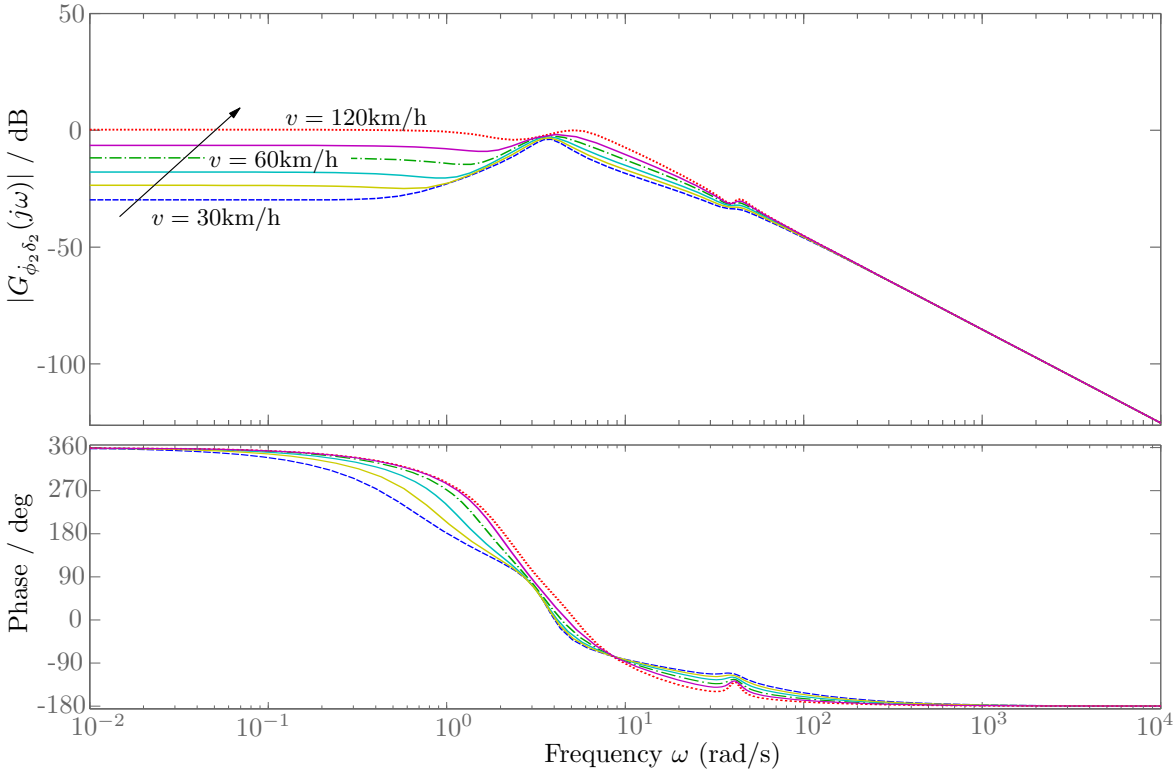

Figure 5.5: Bode diagram of the frequency response $G_{\dot{\phi}_2\delta_2}(j\omega)$ of the roll-transfer function at different TST velocities.

The input matrix $\boldsymbol{b}_{\delta_2}$ is the second column of $\boldsymbol{B}$ from equation (3.71) and the output matrix is the row vector $\boldsymbol{c}_{\dot{\psi}_2} = \begin{bmatrix}0 & 0 & 0 & 1\end{bmatrix}$, which is used to select the semitrailer yaw velocity $\dot{\psi}_2$. Figure 5.4 depicts the *Bode*-diagram for various TST velocities. It shows that the magnitude of the response exponentially increases with velocity and that a velocity of more than 120km/h leads to high amplifications($|G_{\dot{\psi}_2\delta_2}| > 1$) at frequencies between 1rad/s and 10rad/s.

The transfer function from the semitrailer steer angle δ_2 to the roll angular velocity (i.e. $\dot{\phi}_2$) of the trailer can be calculated in order to investigate the roll dynamics of the semitrailer. It can be derived from equation (3.106) with

$$G_{\dot{\phi}_2\delta_2}(s) = \boldsymbol{c}^T_{r\dot{\phi}_2}(s\boldsymbol{I} - \boldsymbol{A}_r)^{-1}\boldsymbol{b}_{r\delta_2} \ . \tag{5.3}$$

Similarly the input matrix $\boldsymbol{b}_{r\delta_2}$ is the second column of $\boldsymbol{B}_r$ from equation (3.106) and the output matrix is the row vector $\boldsymbol{c}_{\dot{\phi}_2} = \begin{bmatrix}0 & 0 & 0 & 0 & 0 & 0 & 1 & 0\end{bmatrix}$, which is used to select the semitrailer roll velocity $\dot{\phi}_2$. Figure 5.5 illustrates the *Bode*-diagram of the roll transfer function for different TST velocities. It also shows that the magnitude of the response exponentially increases with the velocity and that a velocity of more than 120km/h leads to high roll amplifications($|G_{\dot{\phi}_2\delta_2}| > 1$) at frequencies between 2rad/s and 8rad/s.

5.2.2 Validation of the TST-Models

The various TST-models must be validated and compared before they can be used for the assessment of the steering strategies. For the general validation of the models the steering the semitrailer is ignored which means $\delta_2 = 0$. Figure 5.7 depicts the animation screen-shots of a TST entering a

roundabout. The simulation results were calculated with the "Nonlinear Lateral-Yaw Model" $\sum_{\text{TST}}$ and the animation was created with the Toolbox MatCarAnim. Figure 5.7(a) clarifies the single-track model in a 3D-view and figure 5.7(b) shows it from a top-view. Furthermore, the trajectories of the 5^{th}-wheel and the rearmost trailer end are illustrated. Since the trailer is unsteered it offtracks to the inside of the turns, which results in a deviation of the both trajectories. Within this driving maneuver the different models are compared and validated in the following.
Figure 5.8(a) depicts the position-trajectories of the nonlinear ($\sum_{\text{TST}}$), linear ($\sum_{\text{TST,lin}}$) and SimPack ($\sum_{\text{SP}}$) "Lateral-Yaw" model at a velocity of 20km/h and a roundabout radius of 20m. On one hand it shows the positions of the 5^{th}-wheel Ⓒ and on the other hand the trajectories of the rearmost trailer end Ⓔ. Comparing all TST-model it is obvious, that the simulation results of the different systems are broadly similar. In the detail view some small deviations are recognizable which result from the simplifications and assumptions during the derivation. The associated tire forces of the nonlinear and SimPack-model are plotted in figure 5.8(b). Since the front axle is controlled by the steering controller of the virtual driver which sequentially adapts the steer angle to the target path, some small oscillations of the concerning tire force F_{yf1} can be observed. The differences between the models are also very small and can be neglected. Since the linear model uses the same tire model as the nonlinear, the trajectories of the tire forces are almost the same and are not shown.

Remark 5.1. *The illustration also clarifies that the largest tire forces always occur at the rear axle of an unsteered semitrailer. According to section 2.1.1 the tire force depends linearly on the tire slip angle. So in order to reduce this tire force, the semitrailer should be equipped by an active steerable axle which is the focus of this research.*

The roll-extended models contain the same lateral and yaw equations, so the resulting trajectories are also very similar. In particular during the low velocity of 20km/h the roll motion is vanishing small. In order to validate the "Lateral-Yaw-Roll" models, the load transfer ratio (LTR) at a higher velocity can be regarded. Figure 5.9(d) illustrates the LTR-trajectories of the nonlinear and linear "Lateral-Yaw-Roll" models with an unsteered semitrailer and at a velocity of 35km/h. The input of the system is the tractor steer angle δ_1, shown in figure 5.9(a). Furthermore the tire forces (calculated by a saturated tire force law) are depicted in figure 5.9(b). Finally the position-trajectories are shown in figure 5.9(c). Since the TST drives with a high velocity and a relatively large tractor steer angle is applied, the rear tire force of the semitrailer is saturated and the semitrailer is close to a rollover ($\text{LTR}_2 \to 1$). The difference between the nonlinear ($\sum_{\text{TST,Roll}}$) and linear ($\sum_{\text{TST,lin,Roll}}$) roll-extended model is very small, so it can be assumed that the linear model is valid and accurate for the roll investigations.

5.2.3 Track-Following Analysis with the Horizontal Planar Models

According to section 4.2 a controller can steer the semitrailer rearmost axle. Since the tractor with the unsteered semitrailer model is denoted by $\sum_{\text{TST}}$, the model with the implemented steady-state controller (section 4.2.1) can be called $\sum_{\text{TST,FF}}$. As already mentioned, the steady-state controller can be extended to a FFFB-control strategy $\sum_{\text{TST,FFFB}}$ (section 4.2.3), in order to improve the control performance. Furthermore it is clear that the measurements at a real system are disturbed by some noise which is considered in the model named "$\sum_{\text{TST,FFFB}}$+noise".
Figure 5.10 shows the simulation results of these different model configurations during the validated drive maneuver. In detail, figure 5.10(a) clarifies the position-trajectories of the 5^{th}-wheel and rear end. The purpose of this strategy is to follow the 5^{th}-wheel position-trajectory as good as possible. Figure 5.10(b) illustrates the deviation Δ_{EC} to provide an objective comparison of the configurations. As expected, the steady-state control improves the track-tracing significantly. In particular, at corner entry and exit the deviation increases because of the hitch angle dependency (see also figure 4.8). Finally, the FFFB-control strategy leads to the smallest deviation and best performance. In addition, a "worst-case noise" scenario is taken into account which yields peaks in

the trajectory of the semitrailer's steer angle, shown in figure 5.10(c). Nevertheless, the disturbed FFFB-control strategy results in an acceptable track-tracing behavior and the application of filters could further improve the performance.
In addition to the track-tracing performance the tire wear is an important aspect which should be investigated. Figure 5.6 illustrates the summarized lateral tire force $F_{y,\mathrm{sum}}$ of the different TST-models, which is representative for the tire wear. On one hand it shows that $F_{y,\mathrm{sum}}$ can be reduced

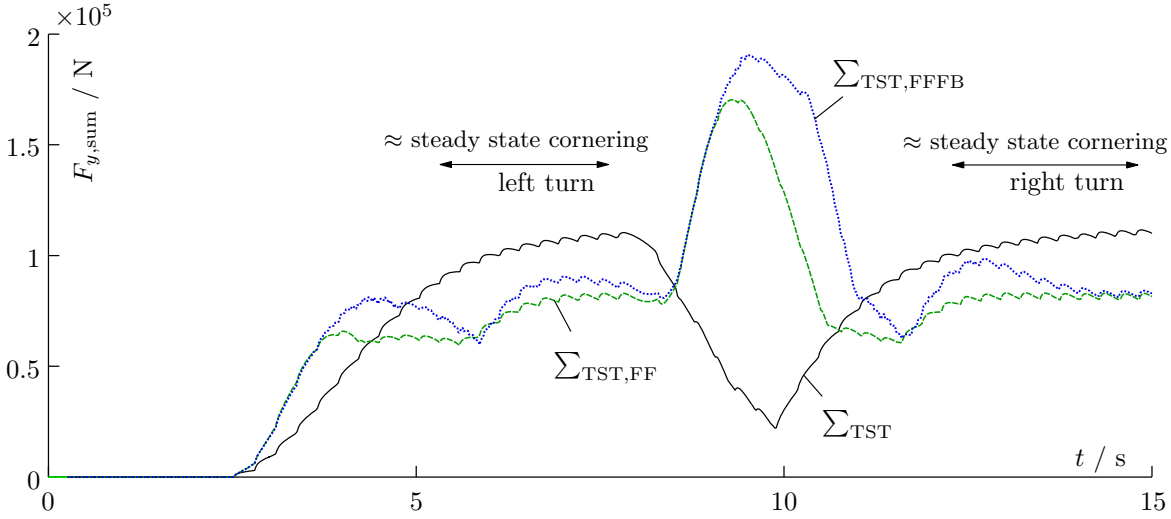

Figure 5.6: Sum of the lateral tire forces, calculated for the different semitrailer steering configurations at a velocity of 20km/h and in the maneuver of entering a roundabout.

during a steady state turn using a semitrailer steering and on the other hand $F_{y,\mathrm{sum}}$ increases during a change of direction. Since the control strategy is developed in order to provide a good trace-tracking i.e. improved maneuverability, the focus of this thesis is not on the tire wear.
Next up, the effect of the path-following FFFB controller is examined at the SimPack-model, which is mentioned in section 3.5. Figure 5.11 compares the steered SimPack-Model $\sum_{\mathrm{TST,SP,FFFB}}$, the steered nonlinear model $\sum_{\mathrm{TST,FFFB}}$ and the SimPack-model with a fixed semitrailer rear axle $\sum_{\mathrm{TST,SP}}$. At the first glance the position trajectories 5.11(a) of the rear-axle steered models are very similar, but on the second, the track deviations according to 5.11(b) show some discrepancies. Since the precise SimPack-model contains several various subsystems with related dynamics, some differences to the simplified nonlinear model are expected and understandable. The limited steer actor performance and reaction time probably explains the delay of the semitrailer steer angle, displayed in figure 5.11(c).

5.2.4 Active-Roll-Damping Analysis with the Roll-extended Models

In the following, the roll dynamics should be investigated. The simulation results of the linear roll-extended TST model $\sum_{\mathrm{TST,lin,Roll}}$ using different control configurations, is shown in figure 5.12. At first the pure FFFB-track-tracing controller is applied ($\sum_{\mathrm{TST,DOF2}}$) during the sharp cornering at the relatively high velocity of 35km/h. On one hand, this can result in a reduced load transfer ratio (LTR) but on the other hand it can also lead to a dynamic excitation and instability. The next configuration has the simplified form of the "Active Roll Damping" at the tractor steering implemented ($\sum_{TST,\hat{\delta}_{1,\mathrm{ARD}}}$). The semitrailer steering is fixed and only the ARD at the front steering of the tractor is simulated. According to figure 5.12(a) the reduction of the LTR is small but no dynamic excitation are caused. The simplified "Active Roll Damping" of equation (4.56) at the semitrailer steering can be switch on in addition ($\sum_{TST,\hat{\delta}_{1\&2,\mathrm{ARD}}}$). It further improves the LTR of

the semitrailer but not as far as expected. Nevertheless, despite of these simultaneous intervention the TST is stable and the rollover risk (LTR) is slightly reduced. The resulting position trajectories are clarified in figure 5.12(d). They show that a small change in the steer angle leads to a large deviation of the position.

Remark 5.2. *Since the "Active Roll Damping" intervenes into the driver steer angle and semitrailer steer angle, the TST may deviate from the course i.e. it can happen that the vehicle swing off the road which is not acceptable.*

In equation (4.57) it is proposed to extend the ARD strategy with a roll-angle proportional part and a deathzone. The simulation results of the linear roll model with a steered ($\sum_{TST,\mathrm{lin,Roll}}$) and unsteered ($\sum_{TST,\delta_{2,\mathrm{ARD}}}$) semitrailer are compared in figure 5.13 – the tractor steer angle is not influenced. Figure 5.13(c) shows, that the semitrailer steer angle is held during the corners, so that the maximal LTR_1 and LTR_2 of the tractor and semitrailer in figure 5.13(b) are essentially improved. The position trajectories in figure 5.13(a) clarifies that in the case of a fixed tractor steer angle application, the TST system still offtracks of the road because of the trailer steer intervention. In conclusion, this steering strategy decreases the risk of a rollover significantly during the investigated maneuvers.

5.3 Figures

This section contains the essential figures of the simulation results. For simulating a time of 20sec, the calculation times approximately resulted:

- Nonlinear-models: about 20 sec
- Linear-model: about 10 sec
- SimPack-model: about 2 min

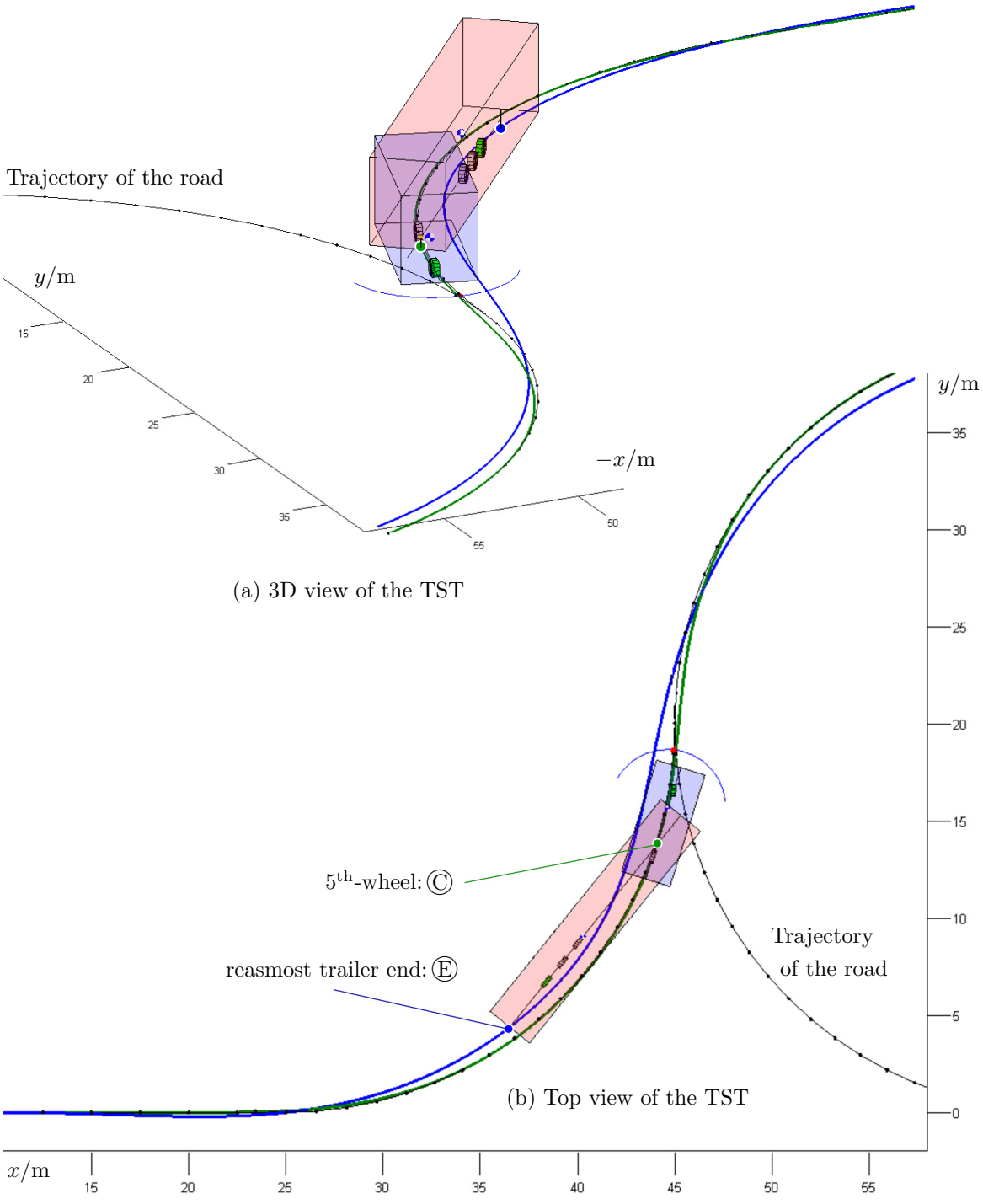

Figure 5.7: Animation of a tractor with an unsteered semitrailer entering a roundabout. The simulation results were calculated with the "Nonlinear Lateral-Yaw Model" $\sum_{\text{TST}}$ and the animation was created with the Toolbox MatCarAnim.

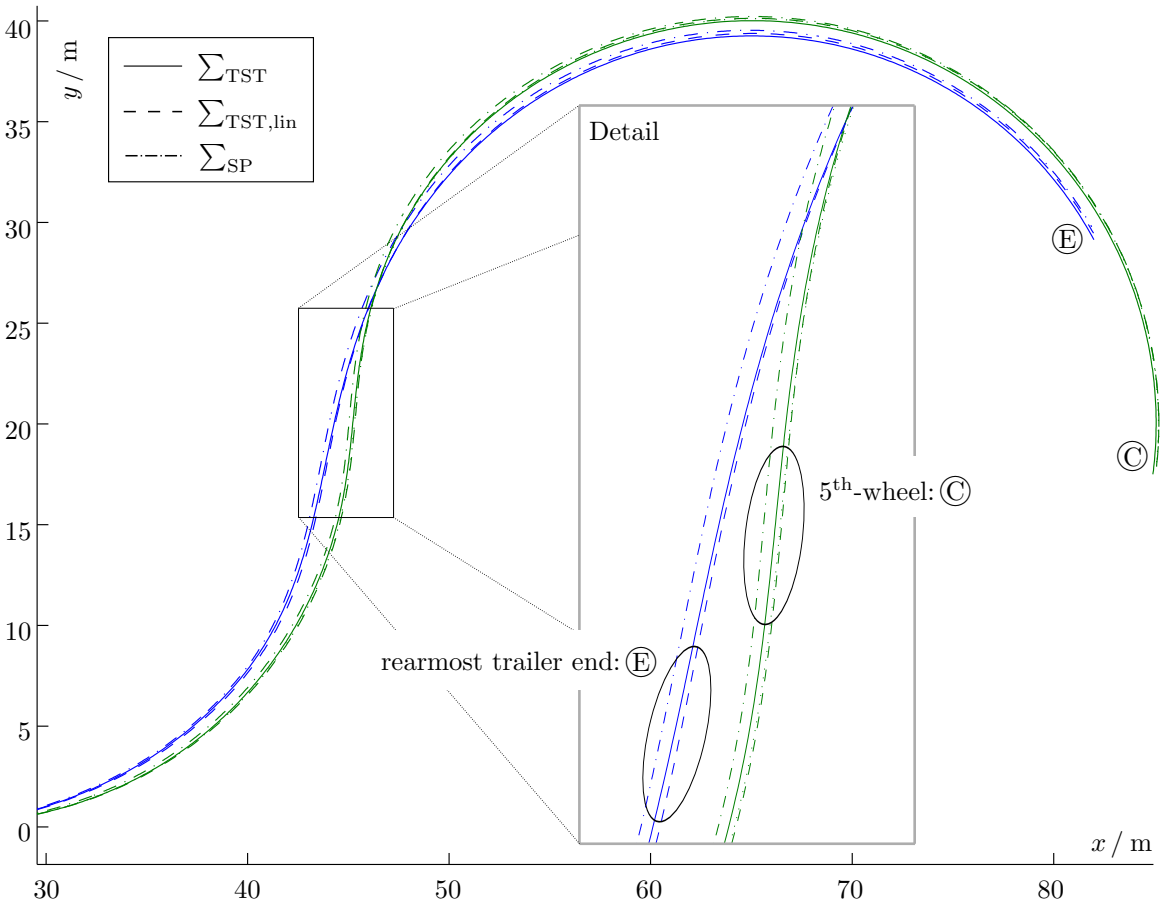

(a) Trajectories of 5th-wheel and rear trailer end position (Nonlinear, Linear & SimPack-model).

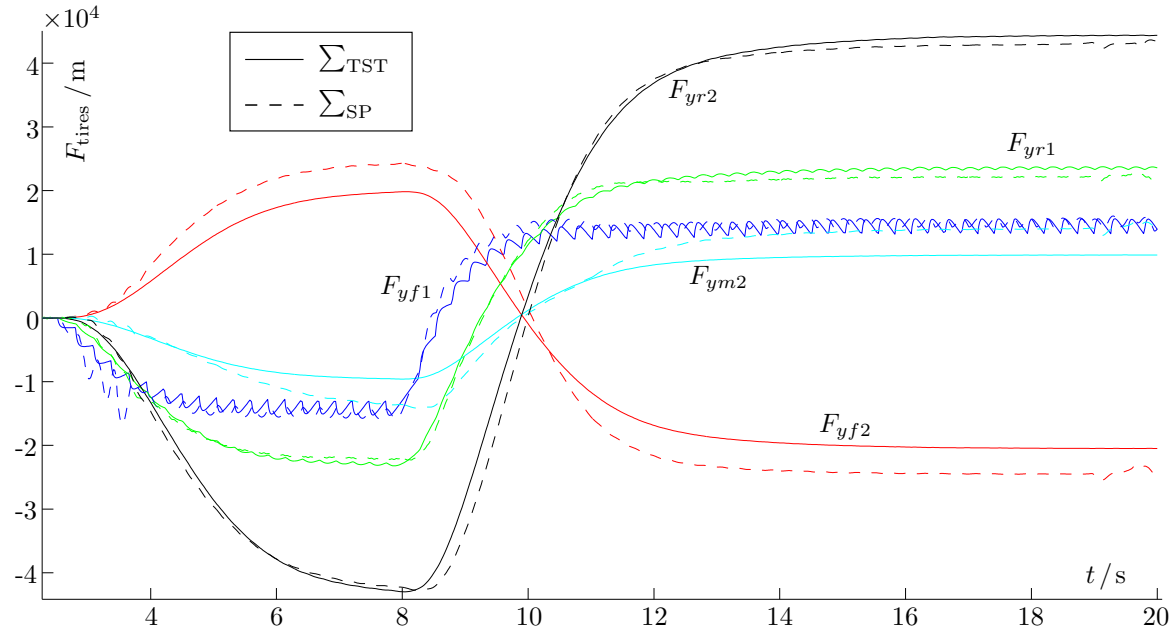

(b) Tire forces of the tractor with the unsteered semitrailer (Nonlinear & SimPack-model).

Figure 5.8: Position-trajectories of the different models with an unsteered semitrailer and at a velocity of 20km/h.

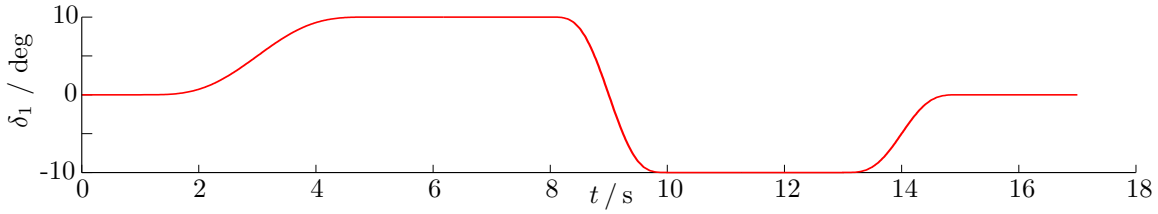

(a) Tractor steer angle

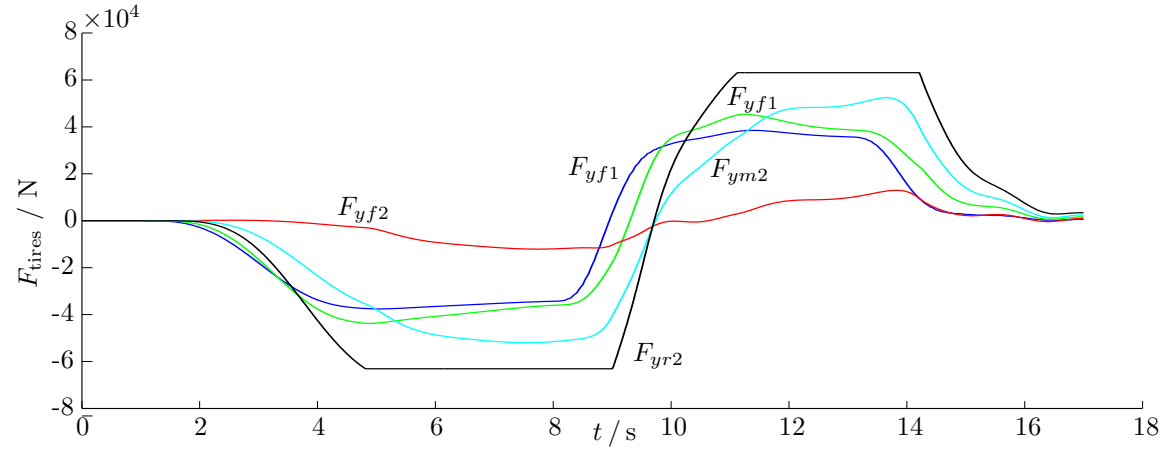

(b) Tire Forces

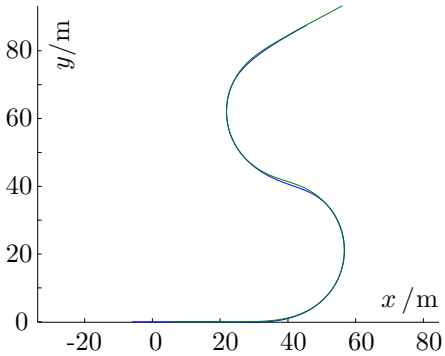

(c) Position trajectories

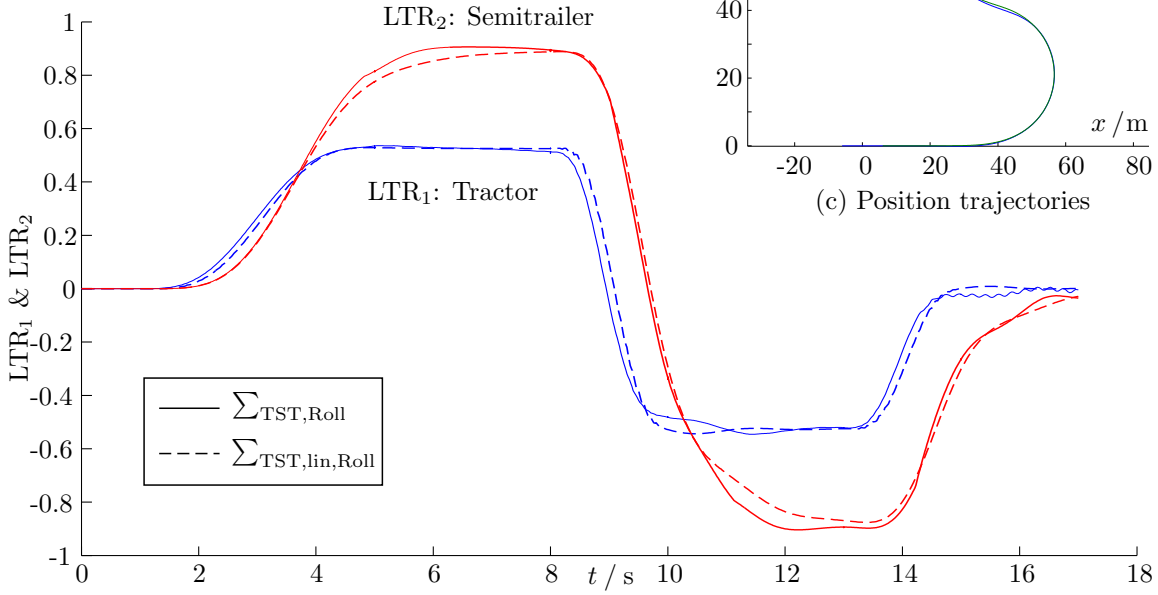

(d) Load transfer ratio (LTR)

Figure 5.9: Trajectories of the nonlinear and linear "Lateral-Yaw-Roll" models with an unsteered semitrailer and at a velocity of 35km/h.

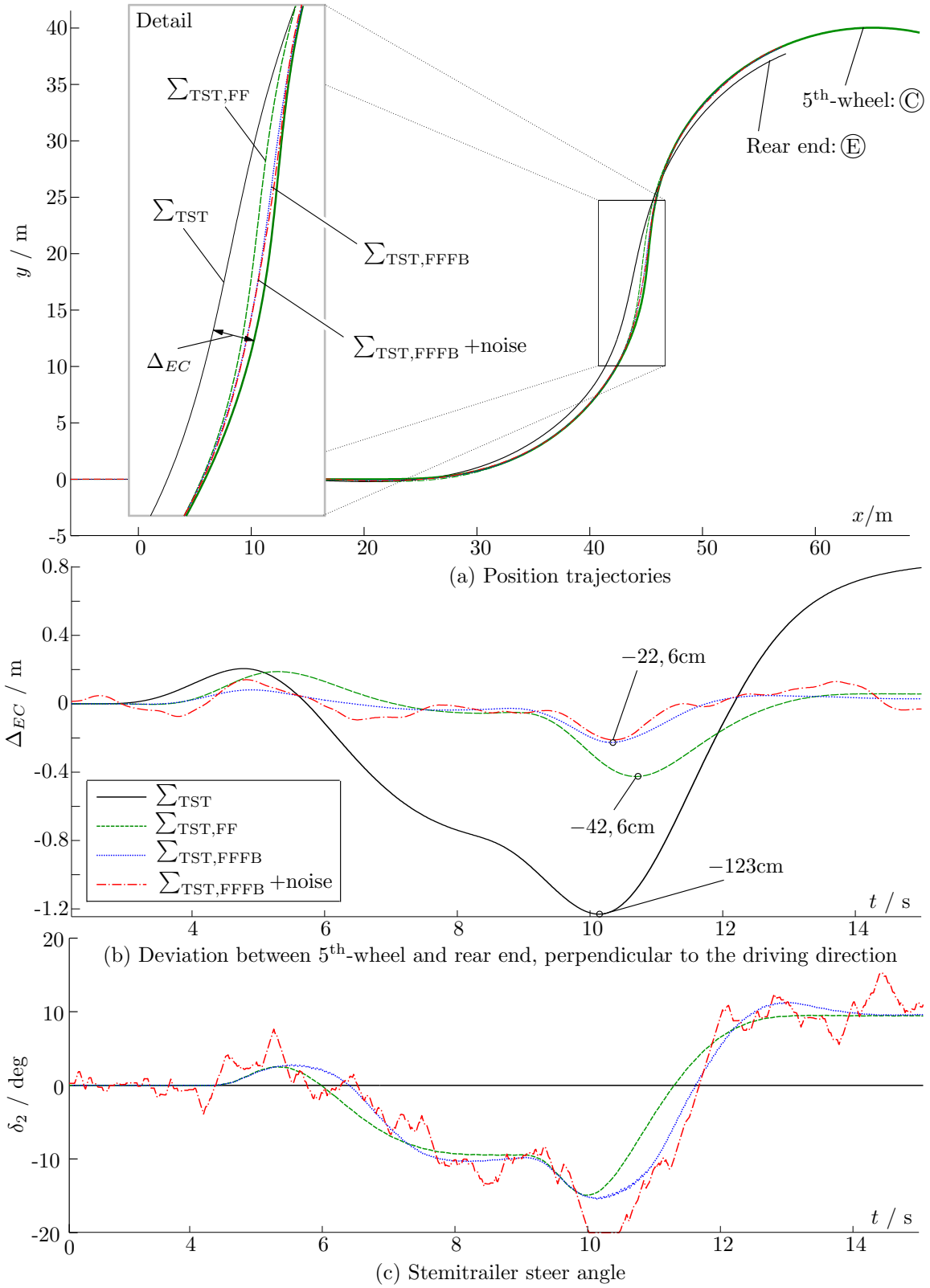

Figure 5.10: Trajectories of the nonlinear "Lateral-Yaw" model with an steered semitrailer and at a velocity of 20km/h.

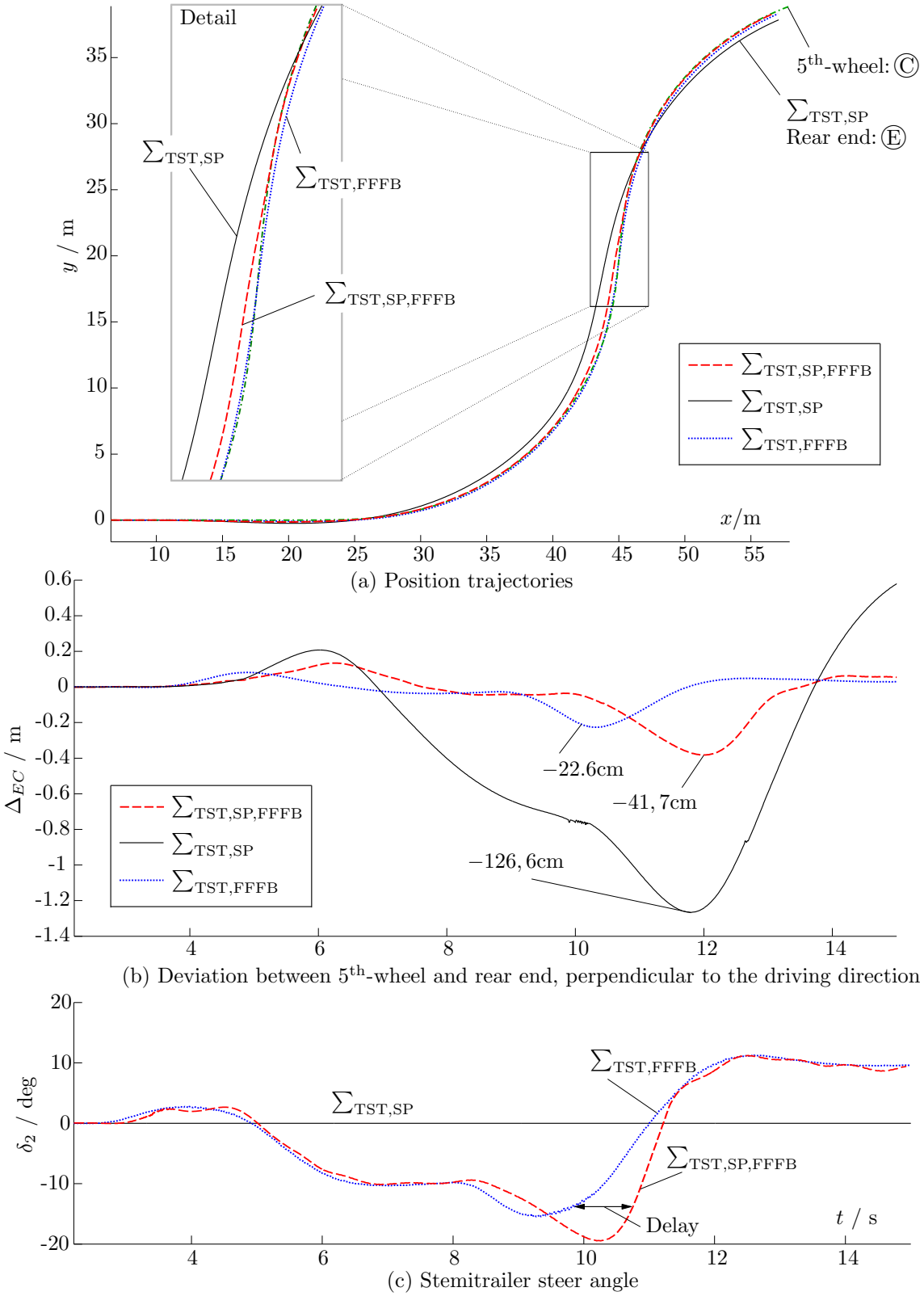

Figure 5.11: Trajectories of the nonlinear ($\sum_{\text{TST}}$) and the SimPack-model ($\sum_{\text{TST,SP}}$) with a steered semitrailer and at a velocity of 20km/h.

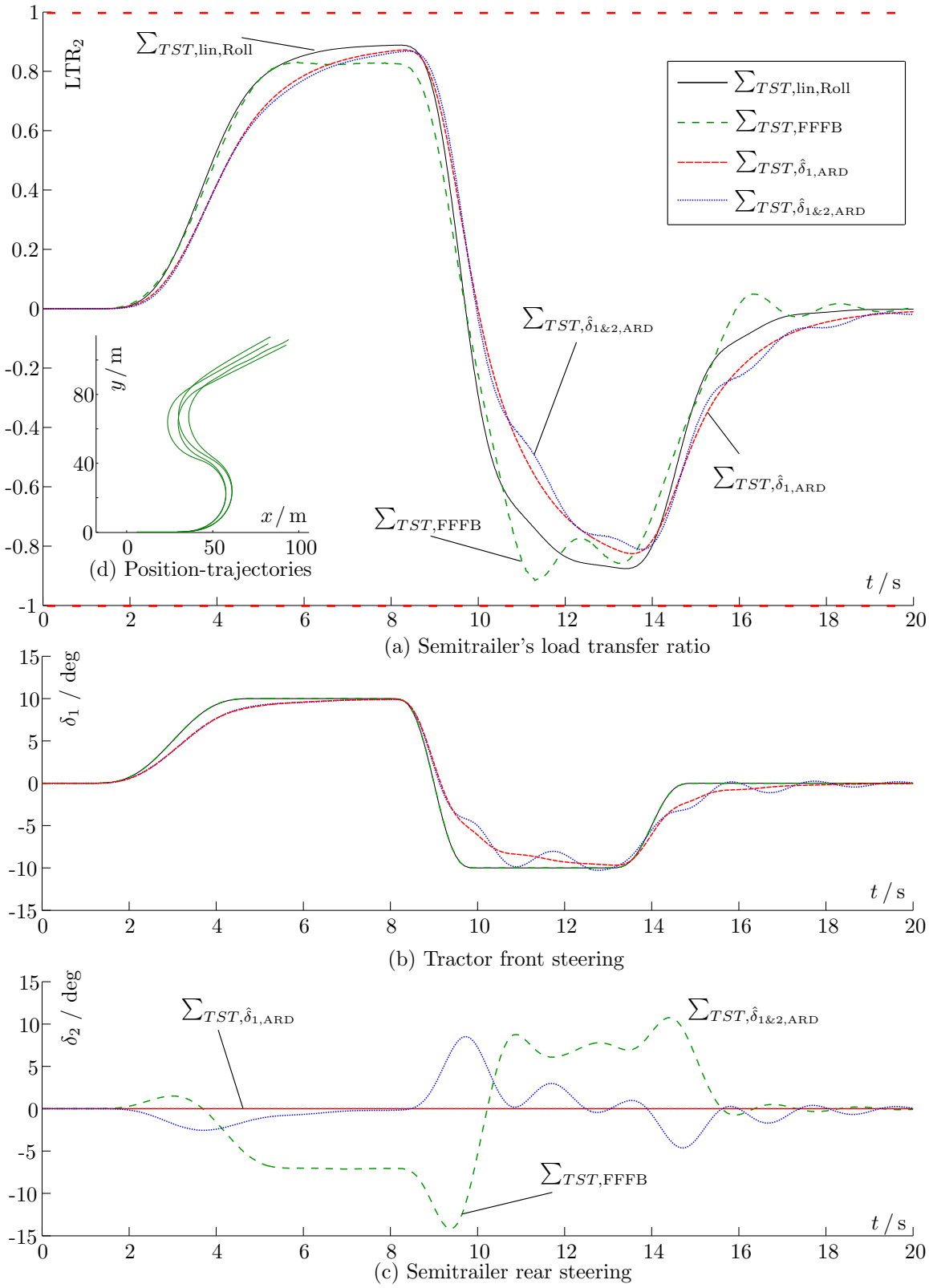

Figure 5.12: Simulation results of the linear roll-extended TST model with the FFFB-track-tracing controller and "Active Roll Damping"(ARD).

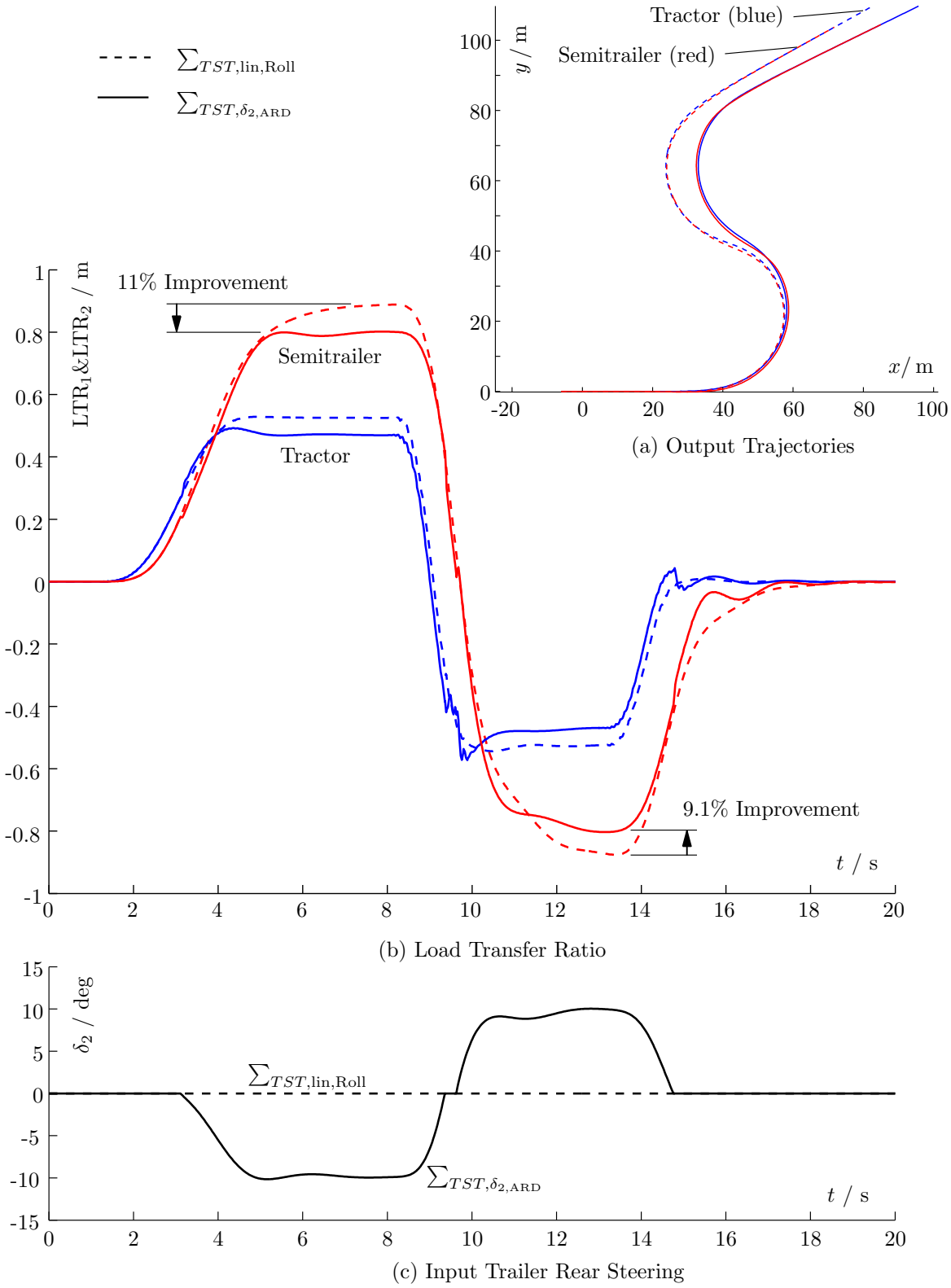

Figure 5.13: Simulation results of the linear roll-extended TST model with the extended "Active Roll Damping"(ARD) control law and a deathzone according to equation (4.57).

Chapter 6

Summary and Outlook

This thesis focuses the modeling and control of articulated tractor-semitrailers (TST). Standard European semitrailers usually utilize an unsteered tri-axle group. They are produced with low financial efforts but have a high tire wear and a reduced maneuverability. The objective of this thesis was to investigate the utilization of a steered rearmost axle of semitrailers in order to improve the performance during low-speed turning maneuvers, high-speed cornering and to react during critical situations such as rollover.

The second chapter introduced some fundamentals of vehicle dynamics with respect to the characterization of the tires, basic vehicle modeling and TST specific approaches. Furthermore, insights of previous research were given and some existing steering and control strategies for a tractor-semitrailer trace-tracking and rollover prevention were presented.

The first challenge during this work was to derive a linear and nonlinear TST single-track model, which take the lateral and yaw motion of the coupled vehicles into account. On the one hand the nonlinear equations of motion (derived by the Newton-Euler approach) characterize the dynamic behavior very accurately, but on the other hand the simplified linear equations can be used for system analysis and for the design of linear model-based controls. The linear model was represented with a saturated tire model and as a fully linear formulation. In addition, the models were extended and re-derived in order to account for the roll motions of the system at high-speed. Finally, the existing multibody simulation (SimPack) model was introduced.

Afterwards the control strategies for the tractor front axle steering and the semitrailer rearmost axle steering were developed and explained. Since the main focus of this thesis was to improve the semitrailer tracking and roll behavior using rear axle steering, multiple control strategies for the semitrailer-steering were designed. Thereby the trajectory of the coupling point is traced with the rear trailer end, reducing offtrack and improving maneuverability of the vehicle. In this scope a steady-state and feedback control strategy was developed. In addition, a feedforward-feedback controller (FFFB) combines both strategies. Furthermore an "active rollover damping"(ARD) control law was proposed, which intervenes with the tractor and / or the trailer steering and aims to reduce the risk of a trailer rollover.

Finally, the derived models and controllers were implemented into the simulation environments. The process chain and simulation structures were illustrated and explained. The models were validated and compared within the simulation results. The influences and improvements of the steering strategies were investigated for a typical maneuver: entering a roundabout at low velocity. It was shown that the FFFB strategy leads to a reliable track-tracing at both, the simplified nonlinear TST model and the precise SimPack model. Moreover the ARD was tested at the tractor and the semitrailer steering. The roll dynamics were simulated during a critical maneuver and the results were analyzed. On the one hand, it was demonstrated that the rollover risk can be significantly reduced using an extended ARD with a deathzone at the semitrailer steerable axle (according to eq. (4.57)), but on the other hand it was shown that the usage of the track-tracing controller at

high velocity may leads to instabilities and to a roll excitation.
In a further research the derived TST models can be used in order to extend the investigation and improvement of the model dynamics using the trailer steering. An optimal path following behavior of the trailer can probably also be realized, designing appropriate observers. The introduced active roll damping strategy is very simple, has a great potential and should be considered in further investigations. Of course, new alternative rollover-prevention-controls could also lead to much better improvements. However, before an universal steering strategy can be implemented on a real semitrailer control device, various control and switching strategies for mixed maneuver (low and high speed / sharp and smooth cornering / different load cases) should be designed and tested intensively.

Appendix A

Model Parameters and Additional Derivations

A.1 Vehicle Parameters

All of the simulation parameters used in this work are listed in the following. The geometrical values are exemplarily visualized in the figures 3.1 and 3.8.

Table A.1: Vehicle geometry

Tractor		Trailer		U.	Description
l_1	1.000			m	Longitudinal distance between vehicle c.g. and front axle
l_2	2.000	b_1	6.000	m	Longitudinal distance between vehicle c.g. and 5$^{\text{th}}$-wheel
l_3	2.600	b_2	0.400	m	Longitudinal distance between vehicle c.g. and 1. rear axle
		b_3	1.700	m	Longitudinal distance between vehicle c.g. and 2. rear axle
		b_4	3.000	m	Longitudinal distance between vehicle c.g. and 3. rear axle
		b_5	3.000	m	Longitudinal distance between rearmost axle and vehicle end
l_T	6.000	l_S	14.00	m	Total length of the vehicle
h_1	0.437	h_2	1.800	m	Height of the c.g. of rolling mass above the roll axis
$h_{r,1}$	0.621	$h_{r,2}$	0.100	m	Height of the roll axis above the ground
z_1	0.479	z_2	1.000	m	Vertical distance between roll center and 5$^{\text{th}}$-wheel
e_1	2.000	e_2	2.095	m	Track width of the vehicle

Table A.2: Vehicle inertia

Tractor		Trailer		Unit	Description
m_1	8200	m_2	34800	kg	Total mass of the vehicle
$I_{xx,1}$	2411	$I_{xx,2}$	20164	kg m^2	Moment of inertia about the x-axis
$I_{zz,1}$	11383	$I_{zz,2}$	223625	kg m^2	Moment of inertia about the z-axis
$I_{xz,1}$	1390	$I_{xz,2}$	14577	kg m^2	Product of inertia about the x and z-axes

Table A.3: Vehicle coupling, suspension and tires

Tractor		Trailer		Unit	Description
c_c	3000e3			Nm/rad	Roll stiffness of 5^{th}-wheel
$k_{f,1}$	380e3			Nm/rad	Roll stiffness of front suspension
$k_{r,1}$	684e3	$k_{r,2}$	2400e3	Nm/rad	Roll stiffness of rear suspension
$k_{ft,1}$	2060e3			Nm/rad	Front tire roll stiffness
$k_{rt,1}$	3337e3	$k_{rt,2}$	5382e3	Nm/rad	Rear tire roll stiffness
$K_{f,1}$	3.2082e5			Nm/rad	Front roll stiffness: $(1/k_f + 1/k_{ft})^{-1}$
$K_{r,1}$	5.6765e5	$K_{r,2}$	1.6547e6	Nm/rad	Rear roll stiffness: $(1/k_r + 1/k_{rt})^{-1}$
c_1	8.8847e5	c_2	1.6547e6	Nm/rad	Total roll stiffness of the vehicle: K_f+K_r
$L_{f,1}$	4.05e3			Nms/rad	Front roll damping of suspension
$L_{r,1}$	6.68e3	$L_{r,2}$	71.7e3	Nms/rad	Rear roll damping of suspension
d_1	10.73e3	d_2	71.7e3	Nms/rad	Total roll damping of the vehicle: L_f+L_r
m_{f1}	7090	m_{f2}	5391	kg	Load on the front / or first rear axle
		m_{m2}	7188	kg	Load on the middle axle
m_{r1}	7573.5	m_{r2}	6772.5	kg	Load on the rear / rearmost axle
C_α	7.5758e6	C_α	7.5758e6	N/(rad kg)	Normalized cornering stiffness (c.s.)
$C_{f,1}$	−5.2692e5	$C_{f,2}$	−4.0065e5	N/rad	c.s. of front axle tires: $-C_\alpha\, g\, m_f$
		$C_{m,2}$	−5.3420e5	N/rad	c.s. of middle axle tires: $-C_\alpha\, g\, m_m$
$C_{r,1}$	−5.6285e5	$C_{r,2}$	−5.0332e5	N/rad	c.s. of rear axle tires: $-C_\alpha\, g\, m_r$

Table A.4: Control parameters, determined by looped parameter tuning

Parameter		Description	Controller	Model
$k_{P,vCtr}$	2e6	Proportional gain	Cruise Control	Nonlinear
$k_{I,vCtr}$	1e6	Integral gain	Cruise Control	Nonlinear
$k_{D,vCtr}$	100	Derivative gain	Cruise Control	Nonlinear
$k_{P,\text{th}}, k_{P,\text{br}}$	280	Proport. gain, throttle/brake	Cruise Control	SimPack
$k_{I,\text{th}}, k_{I,\text{br}}$	100	Integral gain, throttle/brake	Cruise Control	SimPack
$k_{D,\text{th}}, k_{D,\text{br}}$	80	Derivative gain, throttle/brake	Cruise Control	SimPack
k_{P,δ_1}	1	Proportional gain	Tractors Steering	Lin & Nonlin
$k_{P,\delta_1,\text{SP}}$	0.3	Proportional gain	Tractors Steering	SimPack
k_{P,δ_2}	−0.7950	Proportional gain	Steady-State Ctr	All
k_{D,δ_2}	0.7950	Derivative gain	Steady-State Ctr	All
k_a	0.0461	Acceleration gain	Steady-State Ctr	All
$k_{P,\delta_2,\text{FB}}$	4	Proportional gain	Feed-Back Ctr	Lin & Nonlin
$k_{P,\delta_2,\text{FB,SP}}$	7	Proportional gain	Feed-Back Ctr	SimPack
$k_{P2,\text{roll}}$	0.35	Proportional gain	Active Roll Damping	Liner
$k_{I2,\text{roll}}$	1.6	Proportional gain	Active Roll Damping	Liner

A.2 Math Notations

This chapter introduces the math notations of this work. On one hand they are inducted to simplify and shorten the equations and on the other hand they should be conductive to the clear understanding of complex relations.
In expensive equations the trigonometric functions of an arbitrary angle α are abbreviated with

$$\mathrm{s}_\alpha = \sin(\alpha) \qquad \mathrm{c}_\alpha = \cos(\alpha), \tag{A.1}$$

as it was suggested in [PS10]. Whenever a symbol of the Greek alphabet is sub-scripted after a 's' or 'c' letter, it will be treated as the argument of the sinus or cosines function, respectively.
If a vector $\boldsymbol{r}$ or coordinate tuple x is expressed with respect to a reference frame called O^S, the abbreviation will be subscripted before the quantity,

$$_S\boldsymbol{r} \text{ , or } \quad _Sx. \tag{A.2}$$

Otherwise they are related to the initial reference frame O^I. Furthermore the transformation of a reference frame O^T to the frame O^S will be notated with

$$_S\boldsymbol{\phi}_T. \tag{A.3}$$

The description of a trajectory or discrete points of time will be realized with a super-scripted and stapled index or position. So a position trajectory of n values can be exemplarily described by

$$\boldsymbol{r}^{(k)}, \text{ where } k = 1(1)n. \tag{A.4}$$

A.3 Equations of Motion according to the Lagrangian Approach

In the following, the non-linear model in agreement with the Lagrangian equations of motion of second kind is derived. In [dB01] and [FMG06] a model of an articulated vehicle with n-trailers conforming to Lagrange's method was established. The kinematic energy (T) can be written as

$$T \;=\; \frac{1}{2}\sum_{k=1}^{2}\begin{bmatrix}\dot{\boldsymbol{r}}_k^T & \dot{\psi}_k\end{bmatrix}\boldsymbol{M}_k\begin{bmatrix}\dot{\boldsymbol{r}}_k^T & \dot{\psi}_k\end{bmatrix}^T \tag{A.5}$$

where $\boldsymbol{r}_k$ is the position vector of the center of gravity and $\boldsymbol{M}_k$ denotes the mass matrix

$$\boldsymbol{M}_k \;=\; \begin{bmatrix} m_k & 0 & 0 \\ 0 & m_k & 0 \\ 0 & 0 & I_k \end{bmatrix} \tag{A.6}$$

of the corresponding body with index k. With the determination of the generalized coordinates

$$\boldsymbol{q} = \begin{bmatrix} x_2 & y_2 & \psi_2 & \psi_1 \end{bmatrix}^T \;, \tag{A.7}$$

the vector $\begin{bmatrix}\dot{\boldsymbol{r}}_k^T & \dot{\psi}_k\end{bmatrix}^T$ can be expressed by

$$\begin{bmatrix}\dot{\boldsymbol{r}}_k \\ \dot{\psi}_k\end{bmatrix} = \boldsymbol{J}_k\,\dot{\boldsymbol{q}} \;, \tag{A.8}$$

where $\boldsymbol{J}_1$ is the Jacobian matrix of the tractor and $\boldsymbol{J}_1$ of the semitrailer body,

$$\boldsymbol{J}_1 = \begin{bmatrix} 1 & 0 & -b_1\sin\psi_2 & -l_2\sin\psi_1 \\ 0 & 1 & b_1\cos\psi_2 & l_2\cos\psi_1 \\ 0 & 0 & 0 & 1 \end{bmatrix} \qquad \text{and} \qquad \boldsymbol{J}_2 = \begin{bmatrix} 1 & 0 & 0 & 0 \\ 0 & 1 & 0 & 0 \\ 0 & 0 & 1 & 0 \end{bmatrix} \;. \tag{A.9}$$

Substituting (A.8) into (A.5) yields

$$T = \frac{1}{2}\dot{\boldsymbol{q}}^T \boldsymbol{M}(\boldsymbol{q})\,\dot{\boldsymbol{q}} \quad , \text{ where} \qquad \boldsymbol{M}(\boldsymbol{q}) = \sum_{k=1}^{2} \boldsymbol{J}_k^T \boldsymbol{M}_k \boldsymbol{J}_k \tag{A.10}$$

is the global mass matrix. In contrast to the matrix presentation, the kinetic energy can also be calculated segmentally,

$$T = \frac{1}{2}\sum_{k=1}^{2}\sum_{l=1}^{2} M_{[k,l]}\,\dot{q}_{[k]}\,\dot{q}_{[l]} \ . \tag{A.11}$$

According to the methods of the virtual work described in [Sha05], the *D'Alembert-Lagrange's equation* can be derived. For the current MBS with four degree of freedoms it results

$$\sum_{i=1}^{4}\left(\frac{\mathrm{d}}{\mathrm{d}t}\frac{\partial T}{\partial \dot{q}_{[i]}} - \frac{\partial T}{\partial q_{[i]}} - Q_{[i]}\right)\delta q_{[i]} = 0 \ , \tag{A.12}$$

where $\delta\boldsymbol{q}$ is the vector of virtual displacement in generalized coordinates and $\boldsymbol{Q}$ is the vector of generalized forces, respectively, the term $\sum_{i=1}^{4} Q_{[i]}\,\delta q_{[i]}$ characterise the virtual work δW_e of the generalized forces. It can also be calculated with the vector of applied forces $\boldsymbol{F}_e$ and the virtual displacement $\delta\boldsymbol{r}_e$ in Cartesian coordinates in matrix form,

$$\delta W_e = \boldsymbol{Q}^T\,\delta\boldsymbol{q} = \boldsymbol{F}_e^T\,\delta\boldsymbol{r}_e \ . \tag{A.13}$$

Since the virtual displacement in Cartesian coordinates can be written as

$$\delta\boldsymbol{r}_e = \frac{\partial\boldsymbol{r}_e}{\partial\boldsymbol{q}}\,\delta\boldsymbol{q} \ , \tag{A.14}$$

the vector of generalized forces can be evaluated by

$$\boldsymbol{Q}^T = \boldsymbol{F}_e^T\,\frac{\partial\boldsymbol{r}_e}{\partial\boldsymbol{q}} \ , \tag{A.15}$$

where $\boldsymbol{r}_e$ contains all positions of the acting tire forces in Cartesian coordinates. For the vector of the applied tire force in Cartesian coordinates it results

$$\boldsymbol{F}_e = \begin{bmatrix} F_{f1x} \\ F_{f1y} \\ F_{r1x} \\ F_{r1y} \\ F_{f2x} \\ F_{f2y} \\ F_{m2x} \\ F_{m2y} \\ F_{r2x} \\ F_{r2y} \\ F_{1x} \\ F_{1y} \end{bmatrix} = \begin{bmatrix} F_{yf1}\sin(\psi_1+\delta_1) \\ -F_{yf1}\cos(\psi_1+\delta_1) \\ F_{yr1}\sin\psi_1 \\ -F_{yr1}\cos\psi_1 \\ F_{yf2}\sin\psi_2 \\ -F_{yf2}\cos\psi_2 \\ F_{ym2}\sin\psi_2 \\ -F_{ym2}\cos\psi_2 \\ F_{yr2}\sin(\psi_2+\delta_2) \\ -F_{yr2}\cos(\psi_2+\delta_2) \\ F_{\mathrm{aux}}\cos\psi_2 \\ F_{\mathrm{aux}}\sin\psi_2 \end{bmatrix} \ , \tag{A.16}$$

at the positions

$$\boldsymbol{r}_e = \begin{bmatrix} x_{f1} \\ y_{f1} \\ x_{r1} \\ y_{r1} \\ x_{f2} \\ y_{f2} \\ x_{m2} \\ y_{m2} \\ x_{r2} \\ y_{r2} \\ x_1 \\ y_1 \end{bmatrix} = \begin{bmatrix} x_2 + b_1 \cos\psi_2 + (l_1 + l_2)\cos\psi_1 \\ y_2 + b_1 \sin\psi_2 + (l_1 + l_2)\sin\psi_1 \\ x_2 + b_1 \cos\psi_2 - (l_3 - l_2)\cos\psi_1 \\ y_2 + b_1 \sin\psi_2 - (l_3 - l_2)\sin\psi_1 \\ x_2 - b_2 \cos\psi_2 \\ y_2 - b_2 \sin\psi_2 \\ x_2 - b_3 \cos\psi_2 \\ y_2 - b_3 \sin\psi_2 \\ x_2 - b_4 \cos\psi_2 \\ y_2 - b_4 \sin\psi_2 \\ x_2 + b_1 \cos\psi_2 + l_2 \cos\psi_1 \\ y_2 + b_1 \sin\psi_2 + l_2 \sin\psi_1 \end{bmatrix} . \tag{A.17}$$

If the generalized coordinates q_i are linearly independent, Eq. (A.12) leads to *Lagrange's equation of second kind* which is given by

$$\frac{\mathrm{d}}{\mathrm{d}t}\frac{\partial T}{\partial \dot{q}_{[i]}} - \frac{\partial T}{\partial q_{[i]}} = Q_{[i]} \ , \quad i = 1(1)4 \ . \tag{A.18}$$

For the i^{th} generalized coordinate the derivatives can be calculated,

$$\frac{\partial T}{\partial \dot{q}_{[i]}} = \sum_{l=1}^{2} M_{[i,l]} \dot{q}_{[l]} \tag{A.19}$$

$$\frac{\mathrm{d}}{\mathrm{d}t}\frac{\partial T}{\partial \dot{q_{[i]}}} = \sum_{l=1}^{2} M_{[i,l]} \ddot{q}_{[l]} + \sum_{k=1}^{2}\sum_{l=1}^{2} \frac{\partial M_{[i,l]}}{\partial \dot{q}_{[k]}} \, \dot{q}_{[k]} \, \dot{q}_{[l]} \tag{A.20}$$

$$\frac{\partial T}{\partial q_{[i]}} = \frac{1}{2} \sum_{k=1}^{2}\sum_{l=1}^{2} \frac{\partial M_{[k,l]}}{\partial \dot{q}_{[i]}} \, \dot{q}_{[k]} \, \dot{q}_{[l]} \ . \tag{A.21}$$

So the equation of motion for the i^{th} generalized coordinate leads to

$$\sum_{l=1}^{2} M_{[i,l]} \ddot{q}_{[l]} + \sum_{k=1}^{2}\sum_{l=1}^{2} \left(\frac{\partial M_{[i,l]}}{\partial \dot{q}_k} - \frac{1}{2}\frac{\partial M_{[k,l]}}{\partial \dot{q}_{[i]}} \right) \dot{q}_{[k]} \, \dot{q}_{[l]} = Q_{[i]} \ , \quad i = 1(1)4 \ , \tag{A.22}$$

or formulated in matrix form

$$\boldsymbol{M}(\boldsymbol{q}) \, \ddot{\boldsymbol{q}} + \boldsymbol{C}(\boldsymbol{q}, \dot{\boldsymbol{q}}) \, \dot{\boldsymbol{q}} = \boldsymbol{Q}(\boldsymbol{q}) \ . \tag{A.23}$$

After some rearrangements, the equation of motions in matrix-form results

$$\begin{bmatrix} m_1+m_2 & 0 & -b_1 m_1 \mathrm{s}_{\psi_2} & -l_2 m_1 \mathrm{s}_{\psi_1} \\ 0 & m_1+m_2 & b_1 m_1 \mathrm{c}_{\psi_2} & l_2 m_1 \mathrm{c}_{\psi_1} \\ -b_1 m_1 \mathrm{s}_{\psi_2} & b_1 m_1 \mathrm{c}_{psi_2} & m_1 b_1^2 + I_2 & l_2 b_1 m_1 \mathrm{c}_{\psi_1-\psi_2} \\ -l_2 m_1 \mathrm{s}_{\psi_1} & l_2 m_1 \mathrm{c}_{\psi_1} & l_2 b_1 m_1 \mathrm{c}_{\psi_1-\psi_2} & m_1 l_2^2 + I_1 \end{bmatrix} \ddot{\boldsymbol{q}} + \ \ldots$$

$$\begin{bmatrix} 0 & 0 & -\dot{\psi}_2 b_1 m_1 \mathrm{c}_{\psi_2} & -\dot{\psi}_1 l_2 m_1 \mathrm{c}_{\psi_1} \\ 0 & 0 & -\dot{\psi}_2 b_1 m_1 \mathrm{s}_{\psi_2} & -\dot{\psi}_1 l_2 m_1 \mathrm{s}_{\psi_1} \\ -\frac{\dot{\psi}_2 b_1 m_1 \mathrm{c}_{\psi_2}}{2} & -\frac{\dot{\psi}_2 b_1 m_1 \mathrm{s}_{\psi_2}}{2} & \frac{b_1 m_1 (\dot{x}_2 \mathrm{c}_{\psi_2} + \dot{y}_2 \mathrm{s}_{\psi_2} - \dot{\psi}_1 l_2 \mathrm{s}_{\psi_1-\psi_2})}{2} & -\frac{l_2 b_1 m_1 \mathrm{s}_{\psi_1-\psi_2}(2\dot{\psi}_1 - \dot{\psi}_2)}{2} \\ -\frac{\dot{\psi}_1 l_2 m_1 \mathrm{c}_{\psi_1}}{2} & -\frac{\dot{\psi}_1 l_2 m_1 \mathrm{s}_{\psi_1}}{2} & -\frac{l_2 b_1 m_1 \mathrm{s}_{\psi_1-\psi_2}(\dot{\psi}_1 - 2\dot{\psi}_2)}{2} & \frac{l_2 m_1 (\dot{\psi}_2 b_1 \mathrm{s}_{\psi_1-\psi_2} + \dot{x}_2 \mathrm{c}_{\psi_1} + \dot{y}_2 \mathrm{s}_{\psi_1})}{2} \end{bmatrix} \dot{\boldsymbol{q}} \ldots \quad \text{(A.24)}$$

$$= \begin{bmatrix} F_{yf1}\mathrm{s}_{\delta_1+\psi_1} + F_{yr2}\mathrm{s}_{\delta_2+\psi_2} + F_{yf2}\mathrm{s}_{\psi_2} + F_{ym2}\mathrm{s}_{\psi_2} + F_{yr1}\mathrm{s}_{\psi_1} + F_{\mathrm{aux}}\mathrm{c}_{\psi_1} \\ -F_{yf1}\mathrm{c}_{\delta_1+\psi_1} - F_{yr2}\mathrm{c}_{\delta_2+\psi_2} - F_{yf2}\mathrm{c}_{\psi_2} - F_{ym2}\mathrm{c}_{\psi_2} - F_{yr1}\mathrm{c}_{\psi_1} + F_{\mathrm{aux}}\mathrm{s}_{\psi_1} \\ F_{yf2}b_2 + F_{ym2}b_3 - F_{yr1}b_1\mathrm{c}_{\psi_1-\psi_2} - F_{yf1}b_1\mathrm{c}_{\delta_1+\psi_1-\psi_2} + F_{yr2}b_4\mathrm{c}_{\delta_2} + F_{\mathrm{aux}}b_1\mathrm{s}_{\psi_1-\psi_2} \\ F_{yr1}(l_3-l_2) - F_{yf1}\mathrm{c}_{\delta_1}(l_1+l_2) \end{bmatrix}.$$

The trigonometric functions are notated in agreement with (A.1).

A.4 Validation with the Bicycle Model

In this section the derivation of the equations of motion should be validated with the bicycle model derived in section 2.1.2. Therefore, the position vectors to the centers of gravity will be redefined (in contrast to section 3.1.1) **with respect to the tractor** (and not to the semitrailer) as shown in figure 3.1,

$$\boldsymbol{r}_1 = \begin{bmatrix} x_1 \\ y_1 \\ 0 \end{bmatrix} \qquad \text{and} \qquad \boldsymbol{r}_2 = \begin{bmatrix} x_1 - l_2\cos\psi_1 - b_1\cos\psi_2 \\ y_1 - l_2\sin\psi_1 - b_1\sin\psi_2 \\ 0 \end{bmatrix}. \tag{A.25}$$

With the generalized coordinates $\boldsymbol{q}_1 = \begin{bmatrix} x_1 & y_1 & \psi_1 & \psi_2 \end{bmatrix}^T$, the translational Jacobian matrices $\boldsymbol{J}_{T1}$ and $\boldsymbol{J}_{T2}$ for the tractor and semitrailer results in

$$\boldsymbol{J}_{T1} = \frac{\partial \boldsymbol{r}_1}{\partial \boldsymbol{q}_1} = \begin{bmatrix} 1 & 0 & 0 & 0 \\ 0 & 1 & 0 & 0 \\ 0 & 0 & 0 & 0 \end{bmatrix} \quad \text{and} \quad \boldsymbol{J}_{T2} = \frac{\partial \boldsymbol{r}_2}{\partial \boldsymbol{q}_1} = \begin{bmatrix} 1 & 0 & l_2\sin\psi_1 & b_1\sin\psi_2 \\ 0 & 1 & -l_2\cos\psi_1 & -b_1\cos\psi_2 \\ 0 & 0 & 0 & 0 \end{bmatrix}. \tag{A.26}$$

In analogy to (3.4), the local acceleration are

$$\bar{\boldsymbol{a}}_1 = \begin{bmatrix} 0 \\ 0 \\ 0 \end{bmatrix} \quad \text{and} \quad \bar{\boldsymbol{a}}_2 = \begin{bmatrix} l_2\mathrm{c}_{\psi 1}\dot{\psi}_1^2 + b_1\mathrm{c}_{\psi_2}\dot{\psi}_2^2 \\ l_2\mathrm{s}_{\psi 1}\dot{\psi}_1^2 + b_1\mathrm{s}_{\psi_2}\dot{\psi}_2^2 \\ 0 \end{bmatrix} \tag{A.27}$$

and the applied forces $\bar{\boldsymbol{q}}^e$ are identical to (3.10). Conforming to (3.6) this yields

$$\begin{bmatrix} m_1+m_2 & 0 & l_2 m_1 \mathrm{s}_{\psi_1} & b_1 m_1 \mathrm{s}_{\psi_2} \\ 0 & m_1+m_2 & -l_2 m_1 \mathrm{c}_{\psi_1} & -b_1 m_1 \mathrm{c}_{\psi_2} \\ l_2 m_1 \mathrm{s}_{\psi_1} & -l_2 m_1 \mathrm{c}_{\psi_1} & m_2 l_2^2 + I_1 & l_2 b_1 m_2 \mathrm{c}_{\psi_1-\psi_2} \\ b_1 m_1 \mathrm{s}_{\psi_2} & -b_1 m_1 \mathrm{c}_{psi_2} & l_2 b_1 m_2 \mathrm{c}_{\psi_1-\psi_2} & m_2 b_1^2 + I_2 \end{bmatrix} \ddot{\boldsymbol{q}}_1 + \begin{bmatrix} l_2 m_2 \mathrm{c}_{\psi_1}\dot{\psi}_1^2 + b_1 m_2 \mathrm{c}_{\psi_2}\dot{\psi}_2^2 \\ l_2 m_2 \mathrm{s}_{\psi_1}\dot{\psi}_1^2 + b_1 m_2 \mathrm{s}_{\psi_2}\dot{\psi}_2^2 \\ \dot{\psi}_1^2 l_2 b_1 m_2 \mathrm{s}_{\psi_1-\psi_2} \\ -\dot{\psi}_2^2 l_2 b_1 m_2 \mathrm{s}_{\psi_1-\psi_2} \end{bmatrix} \ldots \tag{A.28}$$

$$= \begin{bmatrix} F_{yf1}\mathrm{s}_{\delta_1+\psi_1} + F_{yr2}\mathrm{s}_{\delta_2+\psi_2} + F_{yf2}\mathrm{s}_{\psi_2} + F_{ym2}\mathrm{s}_{\psi_2} + F_{yr1}\mathrm{s}_{\psi_1} + F_{\mathrm{aux}}\mathrm{c}_{\psi_1} \\ -F_{yf1}\mathrm{c}_{\delta_1+\psi_1} - F_{yr2}\mathrm{c}_{\delta_2+\psi_2} - F_{yf2}\mathrm{c}_{\psi_2} - F_{ym2}\mathrm{c}_{\psi_2} - F_{yr1}\mathrm{c}_{\psi_1} + F_{\mathrm{aux}}\mathrm{s}_{\psi_1} \\ F_{yf2}b_2 + F_{ym2}b_3 - F_{yr1}b_1\mathrm{c}_{\psi_1-\psi_2} - F_{yf1}b_1\mathrm{c}_{\delta_1+\psi_1-\psi_2} + F_{yr2}b_4\mathrm{c}_{\delta_2} + F_{\mathrm{aux}}b_1\mathrm{s}_{\psi_1-\psi_2} \\ F_{yr1}(l_3-l_2) - F_{yf1}\mathrm{c}_{\delta_1}(l_1+l_2) \end{bmatrix}.$$

After the transformation (3.17) with the generalized coordinates ${}_T\boldsymbol{q}_1 = \begin{bmatrix} {}_Tx_1 & {}_Ty_1 & \psi_1 & \psi_2 \end{bmatrix}^T$ and the rotation matrix

$$\underbrace{\begin{bmatrix} \dot{x}_1 \\ \dot{y}_1 \\ \dot{\psi}_1 \\ \dot{\psi}_2 \end{bmatrix}}_{\dot{\boldsymbol{q}}_1} = \underbrace{\begin{bmatrix} \cos\psi_1 & -\sin\psi_1 & 0 & 0 \\ \sin\psi_1 & \cos\psi_1 & 0 & 0 \\ 0 & 0 & 1 & 0 \\ 0 & 0 & 0 & 1 \end{bmatrix}}_{{}_I\boldsymbol{\Phi}_T} \underbrace{\begin{bmatrix} {}_T\dot{x}_1 \\ {}_T\dot{y}_1 \\ \dot{\psi}_1 \\ \dot{\psi}_2 \end{bmatrix}}_{{}_T\dot{\boldsymbol{q}}_1} \tag{A.29}$$

to the tractor-fixed reference frame O^T shown in figure 3.2, the tractor related equations of motion can be written by

$$\begin{bmatrix} m_1+m_2 & 0 & 0 & -b_1m_2\mathrm{s}_{\psi_1-\psi_2} \\ 0 & m_1+m_2 & -l_2m_2 & -b_1m_2\mathrm{c}_{\psi_1-\psi_2} \\ 0 & -l_2m_2 & m_2l_2^2+I_1 & l_2b_1m_1\mathrm{c}_{\psi_1-\psi_2} \\ -b_1m_2\mathrm{s}_{\psi_1-\psi_2} & -b_1m_2\mathrm{c}_{\psi_1-\psi_2} & l_2b_1m_1\mathrm{c}_{\psi_1-\psi_2} & m_2b_1^2+I_2 \end{bmatrix} {}_T\ddot{\boldsymbol{q}}_1 + \begin{bmatrix} \dot{\psi}_1^2l_2m_2 + \dot{\psi}_2^2b_1m_2\mathrm{c}_{\psi_1-\psi_2} - \dot{\psi}_1\,{}_T\dot{y}_1(m_1+m_2) \\ -\dot{\psi}_1^2b_1m_2\mathrm{s}_{\psi_1-\psi_2} + \dot{\psi}_1\,{}_T\dot{x}_1(m_1+m_2) \\ -l_2m_2(\dot{\psi}_1\,{}_T\dot{x}_1 - \dot{\psi}_2^2b_1\mathrm{s}_{\psi_1-\psi_2}) \\ -\dot{\psi}_1b_1m_2({}_T\dot{x}_1\mathrm{c}_{\psi_1-\psi_2} + (\dot{\psi}_1l_2 - {}_T\dot{y}_1)\mathrm{s}_{\psi_1-\psi_2}) \end{bmatrix} \ldots \tag{A.30}$$

$$= \begin{bmatrix} F_{\mathrm{aux}} + F_{yr2}\mathrm{s}_{\delta_2-\psi_1+\psi_2} + F_{yf1}\mathrm{s}_{\delta_1} - F_{yf2}\mathrm{s}_{\psi_1-\psi_2} - F_{ym2}\mathrm{s}_{\psi_1-\psi_2} \\ -F_{yr1} - F_{yr2}c_{\delta_2-\psi_1+\psi_2} - F_{yf1}\mathrm{c}_{\delta_1} - F_{yf2}\mathrm{c}_{\psi_1-\psi_2} - F_{ym2}\mathrm{c}_{\psi_1-\psi_2} \\ F_{yr1}l_3 + F_{yf2}l_2\mathrm{c}_{\psi_1-\psi_2} + F_{ym2}l_2\mathrm{c}_{\psi_1-\psi_2} + F_{yr2}l_2\mathrm{c}_{\delta_2-\psi_1+\psi_2} - F_{yf1}l_1\mathrm{c}_{\delta_1} \\ F_{yf2}(b_1+b_2) + F_{ym2}(b_1+b_3) + F_{yr2}\mathrm{c}_{\delta_2}(b_1+b_4) \end{bmatrix}.$$

If one consider the tractor vehicle without the trailer ($m_2 = F_{yf2} = F_{ym2} = F_{yr2} = 0$) and the auxiliary force ($F_{\mathrm{aux}} = 0$), the simplified equation leads to

$$\begin{bmatrix} m_1 & 0 & 0 & 0 \\ 0 & m_1 & 0 & 0 \\ 0 & 0 & I_1 & 0 \\ 0 & 0 & 0 & 0 \end{bmatrix} {}_T\ddot{\boldsymbol{q}}_1 + \begin{bmatrix} -\dot{\psi}_1\,{}_T\dot{y}_1m_1 \\ \dot{\psi}_1\,{}_T\dot{x}_1m_1 \\ 0 \\ 0 \end{bmatrix} = \begin{bmatrix} F_{yf1}\mathrm{s}_{\delta_1} \\ -F_{yf1}\mathrm{c}_{\delta_1} - F_{yr1} \\ -F_{yf1}l_1\mathrm{c}_{\delta_1} + F_{yr1}l_3 \\ 0 \end{bmatrix}, \tag{A.31}$$

respectively with (2.13) and the assumption of small steer angles $\delta_1 << 1$ it yields

$$m_1\,{}_T\ddot{x}_1 - m_1\dot{\psi}_1\,{}_T\dot{y}_1 = C_{\alpha f}\,\alpha_f\,\delta_1 \tag{A.32}$$

$$m_1\,{}_T\ddot{y}_1 + m_1\dot{\psi}_1\,{}_T\dot{x}_1 = -C_{\alpha f}\,\alpha_f - C_{\alpha r}\,\alpha_r \tag{A.33}$$

$$I_1\ddot{\psi}_1 = -C_{\alpha f}\,\alpha_f\,l_1 + C_{\alpha r}\,\alpha_r\,l_3\,. \tag{A.34}$$

The resulted velocity v_1 and the body slip angle β_1 of the tractor are depict in figure (A.1). They

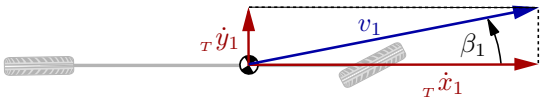

Figure A.1: Explanation of β_1, the body slip angle of the tractor.

are linked to the velocity components (${}_T\dot{x}_1$, ${}_T\dot{y}_1$) and with the assumption of a small body slip angle $\beta_1 << 1$ (equivalent to section 2.1.2) the following conditions can be derived,

$$\cos\beta_1 = \frac{{}_T\dot{x}_1}{v_1} \approx 1 \quad \Leftrightarrow \quad {}_T\dot{x}_1 \approx v_1 \quad \Rightarrow \quad {}_T\ddot{x}_1 \approx \dot{v}_1 \tag{A.35}$$

$$\sin\beta_1 = \frac{{}_T\dot{y}_1}{v_1} \approx \beta_1 \quad \Leftrightarrow \quad {}_T\dot{y}_1 \approx v_1\beta_1 \quad \Rightarrow \quad {}_T\ddot{y}_1 \approx \dot{v}_1\beta_1 + v_1\dot{\beta}_1\,. \tag{A.36}$$

In analogy to (2.16), the front and rear tire slip angles can be calculated by

$$\alpha_f \approx \delta_1 - \frac{\dot{\psi}_1 l_f}{v_1} - \beta_1 \quad \text{and} \quad \alpha_r \approx \frac{\dot{\psi}_1 l_r}{v_1} - \beta_1 \ . \tag{A.37}$$

The next step is to insert the equations (A.35-A.37) in (A.32-A.34), which yields

$$m_1 \dot{v}_1 - m_1 \dot{\psi}_1 v_1 \beta_1 = C_{\alpha f} \left(\delta_1 - \frac{\dot{\psi}_1 l_f}{v_1} - \beta_1 \right) \delta_1 \tag{A.38}$$

$$m_1(\dot{v}_1 \beta_1 + v_1 \dot{\beta}_1) + m_1 \dot{\psi}_1 v_1 = -C_{\alpha f} \left(\delta_1 - \frac{\dot{\psi}_1 l_f}{v_1} - \beta_1 \right) - C_{\alpha r} \left(\frac{\dot{\psi}_1 l_r}{v_1} - \beta_1 \right) \tag{A.39}$$

$$I_1 \ddot{\psi}_1 = -C_{\alpha f} \left(\delta_1 - \frac{\dot{\psi}_1 l_f}{v_1} - \beta_1 \right) l_1 + C_{\alpha r} \left(\frac{\dot{\psi}_1 l_r}{v_1} - \beta_1 \right) l_3 \ . \tag{A.40}$$

For a consideration of the vehicle at constant velocity ($\dot{v} = 0$), the second and third equations leads again to the *Riekert and Schunck's* equations (2.23)

$$m_1 v_1 (\dot{\beta}_1 + \dot{\psi}_1) - (C_{\alpha f} + C_{\alpha r}) \beta_1 - \frac{C_{\alpha f} l_1 - C_{\alpha r} l_3}{v_1} \dot{\psi}_1 = -C_{\alpha f} \delta_1 \tag{A.41}$$

$$I_1 \ddot{\psi}_1 - \frac{1}{v_1} (l_3^2 C_{\alpha r} + l_1^2 C_{\alpha f}) \dot{\psi}_1 - (l_1 C_{\alpha f} - l_3 C_{\alpha r}) \beta_1 = -C_{\alpha f} \delta_1 l_1 \ . \tag{A.42}$$

A.5 Alternative Derivation of the linear TST Model

This section describes an alternative derivation of the linear tractor-semitrailer (TST) model. The equations of motion derived in section 3.3 are obtained by simplifying and linearising the nonlinear TST model. In contrast, the linear model also directly results from a simplified approach of the translational and angular momentum. For of a body with the mass m_i, the directional and lateral acceleration $\ddot{x}_i$ and $\ddot{y}_i$, the moment of inertia I_i and the rotational acceleration $\ddot{\psi}_i$, it can be generally formulated

$$m_i \ddot{x}_i = \sum F_{xi} \ , \qquad m_i \ddot{y}_i = \sum F_{yi} \ , \text{ and} \qquad I_i \ddot{\psi}_i = \sum M_i \ , \tag{A.43}$$

where $\sum F_{xi}$, $\sum F_{xi}$ and $\sum M_i$ characterize the forces and moment acting on the body. Figure A.2 shows the forces acting on the TST. In order to derive linear equations of motion, which describe

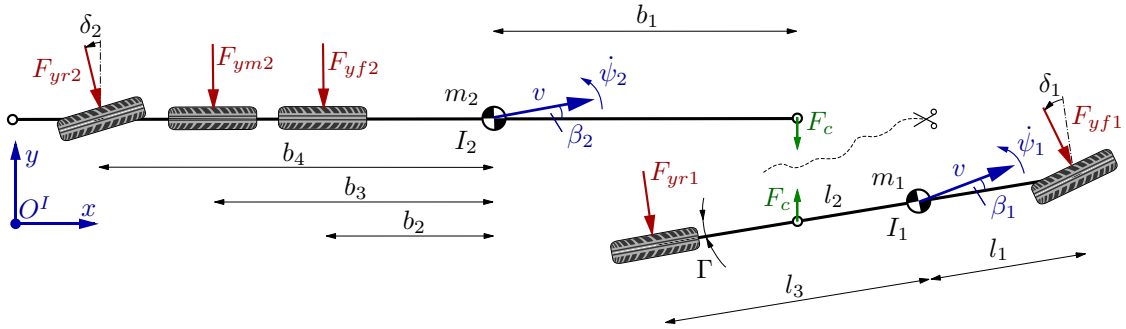

Figure A.2: Single Track Model of Tractor and Semitrailer(TST) with a steered rearmost axle for the derivation of the linear equations.

the lateral and rotational behavior of the TST, the simplifications reported by the enumeration in

section 3.3 have to be taken into account. The lateral acceleration of the tractor can be described by the body angular velocity $\dot{\psi}_1$, the change of the body slip angle β_1 and the constant tractor velocity v with

$$\ddot{y}_1 = v(\dot{\psi}_1 + \dot{\beta}_1) \ . \tag{A.44}$$

So the equilibrium of the forces in the direction of y (lateral) and the momentum around the c.g. of the tractor with the mass m_1 and moment of inertia I_1 yields

$$m_1 v(\dot{\psi}_1 + \dot{\beta}_1) = -F_{yf1} - F_{yr1} + F_c \qquad = Y_{\beta_1}\beta_1 + Y_{\dot{\psi}_1}\dot{\psi}_1 + Y_{\delta_1}\delta_1 + F_c \tag{A.45}$$

$$I_1\ddot{\psi}_1 = -F_{yf1}l_1 + F_{yr1}l_3 - F_c\, l_2 \qquad = N_{\beta_1}\beta_1 + N_{\dot{\psi}_1}\dot{\psi}_1 + N_{\delta_1}\delta_1 - F_c\, l_2 \ , \tag{A.46}$$

where the force F_c represents the internal force at the hitch. The tire forces at the front and rear wheel, F_{yf1} and F_{yr1}, can also be linearly described by the terms Y_{β_1}, $Y_{\dot{\psi}_1}$ and Y_{δ_1}, the caused torsional moment by N_{β_1}, $N_{\dot{\psi}_1}$ and N_{δ_1}. Their explicit calculation will be explained later on.
In analogy, the equations for the semitrailer can be written

$$m_2 v(\dot{\psi}_2 + \dot{\beta}_2) = -F_{yf2} - F_{yr2} - F_{yr1} - F_c \qquad = Y_{\beta_2}\beta_2 + Y_{\dot{\psi}_2}\dot{\psi}_2 + Y_{\delta_2}\delta_2 - F_c \tag{A.47}$$

$$I_2\ddot{\psi}_2 = \quad F_{yf2}b_2 + F_{ym2}b_3 + F_{yr2}b_4 - F_c b_1 \qquad = N_{\beta_2}\beta_2 + N_{\dot{\psi}_2}\dot{\psi}_2 + N_{\delta_2}\delta_2 - F_c b_1 \ . \tag{A.48}$$

The internal hitch force F_c can either be eliminated by using (A.45) and (A.47),

$$m_2 v(\dot{\psi}_2 + \dot{\beta}_2) = Y_{\beta_2}\beta_2 + Y_{\dot{\psi}_2}\dot{\psi}_2 + Y_{\delta_2}\delta_2 - m_1 v(\dot{\psi}_1 + \dot{\beta}_1) + Y_{\beta_1}\beta_1 + Y_{\dot{\psi}_1}\dot{\psi}_1 + Y_{\delta_1}\delta_1 \ , \tag{A.49}$$

or by using (A.45) and (A.48),

$$I_2\ddot{\psi}_2 = N_{\beta_2}\beta_2 + N_{\dot{\psi}_2}\dot{\psi}_2 + N_{\delta_2}\delta_2 - m_1 v(\dot{\psi}_1 + \dot{\beta}_1)b_1 + Y_{\beta_1}\beta_1 b_1 + Y_{\dot{\psi}_1}\dot{\psi}_1 b_1 + Y_{\delta_1}\delta_1 b_1 \ , \tag{A.50}$$

or in conclusion by using (A.45) and (A.46),

$$I_1\ddot{\psi}_1 = N_{\beta_1}\beta_1 + N_{\dot{\psi}_1}\dot{\psi}_1 + N_{\delta_1}\delta_1 - m_1 v(\dot{\psi}_1 + \dot{\beta}_1)l_2 + Y_{\beta_1}\beta_1 l_2 + Y_{\dot{\psi}_1}\dot{\psi}_1 l_2 + Y_{\delta_1}\delta_1 l_2 \ . \tag{A.51}$$

The body slip angle of the tractor β_1 and the slip angular velocity $\dot{\beta}_1$ can be substituted using the kinematic coupling constraints (3.37) and (3.38). Moreover, the derivation of (3.19) with respect to the time leads to the additional equation

$$\dot{\Gamma} = \dot{\psi}_1 - \dot{\psi}_2 \ . \tag{A.52}$$

Furthermore, the generalized coordinates

$$\boldsymbol{q}_{\text{lin}} = \begin{bmatrix} \Gamma & \dot{\psi}_1 & \beta_2 & \dot{\psi}_2 \end{bmatrix}^T \tag{A.53}$$

and the input vector

$$\boldsymbol{u} = \begin{bmatrix} \delta_1 & \delta_2 \end{bmatrix}^T \tag{A.54}$$

will be defined. After some rearrangements, the equations (A.51)-(A.52) can be written in matrix form as

$$\begin{bmatrix} 0 & m_1 l_2 & (m_1+m_2)v & m_1 b_1 \\ 0 & m_1 l_2 b_1 & m_1 b_1 v & m_1 b_1^2 + I_2 \\ 0 & m_1 l_2^2 + I_1 & m_1 l_2 v & m_1 l_2 b_1 \\ 1 & 0 & 0 & 0 \end{bmatrix} \dot{\boldsymbol{q}}_{\text{lin}} + \begin{bmatrix} Y_{\beta_1} & -Y_{\dot{\psi}_1} - Y_{\beta_1}\frac{l_2}{v} & -Y_{\beta_2} - Y_{\beta_1} & (m_1+m_2)v - Y_{\dot{\psi}_2} - Y_{\beta_1}\frac{b_1}{v} \\ Y_{\beta_1} b_1 & -(Y_{\dot{\psi}_1} + Y_{\beta_1}\frac{l_2}{v})b_1 & -N_{\beta_2} - Y_{\beta_1} b_1 & m_1 v b_1 - N_{\psi_2} - Y_{\beta_1}\frac{b_1^2}{v} \\ N_{\beta_1} + Y_{\beta_1} l_2 & -N_{\psi_1} - Y_{\dot{\psi}_1} l_2 - Y_{\beta_1}\frac{l_2^2}{v} - N_{\beta_1}\frac{l_2}{v} & -N_{\beta_1} - Y_{\beta_1} l_2 & m_1 l_2 v - (N_{\beta 1} + Y_{\beta_1} l_2)\frac{b_1}{v} \\ 0 & -1 & 0 & 1 \end{bmatrix} \boldsymbol{q}_{\text{lin}} \tag{A.55}$$
$$\ldots = \begin{bmatrix} Y_{\delta_1} & Y_{\delta_2} \\ Y_{\delta_1} b_1 & N_{\delta_2} \\ N_{\delta_1} + Y_{\delta_1} l_2 & 0 \\ 0 & 0 \end{bmatrix} \boldsymbol{u} \,,$$

which is equal to (3.65). The explicit linear model equations

$$\underbrace{\begin{bmatrix} 0 & m_1 l_2 & (m_1+m_2)v & m_1 b_1 \\ 0 & m_1 l_2 b_1 & m_1 b_1 v & m_1 b_1^2 + I_2 \\ 0 & m_1 l_2^2 + I_1 & m_1 l_2 v & m_1 l_2 b_1 \\ 1 & 0 & 0 & 0 \end{bmatrix}}_{\tilde{\boldsymbol{M}}} \dot{\boldsymbol{q}}_{\text{lin}} + \ldots$$

$$\underbrace{\begin{bmatrix} C_{f1} + C_{r1} & C_{r1}\frac{l_3 - l_2}{v} - C_{f1}\frac{l_1 + l_2}{v} & -(C_{f2} + C_{m2} + C_{r2} + C_{f1} + C_{r1}) & (m_1+m_2)v + C_{f2}\frac{b_2}{v} + C_{m2}\frac{b_3}{v} + C_{r2}\frac{b_4}{v} - (C_{f1}+C_{r1})\frac{b_1}{v} \\ C_{f1} b_1 + C_{r1} b_1 & C_{r1} b_1 \frac{l_3 - l_2}{v} - C_{f1} b_1 \frac{l_1 + l_2}{v} & C_{f2} b_2 + C_{m2} b_3 + C_{r2} b_4 - C_{r1} b_1 - C_{f1} b_1 & m_1 v b_1 - C_{f2}\frac{b_2^2}{v} - C_{m2}\frac{b_3^2}{v} - C_{r2}\frac{b_4^2}{v} - C_{r1}\frac{b_1^2}{v} - C_{f1}\frac{b_1^2}{v} \\ C_{f1}(l_1+l_2) - C_{r1}(l_3 - l_2) & -C_{r1}\frac{(l_3 - l_2)^2}{v} - C_{f1}\frac{(l_1+l_2)^2}{v} & C_{r1}(l_3 - l_2) - C_{f1}(l_1 + l_2) & m_1 l_2 v + C_{r1} b_1 \frac{l_3 - l_2}{v} - C_{f1} b_1 \frac{l_1 + l_2}{v} \\ 0 & -1 & 0 & 1 \end{bmatrix}}_{\tilde{\boldsymbol{D}}} \boldsymbol{q}_{\text{lin}} \tag{A.56}$$

$$\ldots = \underbrace{\begin{bmatrix} -C_{f1} & -C_{r2} \\ -C_{f1} b_1 & C_{r2} b_4 \\ -C_{f1}(l_1 + l_2) & 0 \end{bmatrix}}_{\tilde{\boldsymbol{H}}} \boldsymbol{u}.$$

can be obtained by expressing the tire forces not with the terms Y_{β_1}, $Y_{\dot{\psi}_1}$, Y_{δ_1}, N_{β_1}, $N_{\dot{\psi}_1}$ and N_{δ_1}, but with the explicit description according to (3.28)-(3.31) as explained in the following.

In order to find the relation between the Y-/N- parameters and the tire forces, the right side of the equations (A.45)-(A.46) can be used,

$$-F_{yf1}-F_{yr1} \overset{(3.28)}{=} -C_{f1}\alpha_{f1}-C_{r1}\alpha_{r1} = Y_{\beta_1}\beta_1 + Y_{\dot{\psi}_1}\dot{\psi}_1 + Y_{\delta_1}\delta_1 \tag{A.57}$$

$$-F_{yf1}l_1+F_{yr1}l_3 \overset{(3.28)}{=} -C_{f1}\alpha_{f1}l_1+C_{r1}\alpha_{r1}l_3 = N_{\beta_1}\beta_1 + N_{\dot{\psi}_1}\dot{\psi}_1 + N_{\delta_1}\delta_1 \tag{A.58}$$

$$-F_{yf2}-F_{yr2}-F_{yr1} \overset{(3.29)}{=} -C_{f2}\alpha_{f2}-C_{r2}\alpha_{r2}-C_{r1}\alpha_{r1} = Y_{\beta_2}\beta_2 + Y_{\dot{\psi}_2}\dot{\psi}_2 + Y_{\delta_2}\delta_2 \tag{A.59}$$

$$F_{yf2}b_2+F_{ym2}b_3+F_{yr2}b_4 \overset{(3.29)}{=} C_{f2}\alpha_{f2}b_2+C_{m2}\alpha_{r2}b_3+C_{r2}\alpha_{r1}b_4 = N_{\beta_2}\beta_2 + N_{\dot{\psi}_2}\dot{\psi}_2 + N_{\delta_2}\delta_2\ . \tag{A.60}$$

With the substitution of the slip angles (3.30)-(3.31) and equating the coefficients, the Y-/N-parameters can be determined equal to (3.66)-(3.69). They are also called the partial derivatives of the lateral tire forces $F_{\text{tractor tires}}$ and $F_{\text{semitrailer tires}}$ and tire yaw moments $M_{\text{tractor tires}}$ and $M_{\text{semitrailer tires}}$,

$$Y_{\beta_1}=\frac{\partial}{\partial\beta_1}F_{\text{tractor tires}} \quad Y_{\dot{\psi}_1}=\frac{\partial}{\partial\dot{\psi}_1}F_{\text{tractor tires}} \quad Y_{\delta_1}=\frac{\partial}{\partial\delta_1}F_{\text{tractor tires}} \tag{A.61}$$

$$N_{\beta_1}=\frac{\partial}{\partial\beta_1}M_{\text{tractor tires}} \quad N_{\dot{\psi}_1}=\frac{\partial}{\partial\dot{\psi}_1}M_{\text{tractor tires}} \quad N_{\delta_1}=\frac{\partial}{\partial\delta_1}M_{\text{tractor tires}} \tag{A.62}$$

$$Y_{\beta_2}=\frac{\partial}{\partial\beta_2}F_{\text{semitrailer tires}} \quad Y_{\dot{\psi}_2}=\frac{\partial}{\partial\dot{\psi}_2}F_{\text{semitrailer tires}} \quad Y_{\delta_2}=\frac{\partial}{\partial\delta_2}F_{\text{semitrailer tires}} \tag{A.63}$$

$$N_{\beta_2}=\frac{\partial}{\partial\beta_2}M_{\text{semitrailer tires}} \quad N_{\dot{\psi}_2}=\frac{\partial}{\partial\dot{\psi}_2}M_{\text{semitrailer tires}} \quad N_{\delta_2}=\frac{\partial}{\partial\delta_2}M_{\text{semitrailer tires}}\ . \tag{A.64}$$

A.6 Symbolic derivation of the equations of motion using MATLAB

In this section are some MATLAB-Codes listed, which are tested in MATLAB 7.12.0 (R2011a) and whereby the *Symbolic-Toolbox* is used.

Listing A.1: MATLAB-Code for the derivation of the nonlinear equations of motion of the TST according the Newton Euler approach by using the *Symbolic-Toolbox*.

```
%% Calc Nonlinear Equation of Tractor-Semitrailer with Newton-Euler-Equ
% --> general coordinates x2 and y2 describes the semitrailer c.g.;
%     psi2 and psi1 describes the orientation angles
%
% references:
% #1 Book (PoppSchiehlen2010) Popp, K. & Schiehlen, W.
%    Ground Vehicle Dynamics
%    Springer-Verlag Berlin Heidelberg, 2010
% #2 A. A. Shabana. Dynamics of Multibody Systems.
%    Cambridge University Press, Cambridge, 3 edition, 2005.

% generalized coordinates:
syms x2 y2 psi2 psi1 Dx2 Dy2 Dpsi2 Dpsi1 D2x2 D2y2 D2psi2 D2psi1
syms m1 I1 m2 I2 l_1 l_2 l_3 b_1 b_2 b_3 b_4 t_

% generalized coordinates
q   = [x2;    y2;     psi2;   psi1];
```

```
Dq  = [Dx2;   Dy2;    Dpsi2;  Dpsi1];
D2q = [D2x2;  D2y2;   D2psi2; D2psi1];

% Position and Rotation of the tractor's(r_1) and semitrailer's(r_2) c.g.
r_1 = [x2+b_1*cos(psi2)+l_2*cos(psi1); y2+b_1*sin(psi2)+l_2*sin(psi1); 0];
r_2 = [x2;                            y2;                             0];
omegl_1 = [0;                         0;                        Dpsi1];
omegl_2 = [0;                         0;                        Dpsi2];

% ------------------------------------------------------------------------
% prepare timedependent auxiliary variables als Taylor-Series for
% implicit derivative
x2_ = x2 + Dx2*t_ + 1/2*D2x2*t_^2;
y2_ = y2 + Dy2*t_ + 1/2*D2y2*t_^2;
psi2_ = psi2 + Dpsi2*t_ + 1/2*D2psi2*t_^2;
psi1_ = psi1 + Dpsi1*t_ + 1/2*D2psi1*t_^2;
q_ = [x2_;    y2_;     psi2_;   psi1_];

% Calculate the velocities
% substitute the auxiliary terms
r_1_ = subs(r_1,q,q_);
r_2_ = subs(r_2,q,q_);
% Now it is possible to obtain the time derive explicitly, because
% the quantities are explicitly dependent of the time
v_1_ = diff(r_1_,'t_');
v_2_ = diff(r_2_,'t_');
% Set t_=0 to eliminate the nonrelevant auxilliary terms
v_1 = subs(v_1_,t_,0);
v_2 = subs(v_2_,t_,0);

% Calculate the accelerations
l_1_ = diff(v_1_,'t_');
l_2_ = diff(v_2_,'t_');
% Set t_=0 to eliminate the nonrelevant auxilliary terms
ac_1 = subs(l_1_+t_,t_,0);
ac_2 = subs(l_2_+t_,t_,0);

% Jacobian-Matrices
J_T1 = jacobian(r_1,q);
J_T2 = jacobian(r_2,q);
J_R1 = jacobian(omegl_1,Dq);
J_R2 = jacobian(omegl_2,Dq);
J = [J_T1; J_T2; J_R1; J_R2];

% Calculate the local accelleration:
% ai = Ji*D2q + ai_lok --> ai_lok = ai - Ji*D2q
l_1q = simplify(ac_1-J_T1*D2q);
l_2q = simplify(ac_2-J_T2*D2q);

% Vector of generalized gyroscopic forces including the Coriolis and
% centrifugal forces as well as the gyroscopic torques (#1, Pages 67, 75)
k_dash = simplify([m1*l_1q; m2*l_2q; zeros(6,1)]);

% Def Mass / Interia
M_glob = [m1*eye(3,3) zeros(3,3)   zeros(3,3)   zeros(3,3); ...
          zeros(3,3)   m2*eye(3,3) zeros(3,3)   zeros(3,3); ...
          zeros(6,12)];
M_glob(9,9) = I1;
M_glob(12,12) = I2;

% ------------------------------------------------------------------------
% Consider the Tire-Forces in x,y,z on each body --> Calc q_e - Vector (#1)
syms F_yf1 F_yr1 F_yf2 F_ym2 F_yr2 F_aux delta1 delta2
q_dash_e = ...
    [ F_yf1*sin(psi1+delta1) + F_yr1*sin(psi1) + F_aux*cos(psi1); ...
     -F_yf1*cos(psi1+delta1) - F_yr1*cos(psi1) + F_aux*sin(psi1); ...
```

```
      0; ...
      F_yf2*sin(psi2) + F_ym2*sin(psi2) + F_yr2*sin(psi2+delta2);...
     -F_yf2*cos(psi2) - F_ym2*cos(psi2) - F_yr2*cos(psi2+delta2);...
      0; ...
      0; ...
      0; ...
     -F_yf1*l_1*cos(delta1) + F_yr1*l_3; ...
      0; ...
      0; ...
      F_yf2*b_2 + F_ym2*b_3 + F_yr2*b_4*cos(delta2)];

% ------------------------------------------------------------------------
%% Equations of motion (Neuton-Euler) in I-sys
%  M_glob(q,q_dot)*J*D2q + k_dash(q,q_dot) = q_dash_e + Q*lambda
% J'*| M_glob(q,q_dot)*J*D2q + k_dash(q,q_dot) = q_dash_e + Q*lambda
% --> J'*Q = 0
M = simplify(J.'*M_glob*J)
k = simplify(J.'*k_dash)
q_e = simplify(J.'*q_dash_e)
```

Listing A.2: MATLAB-Code for the transformation of equations of motion to the trailer-fixed reference frame by using the *Symbolic-Toolbox*.

```
%% Transfer Equations of Motions to the trailer-fixed reference frame:
% Prepare Transformation I-sys to S-sys according #1:
%  S_Phi_I*|  M(q,q_dot)*D2q + k(q,q_dot) = q_e
%
%  with: q_dot = I_Phi_S * q_dot_s
%   --> q_dot2 = I_Phi_S * q_dot2_s + I_Phi_S_dot * q_dot_s

% generalized coordinates
syms x2 y2 psi2 psi1 Dx2 Dy2 Dpsi2 Dpsi1 D2x2 D2y2 D2psi2 D2psi1 t_
q   = [x2;    y2;     psi2;   psi1];
q_s =   [x2 y2 psi2 psi1].';
Dq_s =  [Dx2 Dy2 Dpsi2 Dpsi1].';
D2q_s = [D2x2 D2y2 D2psi2 D2psi1].';
I_Phi_S = [cos(psi2) -sin(psi2) 0   0;
           sin(psi2)  cos(psi2) 0   0;
           0          0         1   0;
           0          0         0   1];
% Calc time derivative:
% prepare timedependent auxiliary variables als Taylor-Series for
% implicit derivative
x2_ = x2 + Dx2*t_ + 1/2*D2x2*t_^2;
y2_ = y2 + Dy2*t_ + 1/2*D2y2*t_^2;
psi2_ = psi2 + Dpsi2*t_ + 1/2*D2psi2*t_^2;
psi1_ = psi1 + Dpsi1*t_ + 1/2*D2psi1*t_^2;
q_ = [x2_;    y2_;     psi2_;   psi1_];
% substitute the auxiliary terms
I_Phi_S_ = subs(I_Phi_S,q,q_);
% Now it is possible to obtain the time derive explicitly, because
% the quantities are explicitly dependent of the time
I_Phi_S_dot_ = diff(I_Phi_S_,'t_');
% Set t_=0 to eliminate the nonrelevant auxilliary terms
I_Phi_S_dot = subs(I_Phi_S_dot_,t_,0);

% ------------------------------------------------------------------------
%% Do Trafo
M_s = simplify(I_Phi_S.'*M*I_Phi_S)
k_s = simplify(I_Phi_S.'*M*I_Phi_S_dot*Dq_s + ...
               I_Phi_S.'*k)
q_e_s = simplify(I_Phi_S.'*q_e)
```

Listing A.3: MATLAB-Code for the derivation of the roll-extended single-track model of the TST using the *Symbolic-Toolbox*.

```
syms Gamma Dpsi_1 Dpsi_2 beta_1 beta_2 phi_1 phi_2 Dphi_1 Dphi_2 delta_1 delta_2
syms DGamma D2psi_1 D2psi_2 Dbeta_1 Dbeta_2 D2phi_1 D2phi_2 delta_1 delta_2
syms m1 m2 g l_2 b_1 v_1 v_2 h_1 h_2 z_1 z_2 d_1 d_2 c_1 c_2 c_c
syms Iz2 Iyy2 Ixz2 Ixx2 Iz1 Iyy1 Ixz1 Ixx1
syms Y_beta1 Y_r1 Y_delta1 Y_beta2 Y_r2 Y_delta2 F_c
syms N_beta1 N_r1 N_delta1 N_beta2 N_r2 N_delta2
syms Dphi_1_ Dphi_2_ % auxilliary vars for state-space-representation
% ------------------------------ Tractor ------------------------------------
% lateral1 equ:
lateral1_str = strcat('m1*v_1*(Dpsi_1 + Dbeta_1) - m1*D2phi_1*h_1 = ', ...
                'Y_beta1*beta_1 + Y_r1*Dpsi_1 + Y_delta1*delta_1 + F_c');
F_c1 = solve(lateral1_str,'F_c');
lateral1 = m1*v_1*(Dpsi_1 + Dbeta_1) - m1*D2phi_1*h_1 ...
            - Y_beta1*beta_1 - Y_r1*Dpsi_1 - Y_delta1*delta_1 - F_c ; % = 0

% yaw1 equ:
yaw1 = Iz1*D2psi_1 - Ixz1*D2phi_1 ...
         - N_beta1*beta_1 - N_r1*Dpsi_1 - N_delta1*delta_1 + F_c*l_2; % = 0

% roll1 equ:
roll1 = (Ixx1 + m1*h_1^2)*D2phi_1 - m1*v_1*(Dpsi_1 + Dbeta_1)*h_1 ...
        - Ixz1*D2psi_1 - m1*g*h_1*phi_1 + c_1*phi_1  + d_1*Dphi_1 ...
        + c_c*(phi_1-phi_2) + F_c*z_1; % = 0

% ------------------------------ Semitrailer --------------------------------
% lateral2 equ:
lateral2 = m2*v_2*(Dpsi_2 + Dbeta_2) - m2*D2phi_2*h_2 ...
             - Y_beta2*beta_2 - Y_r2*Dpsi_2 - Y_delta2*delta_2 + F_c; % = 0

% yaw2 equ:
yaw2 = Iz2*D2psi_2 - Ixz2*D2phi_2 ...
        - N_beta2*beta_2 - N_r2*Dpsi_2 - N_delta2*delta_2 + F_c*b_1'; % = 0

% roll2 equ:
roll2 = (Ixx2 + m2*h_2^2)*D2phi_2  - m2*v_2*(Dpsi_2 + Dbeta_2)*h_2 ...
          - Ixz2*D2psi_2 - m2*g*h_2*phi_2 + c_2*phi_2 + d_2*Dphi_2 ...
          - c_c*(phi_1-phi_2) - F_c*z_2'; % = 0

% ------------------------- Coupling Conditions -----------------------------
beta_1_ = -Gamma + beta_2 + l_2/v_2*Dpsi_1 + b_1/v_1*Dpsi_2 ...
                              + z_1/v_1*Dphi_1 - z_2/v_2*Dphi_2;

Dbeta_1_ = Dpsi_2 - Dpsi_1 + Dbeta_2 + l_2/v_1*D2psi_1 ...
            + b_1/v_2*D2psi_2 + z_1/v_1*D2phi_1  - z_2/v_2*D2phi_2;

kin_constraint = Dpsi_2 - Dpsi_1 + Dbeta_2 - Dbeta_1 + l_2/v_1*D2psi_1 ...
            + b_1/v_2*D2psi_2 + z_1/v_1*D2phi_1  - z_2/v_2*D2phi_2; % = 0

Gamma_constraint = DGamma - Dpsi_1 + Dpsi_2;

% -------------------------------------------------------------------------
%% Elliminate Fc to derive the linear equations of motion
q_rlin = [Gamma; Dpsi_1; beta_2; Dpsi_2; Dphi_1; phi_1; Dphi_2; phi_2];
Dq_rlin = [DGamma; D2psi_1; Dbeta_2; D2psi_2; D2phi_1; Dphi_1_; D2phi_2; Dphi_2_];
u_lin = [delta_1; delta_2];

subs_old = {'beta_1';'Dbeta_1'};  % Prepare the constraint substitutions
subs_new = [beta_1_;Dbeta_1_];

% Row1 lateral1 --> lateral2
lat1lat2 = subs(subs(lateral2,'F_c',F_c1),subs_old,subs_new);

% Row2 lateral1 --> yaw2
```

```
lat1yaw2 = subs(subs(yaw2,'F_c',F_c1),subs_old,subs_new);

% Row3 lateral1 --> yaw1
lat1yaw1 = subs(subs(yaw1,'F_c',F_c1),subs_old,subs_new);

% Row5 lateral1 --> roll1
lat1roll1 = subs(subs(roll1,'F_c',F_c1),subs_old,subs_new);

% Row6 lateral1 --> roll2
lat1roll2 = subs(subs(roll2,'F_c',F_c1),subs_old,subs_new);

M_r = sym('M_r', [length(q_rlin),length(q_rlin)]);
for idx = 1:length(q_rlin)
    M_r(1,idx) = simplify(diff(lat1lat2,Dq_rlin(idx)));
    M_r(2,idx) = simplify(diff(lat1yaw2,Dq_rlin(idx)));
    M_r(3,idx) = simplify(diff(lat1yaw1,Dq_rlin(idx)));
    M_r(4,idx) = simplify(diff(Gamma_constraint,Dq_rlin(idx)));
    M_r(5,idx) = simplify(diff(lat1roll1,Dq_rlin(idx)));
    M_r(6,idx) = simplify(diff(lat1roll2,Dq_rlin(idx)));
    M_r(7,idx) = simplify(diff(Dphi_1_,Dq_rlin(idx)));
    M_r(8,idx) = simplify(diff(Dphi_2_,Dq_rlin(idx)));
end
M_r       % Display the matrix

P_r = sym('P_r', [length(q_rlin),length(q_rlin)]);
for idx = 1:length(q_rlin)
    P_r(1,idx) = -simplify(diff(lat1lat2,q_rlin(idx)));
    P_r(2,idx) = -simplify(diff(lat1yaw2,q_rlin(idx)));
    P_r(3,idx) = -simplify(diff(lat1yaw1,q_rlin(idx)));
    P_r(4,idx) = -simplify(diff(Gamma_constraint,q_rlin(idx)));
    P_r(5,idx) = -simplify(diff(lat1roll1,q_rlin(idx)));
    P_r(6,idx) = -simplify(diff(lat1roll2,q_rlin(idx)));
    P_r(7,idx) = -simplify(diff(-Dphi_1,q_rlin(idx)));
    P_r(8,idx) = -simplify(diff(-Dphi_2,q_rlin(idx)));
end
P_r       % Display the matrix

H_r = sym('H_r', [length(q_rlin),length(u_lin)]);
for idx = 1:length(u_lin)
    H_r(1,idx) = -simplify(diff(lat1lat2,u_lin(idx)));
    H_r(2,idx) = -simplify(diff(lat1yaw2,u_lin(idx)));
    H_r(3,idx) = -simplify(diff(lat1yaw1,u_lin(idx)));
    H_r(4,idx) = -simplify(diff(Gamma_constraint,u_lin(idx)));
    H_r(5,idx) = -simplify(diff(lat1roll1,u_lin(idx)));
    H_r(6,idx) = -simplify(diff(lat1roll2,u_lin(idx)));
    H_r(7,idx) = -simplify(diff(-Dphi_1,u_lin(idx)));
    H_r(8,idx) = -simplify(diff(-Dphi_2,u_lin(idx)));
end
H_r       % Display the matrix
```

Appendix B

Vehicle Animation with MatCarAnim

Within this work, an animation- or visualization-toolbox named as *MatCarAnim* was developed for the MATLAB®-enviroment. It was tested in MATLAB®-R2011b.
The *Toolbox* contains various MATLAB® *m-Functions* structured in figure B.2, which provide visualization and animation tools like "coordinate transformations" and functions for the creation of basic drawings. Furthermore it uses a structure variable, which allows the storage of model parameters and settings. It is shown in figure B.3 and allows arbitrary extensions. The whole toolbox functions and documentation will be provided soon, on the MATHWORKS file exchange website http://www.mathworks.com/matlabcentral/fileexchange/.

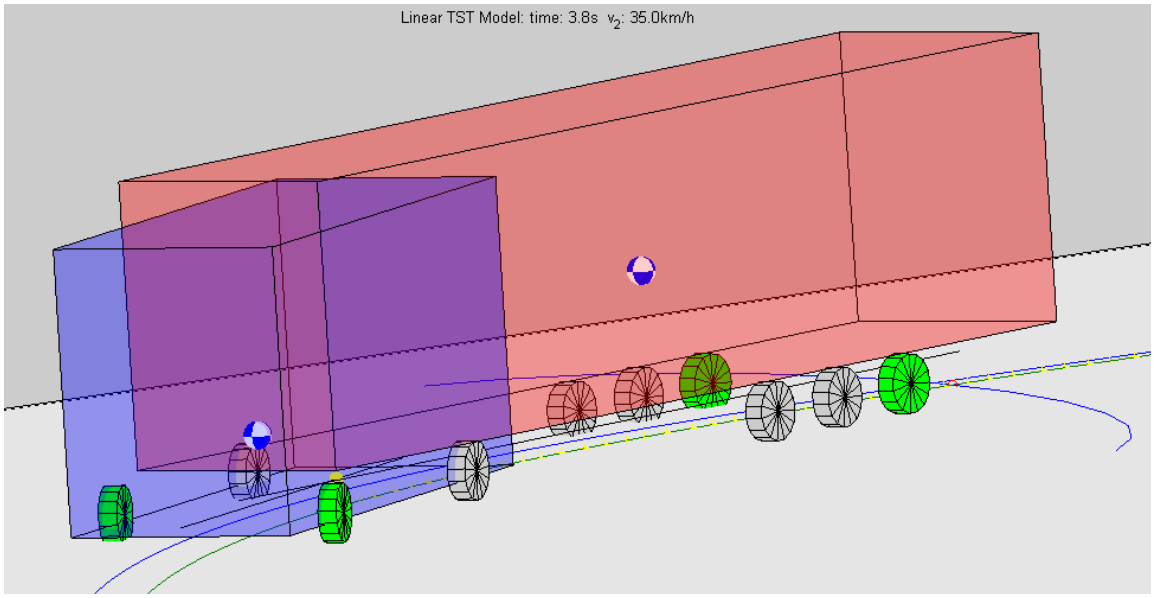

Figure B.1: 3D view of a tractor-semitrailer with a steerable rearmost axle, created by the MATCARANIM toolbox.

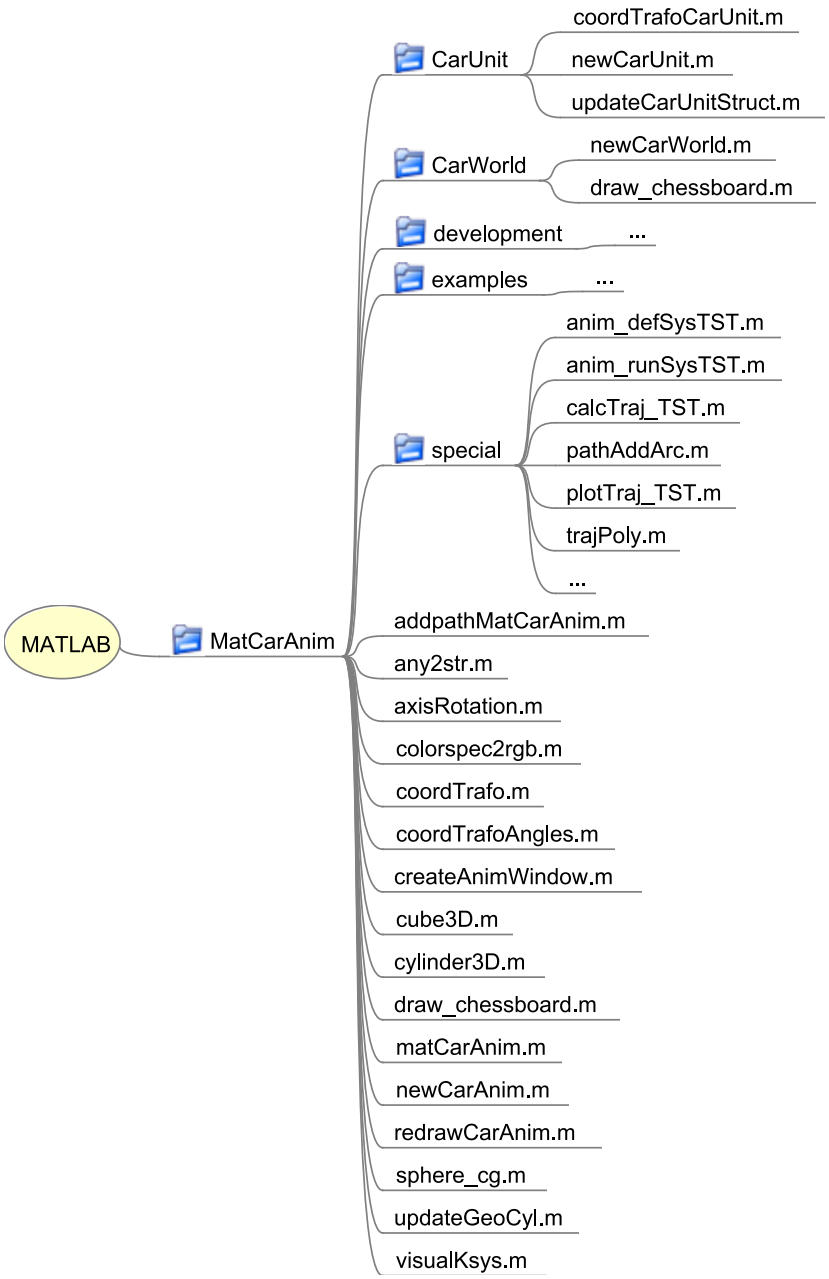

Figure B.2: Structure of the MatCarAnim-software.

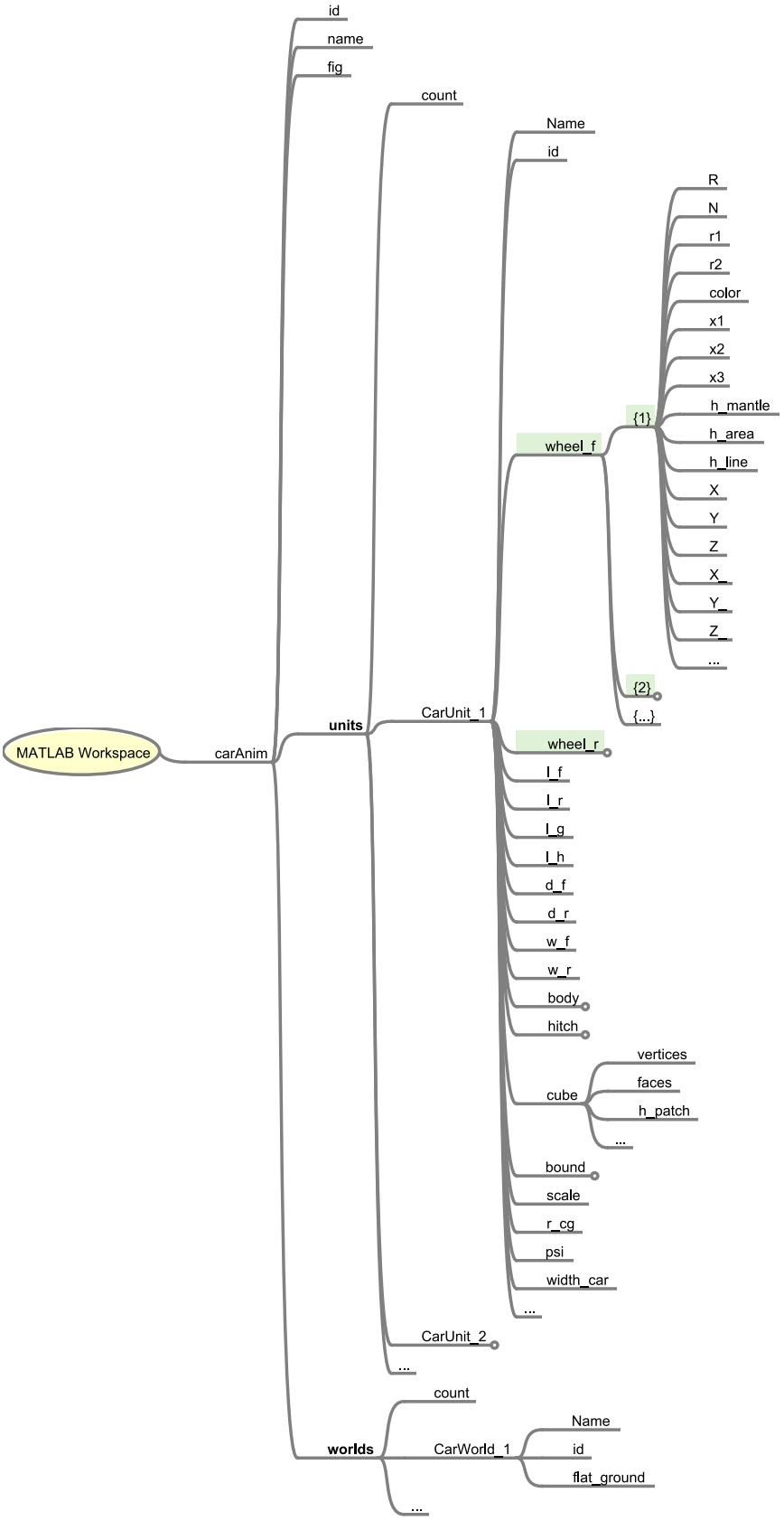

Figure B.3: Structure of the MatCarAnim-struct.

List of Figures

Bibliography

[AO98] J. Ackermann and D. Odenthal. Robust steering control for active rollover avoidance of vehicles with elevated center of gravity. Technical report, DLR, German Aerospace Center, Institute of Robotics and System Dynamics, 1998.

[AO99] J. Ackermann and D. Odenthal. Damping of vehicle roll dynamics by gain scheduled active steering. Technical report, DLR, German Aerospace Center, Institute of Robotics and System Dynamics, Oberpfaffenhofen, D-82230 Wessling, Germany, 1999.

[Boe11] S. Boehl. Lenkstrategie für einen aktiv gelenkten Sattelauflieger. Semesterthesis, Institute for Dynamic Systems and Control - Swiss Federal Institute of Technology (ETH) Zürich, 2011.

[CC08] C. Cheng and D. Cebon. Improving roll stability of articulated heavy vehicles using active semi-trailer steering. *Vehicle System Dynamics: International Journal of Vehicle Mechanics and Mobility*, Vol. 46, Supplement:373–388, 2008.

[CP01] B. Chen and H. Peng. Differential-braking-based rollover prevention for sport utility vehicles with human-in-the-loop evaluations. *Vehicle System Dynamics: International Journal of Vehicle Mechanics and Mobility*, Vol. 36, No. 4-5:359–389, 2001.

[dB01] D. d. Bruin. *Lateral Guidance of All-Wheel Steered Multiple-Articulated Vehicles*. Dissertation, Technische Universiteit Eindhoven, 2001.

[FMG06] C. Fletcher, C. Manzie, and M. Good. Trailer Steering: An Australian Research Perspective and Application for By-Wire Control. Technical report, Ninth International Symposium on Heavy Vehicle Weights and Dimensions. June 18-22, Penn State, State College, Pennsylvania, 2006.

[FW07] P. S. Fancher and C. B. Winkler. Directional performance issues in evaluation and design of articulated heavy vehicles. *Vehicle System Dynamics: International Journal of Vehicle Mechanics and Mobility*, Vol. 45, No. 7-8:607–647, 2007.

[Gil92] T. D. Gillespie. *Fundamentals of Vehicle dynamics*. Society of Automotive Engineers, Warrendale, PA, 1992.

[Hor63] I. M. Horowitz. *Synthesis of feedback systems*. Academic Press, New York, 1963.

[Jaz09] R. N. Jazar. *Vehicle Dynamics: Theory and Application*. Springer-Verlag Berlin Heidelberg, 2009.

[KS88] I. Kageyama and Y. Saito. Stabilization of articulated vehicles by semiactive control method. *Vehicle System Dynamics: International Journal of Vehicle Mechanics and Mobility*, Vol. 17, Supplement 1:199–209, 1988.

[Lun08] J. Lunze. *Regelungstechnik 1 - Systemtheoretische Grundlagen, Analyse und Entwurf einschleifiger Regelungen*. Springer-Verlag Berlin Heidelberg, 2008.

[OBA99] D. Odenthal, T. Bünte, and J. Ackermann. Nonlinear steering and braking control for vehicle rollover avoidance. Technical report, DLR, German Aerospace Center, Institute of Robotics and System Dynamics, 1999.

[ORJC10] A. M. C. Odhams, R. L. Roebuck, B. A. Jujnovich, and D. Cebon. Active steering of a tractor-semi-trailer. *Proceedings of the Institution of Mechanical Engineers, Part D: Journal of Automobile Engineering*, Vol. 225:847–869, 2010.

[Pac02] H. Pacejka. *Tyre and Vehicle Dynamics*. Number 0750651415. Elsevier Butterworth-Heinemann, 2002.

[PS10] K. Popp and W. Schiehlen. *Ground Vehicle Dynamics*. Springer-Verlag Berlin Heidelberg, 2010.

[SAE76] Vehicle dynamics terminology, SAE J670e, Warrendale, PA, 1976.

[Sam00] D. John M. Sampson. *Active Roll Control of Articulated Heavy Vehicles*. Dissertation, Cambridge University Engineering Department, 2000.

[SC98] D. J. M. Sampson and D. Cebon. An investigation of roll control system design for articulated heavy vehicles. Technical report, Cambridge University Engineering Department, 1998.

[SC03] D. J. M. Sampson and D. Cebon. Achievable roll stability of heavy road vehicles. *Proceedings of the Institution of Mechanical Engineers, Part D: Journal of Automobile Engineering*, Vol. 217:217–287, 2003.

[Seg57] L. Segel. Theoretical prediction and experimental substantiation of the response of the automobile to steering control. *Proceedings of the IMechE Automobile Division*, pages 310–330, 1956-1957.

[Sha05] A. A. Shabana. *Dynamics of Multibody Systems*. Cambridge University Press, Cambridge, 3 edition, 2005.

[SMC99] D. J. M. Sampson, G. McKevitt, and D. Cebon. The development of an active roll control system for heavy vehicles. Technical report, Cambridge University Engineering Department, 1999.

[SW99] R. Schwertassek and O. Wallrapp. *Dynamik flexibler Mehrkörpersysteme (in German)*. Vieweg, Braunschweig, 1999.

[vdV11] B. v. d. Velden. Steering Control of Semi-Trailers – Model-Based Vehicle Dynamics Control for Rollover Prevention. Master's thesis, Institute for Dynamic Systems and Control - Swiss Federal Institute of Technology (ETH) Zürich, 2011.

[Viv12] M. Vivaldelli. Semi-Trailer Steering Strategies – Model-Based Vehicle Dynamics Controllers for Reversing Manoeuvres. Masterthesis, Institute for Dynamic Systems and Control - Swiss Federal Institute of Technology (ETH) Zürich, Swiss Federal Institute of Technology (ETH) Zürich, 2012.

[Win98] C. B. Winkler. Simplified analysis of the steady-state turning of complex vehicles. *Vehicle System Dynamics: International Journal of Vehicle Mechanics and Mobility*, Vol. 29:141–180, 1998.

[Zom83] A. Zomotor. *Fahrwerktechnik: Fahrverhalten*. VOGEL Buchverlag Wuerzburg, 1983.

ETH
Eidgenössische Technische Hochschule Zürich
Swiss Federal Institute of Technology Zurich

Institute for Dynamic Systems and Control
Prof. Dr. R. D'Andrea, Prof. Dr. L. Guzzella

Title of work:

Lateral Dynamics of Multiaxle Vehicles

Thesis type and date:

Master Thesis, July 2013

Supervision:

M. Alberding (ETH Zurich)
Prof. Dr. L. Guzzella (ETH Zurich)
Prof. Dr. W. Schiehlen (University of Stuttgart)
Prof. Dr. P. Eberhard (University of Stuttgart)

Student:

Name:	Johannes Stoerkle
E-mail:	johannesstoerkle@yahoo.de
Legi-Nr.:	12-909-909
Semester:	1

Statement regarding plagiarism:

By signing this statement, I affirm that I have read the information notice on plagiarism, independently produced this paper, and adhered to the general practice of source citation in this subject-area.

Information notice on plagiarism:

http://www.ethz.ch/students/semester/plagiarism_s_en.pdf

Zurich, 10. 12. 2013: _____